



universität
wien

MASTERARBEIT

Titel der Masterarbeit

„Synthese, Charakterisierung und elektrochemische
Untersuchung von Nitro und Nitrosyl
Rutheniumkomplexen mit Azolheterocyclen als
potentielle tumorhemmende Therapeutika“

verfasst von

Ewelina Orłowska Bsc.

angestrebter akademischer Grad

Master of Science (MSc)

Wien, 2013

Studienkennzahl lt.
Studienblatt:

A 066 862

Studienrichtung lt.
Studienblatt:

Masterstudium Chemie

Betreut von:

ao. Univ.-Prof. Dr. Vladimir Arion



universität
wien

MASTER THESIS

„Synthesis, characterization and electrochemical studies
of ruthenium-nitro and -nitrosyl complexes with azole
heterocycles as potential anticancer drugs“

Author

Ewelina Orłowska Bsc.

Intended academic degree

Master of Science (MSc)

Vienna, 2013

Subject:

Chemistry

Supervisor:

ao. Univ.-Prof. Dr. Vladimir Arion

Meinen Eltern

Acknowledgements

I want to thank all the people who helped me during my master thesis:

O. Univ.-Prof. Dr. Dr. Bernhard K. Keppler for the opportunity to work in his skilled and experienced group.

Ao. Univ.-Prof. Dr. Vladimir Arion for being an excellent supervisor.

Univ.-Prof. Dominique Luneau for his great supervision and Univ.-Prof. Jean Bernard Tommasino for the explanations on electrochemistry and the help during my work in France.

Mag Alex Roller and Dr. Guillaume Pilet for the X-ray diffraction measurements.

Univ.-Prof. Peter Rapta for the EPR measurements.

Mag. Anotolie Dobrov, Mag. Aliona Luganschi, Anna Rathgeb Bsc., Josef Plangger and Peter Unteregger for the ESI-MS measurements.

Ao. Univ.-Prof. Mag. Dr. Markus Galanski, Dipl.-Chem. Paul-Steffen Kuhn, Dipl.-Ing. Melanie Schmidlehner, Mag. Michael Primik, Mag. Verena Pichler and Samuel Meier Msc. for measuring the NMR spectra.

Mag. Johannes Theiner and all members of the microanalytical Laboratory for the elemental analyses.

Mag. Elfriede Limberger for her help regarding administrative concerns.

Mihai Odoeanu for the material supplies.

My laboratory colleagues Anna Rathgeb Bsc. and Sonja Platzler Bsc. for the great working atmosphere.

Abstract

Nowadays ruthenium complexes seem to be the most promising alternatives to platinum complexes in the research field of metal-based anticancer compounds. The possibility to tune different properties of ruthenium, such as redox potential, substitution rate or ligand affinity, and increasing knowledge about the biological activity of ruthenium complexes makes this metal worth of investigation. The discovery that nitric oxide is one of the most important physiological regulators had a stimulating effect on the coordination and biological chemistry of this non-innocent ligand. NO plays an important role in many different biological processes, such as neurotransmission, blood pressure control, antioxidant action and immunological responses. The control of NO concentration, which is needed to obtain the required effect, could be achieved with carriers like metal complexes. The controlled NO-releasing or scavenging complexes are, therefore, of great interest for medical purposes. It has been reported that in several types of cancer the apoptosis of the cancer cells is greatly increased in the presence of nitric oxide. Having the metal complex with nitrosyl could induce the anticancer activity or improve the already observed effects.

Ruthenium compounds with one and two azole heterocycles (NAMI-A and KP1019 analogues), which have been synthesized many years ago, are currently studied in phases I-II clinical trials as potential anticancer drugs. Combining those promising compounds with the non-innocent ligand NO gives the opportunity to create metal-nitrosyls with encouraging properties. Of particular interest is the synthesis of ruthenium-nitrosyl complexes with four azole heterocycles. The higher azole-to-chloride ratio decreases the reduction potential of those compounds, which results in higher antiproliferative activity.

The aim of this work was the synthesis and characterisation of ruthenium nitro and nitrosyl compounds with four azole heterocycles, their electrochemical studies and investigation of the stability of Ru-NO bond.

Zusammenfassung

Heutzutage scheinen die Rutheniumverbindungen die beste Alternative zu den Platin Komplexen in dem Forschungsfeld der Metall-basierten Anti-Krebs-Verbindungen zu sein. Die Möglichkeit zur Steuerung von verschiedenen Eigenschaften des Rutheniums, wie zum Beispiel das Redox Potential, Substitutionsgeschwindigkeit oder Affinität zu Liganden und wachsendes Wissen über die biologische Aktivität von Ruthenium, machen dieses Metall weiterer Erforschung würdig. Die Entdeckung des Stickstoffmonoxides als einer der wichtigsten physiologischen Regulators hatte eine stimulierende Wirkung auf die Koordinations- und biologische Chemie von diesem 'nicht-unschuldigen' Liganden. NO spielt eine wichtige Rolle in vielen biologischen Prozessen wie Neurotransmission, Kontrolle des Blutdrucks, antioxidative Wirkung und Immunreaktionen. Die Kontrolle der NO-Konzentration, die notwendig zum Erreichen des gewünschten Effektes ist, kann mit Trägern wie Metall-Komplexe erfolgen. Die NO-freisetzende oder abfangende Komplexe sind daher von großem Interesse für medizinische Zwecke. Es wurde berichtet, dass in Gegenwart von Stickstoffmonoxid die Apoptose von Krebszellen beschleunigt wird. Somit ist es möglich mit Metall-Nitrosyl Komplexen die Anti-Krebs-Aktivität zu induzieren oder bereits bestehende zu verbessern.

Rutheniumkomplexe mit einem und zwei Azolheterocyclen wie KP1019 und NAMI-A, wurden vor vielen Jahren synthetisiert und befinden sich gerade in der Phase I-II von den klinischen Studien als potentielle Antikrebsmedikamente. Die Kombination von diesen Komplexen mit NO Ligand gibt eine Möglichkeit zur Herstellung von Verbindungen mit vielversprechenden Eigenschaften. Von besonderem Interesse ist die Synthese von Ruthenium-Nitrosyl-Komplexen mit vier Azolheterocyclen. Mit dem höheren Azol-zum-Chlorid-Verhältnis nimmt das Reduktions-Potential von solchen Verbindungen ab, gefolgt von der höheren antiproliferativen Aktivität.

Ziel dieser Arbeit war die Synthese, Charakterisierung und elektrochemische Untersuchungen von Ruthenium'-nitro- und -nitrosyl-Komplexen mit vier Azol Heterocyclen.

Abbreviations

3,5-Dimepz	3,5-dimethylpyrazole
4-pic	4-picoline
ADP	adenosine diphosphate
Anal. Calc.	analysis calculated
cGMP	cyclic guanosine monophosphate
<i>conc.</i>	concentrated
CV	cyclic voltammetry or voltammogramm
d (NMR)	duplett
DMF	dimethyl formamide
DMSO	dimethyl sulfoxide
DNA	deoxyribonucleic acid
$E_{1/2}$	half-wave potential
E_p	peak potential
ESI	electrospray ionisation
EPR	electron paramagnetic resonance
g	grams
GC	guanine cyclase
h	hour
Hpz	1 <i>H</i> -pyrazole
Hind	1 <i>H</i> -indazole
IR	infra-red
KP 1019	(IndH)[<i>trans</i> -RuCl ₄ (Ind) ₂]
λ_{max}	wavelength of absorption peak (UV/VIS)
m (Yield)	mass
min	minutes
mg	milligrams
mL	millilitres
M_w	molecular weight
<i>m/z</i>	molecular mass/charge-ratio
n	molar number
NAMI-A	(ImH)[<i>trans</i> -RuCl ₄ (Im)(DMSO)]
NO	nitric oxide
NOS	nitric oxide synthase
OEP	octaethylporphyrin
PARP	poly ADP ribose polymerase
RNA	ribonucleic acid
R.T.	room temperature
TPP	tetraphenylporphyrin
UV	ultra violet
V	volume
VIS	visible

Table of Content

Acknowledgements	7
Abstract	9
Zusammenfassung	11
Abbreviations	13
Table of content	15
1 Introduction	17
1.1 Cancer.....	17
1.1.1 Cancer occurrence and mortality.....	17
1.1.2 Carcinogenesis and risk factors.....	18
1.2 Cancer therapy.....	21
1.2.1 Platin analogues as anticancer agents.....	22
1.2.2 New metal complexes against cancer.....	25
1.2.3 Ruthenium complexes as promising alternative to Cisplatin.....	26
1.2.4 Modes of action of ruthenium drugs.....	27
1.3 Nitric oxide.....	33
1.3.1 NO as non-innocent ligand.....	34
1.4 Ruthenium NO complexes.....	36
1.4.1 Electronic structure alternatives.....	36
1.4.2 NO release in ruthenium complexes.....	37
1.4.3 antiproliferative activity.....	39
1.4.4 Ruthenium NO complexes withazole heterocycles.....	39
1.5 References.....	42
2 General Part	48
3 Supporting information	79
4 Curriculum vitae	91

1 Introduction

1.1 Cancer

1.1.1 Cancer occurrence and mortality

The development of drugs against bacterial diseases, the improvement of the life standard and security changed the leading causes of death under men population upon the time. In the last centuries the biggest part of population died because of the bacterial diseases like malaria. Today, in the developed countries, the main cause of death after cardiovascular diseases is cancer.¹ In Austria on average 20 thousand people died in 2011 due to cancer, which was 26.1% of all deaths (Figure 1).² Worldwide cancer is the leading cause of death after cardiovascular, infectious and parasitic diseases.¹

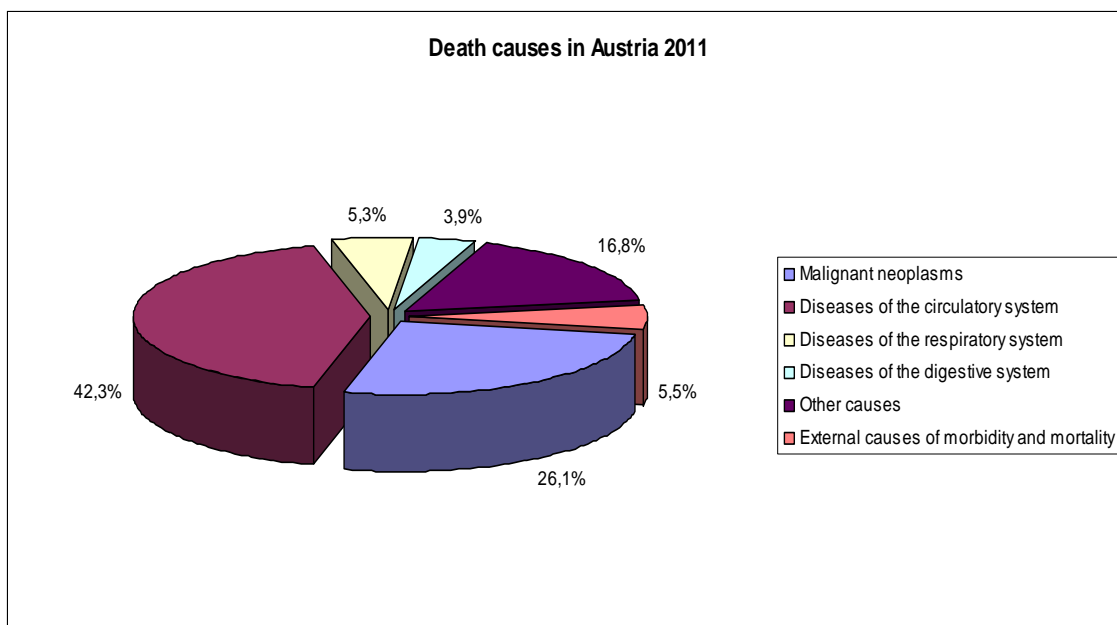


Figure 1. Death causes in Austria in 2011.²

The leading types of cancer with the biggest mortality rates are lung, stomach, liver and colorectal cancer (Figure 2).³ On the other hand breast and prostate cancer occur often but the mortality is much lower.

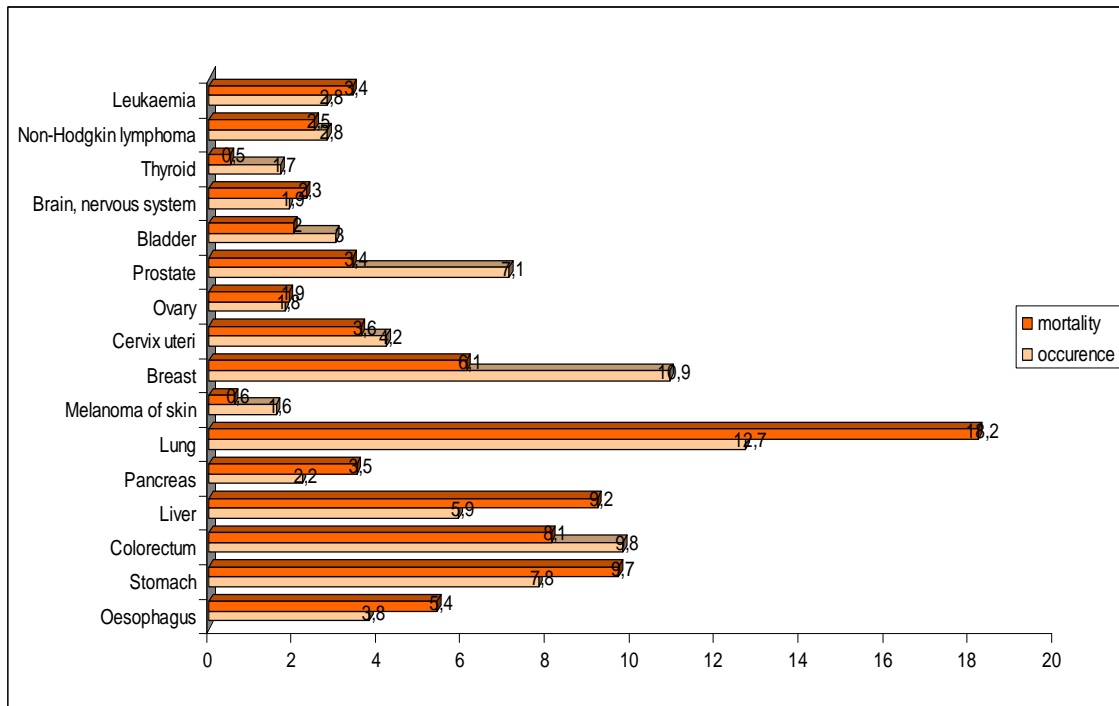


Figure 2. Occurrence of cancer types and their mortality for both sexes in 2008 worldwide.

Due to increasing lifespan and decrease from infectious and parasitic diseases, deaths from cancer worldwide are projected to continue to rise to over 13.1 million in 2030.⁴ Considering these facts, the research activity on tumour therapy and anticancer agents is going to increase permanently and became the most important task in medicine field.

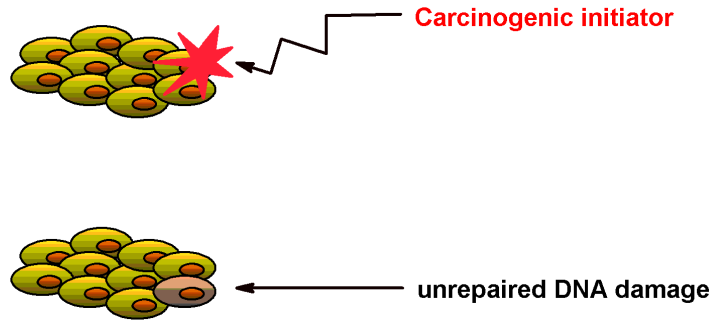
1.1.2 Carcinogenesis and risk factors

Cancer or malignant neoplasm is a group of diseases which all have the unregulated cell grow in common. Cancer is generally classified in dependence of the cell type which started to change. For example the cancer derived from epithelial cells is called Carcinoma and this kind of cancer includes many common cancers like pancreas- or lung cancer.

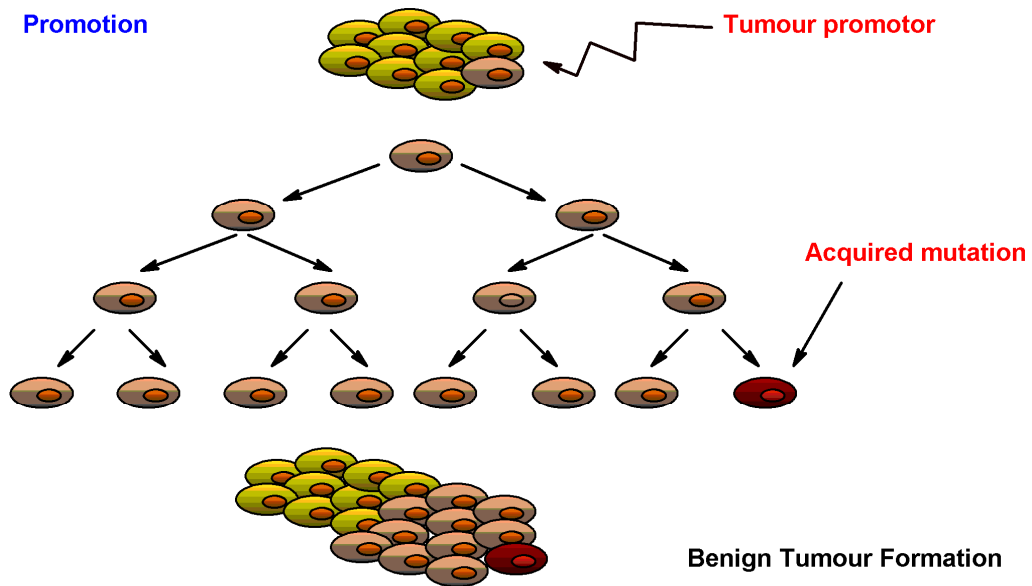
Carcinogenesis is the process where the healthy cells undergo several mutations and transform into tumour cells.^{5,6} It is a multistage process which can take long time and requires the repair mechanisms to fail (Figure 3). If the damage occurs and would not be repaired, the promotion of the tumour can begin. The last step in tumour progression is the change from benign to malignant tumour, which is followed with

invasion to the surrounding tissue. The changed cells can spread in the body using the blood supply and affect other organs. Such behaviour is called metastasis.

Initiation



Promotion



Progression



Figure 3. Schematic view of the three step carcinogenesis.⁷

Besides genetic factors there are many other exogenic agents⁸ which promote tumour formation and grow. They can be divided in following groups:

- chemical factors, such as tobacco smoke, alcohol, benzene and asbestos;
- physical factors, such as ultraviolet and ionizing radiation;
- biological carcinogens, such as infections from oncoviruses (hepatitis B and hepatitis C viruses) bacteria or parasites.

Other risk factors are wrong diet (lack of vegetables and fruits), overweight, no physical activity and ageing. Due to ageing, the cellular repair mechanisms are less effective which increases the possibility of mutation and cancer promotion.

1.2 Cancer therapy

For a long time there was no cure for cancer. The first way to treat tumour was the surgical approach. In the present there are also other strategies for a cancer treatment, like chemotherapy and radiation. Chemotherapy is particularly important and the mostly used method if the tumour already began to spread in other parts of the organism. For the tumours like Leukemia and Lymphoma the use of chemotherapy is essential because those tumours are always widespread. Also to prevent the re-growth of the tumour after the surgical removal is chemotherapy very important. The drugs used in the chemotherapy are supposed to damage the tumour tissue as selective as possible. Those chemotherapeutic agents have different modes of action and can be divided in following groups (according to ATC^a):⁹

- Alkylating antineoplastic agents are the oldest group and cause the alkylation of DNA which leads to cell death. The alkylation takes place on the guanine base of DNA, at the number 7 nitrogen atom of the purine ring. Classical alkylating agents are chlorambucil, carmustine and mechlorethamine.
- Antimetabolites such as antifolates, purine and pyrimidine analogues which prevent the use of metabolite (purine, pyrimidine, folic acid), stop cell growth and cell division.
- Plant alkaloids and other natural products. They inhibit cell division by preventing microtubules function. An example of plant alkaloid with antitumour activity is stilbenoid combretastatin A-4 (Figure 4) found in *Combretum caffrum*.¹⁰
- Cytotoxic antibiotics and related substances which have the ability (depending on the type) to inhibit transcription, intercalate DNA, inhibit topoisomerase II, and cause breaks in DNA.
- Other agents (Platinum analogues, inhibitors of Topoisomerase I and II, intercalating agents, anti-mitotic agents).

^aATC stands for Anatomical Therapeutic Chemical classification system. It is hosted by World Health Organisation (WHO).

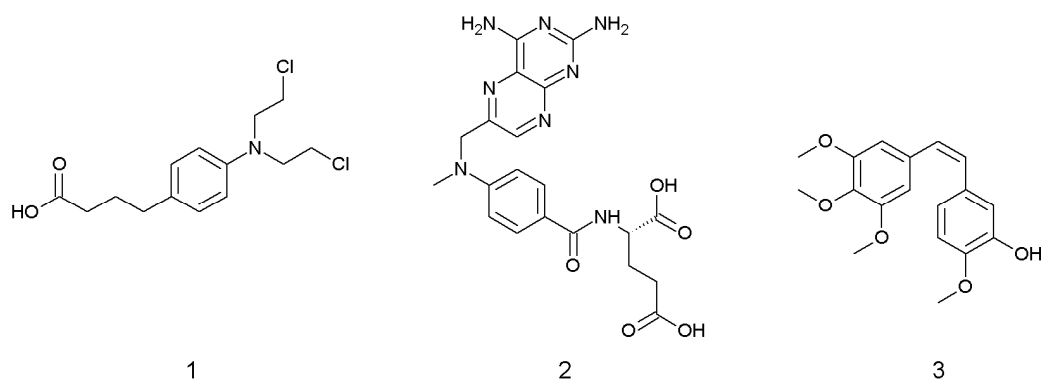


Figure 4. Some of chemotherapeutic agents Chloroambucil (1), Methotrexate (2) and Combretastatin A-4 (3).

The group of other agents includes platinum analogues, which are the group of most effective drugs. They bind to DNA, change the structure of it so that it loses its function. This group will be discussed in more detail. Also very important class are inhibitors of Topoisomerase I and II, which bind to Topoisomerase I and II α – the key enzymes in cell division process.^{11,12} Bound drug prevents the ligation step of the cell cycle and generate double and single stranded breaks that damage the integrity of the genome. Intercalating agents are a group of drugs which bind non-covalently to DNA and in this way they prevent the binding of polymerases to DNA which makes the cell division impossible. A few examples of chemotherapeutic agents are shown in Figure 4.

Most of those drugs are used in combination with each other to increase the effect. For example ECF is the name of the chemotherapeutic agent which contains epirubicin (intercalating agent), cisplatin and 5-fluorouracil (antimetabolite).¹³

1.2.1 Platinum analogues as anticancer agents

Before the Platinum drugs were discovered other metal complexes were tried out in cancer therapy. The one historical example was Fowler's solution,¹⁴ which contains 1% potassium arsenite. It was mainly used for a treatment of leukemia, but it was abandoned because of its toxic and carcinogenic properties.

Cisplatin, the first worldwide approved and still playing the major role in the chemotherapy drug, was first synthesized by Michele Peyrone.¹⁵ The substance was forgotten for about 100 years until the microbiologist Barnett Rosenberg made his

experiment in 1969. He was investigating the influence of an electrical field on bacteria growth and division. For this investigation he used platinum electrodes and ammonium chloride solution with *Escherichia coli*. The bacteria grew to about 300 times of their normal size but they did not divide.¹⁶ Rosenberg thought, it was the electrical field that inhibits the division. However, after he tried the same experiment with carbon electrodes, the bacteria divided as usual. Due to the experimental conditions ammonium hexachloroplatinate(IV), $(\text{NH}_4)_2[\text{PtCl}_6]$ was formed. After sunlight irradiation a photoreaction took place, generating *cis*-diamminetetrachloroplatinum(IV) $\text{cis-}[\text{PtCl}_4(\text{NH}_3)_2]$, which was reduced to *cis*-diamminedichloroplatinum(II), $\text{cis-}[\text{PtCl}_2(\text{NH}_3)_2]$, known as cisplatin.¹⁷ More experiments have shown that cisplatin was a very good candidate for a development as an antitumour agent.^{18,19} In 1978 FDA approved cisplatin for clinical use¹⁶ and today it is still very efficient drug against several cancers, such as testicular and ovarian carcinomas. Although cisplatin shows remarkable activity against many tumours, it has also two major disadvantages. First are the side effects, such as dose-limiting nephrotoxicity, ototoxicity, neurotoxicity and nausea. The second is primary and developed resistance of many tumours against cisplatin.²⁰ Those downsides of cisplatin led to the development of new platinum analogues. During the last 40 years of research two of them were approved for the clinical use worldwide, namely carboplatin and oxaliplatin (Figure 5) and only few regionally.

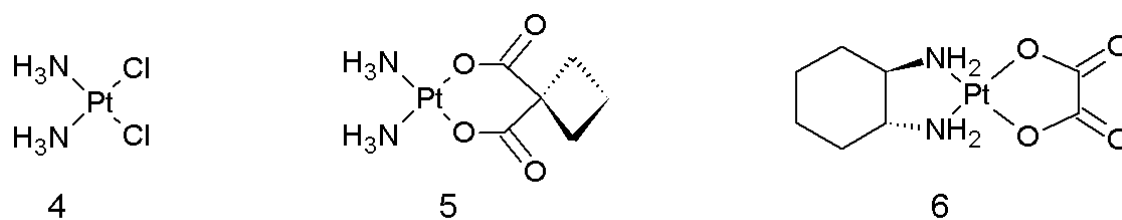


Figure 5. Cisplatin (4), Carboplatin (5) and Oxaliplatin (6).

In case of carboplatin the labile chlorido ligands were replaced with more stable 1,1-cyclobutanedicarboxylato so that the typical side effects of cisplatin do not occur.²¹ However, other side effects are present and the administered dose has to be much higher to obtain similar effects as with cisplatin.²² Oxaliplatin seems to have other mode of action than *cis*- und carboplatin. The accumulation in tumour cells and DNA adducts are believed to be different from those observed with cisplatin and the evidence for that is efficiency in some cisplatin resistant cancers.²³ The three

regionally approved platinum analogues are heptaplatin in South Korea, nedaplatin in Japan and lobaplatin in China (Figure 6)²⁴.

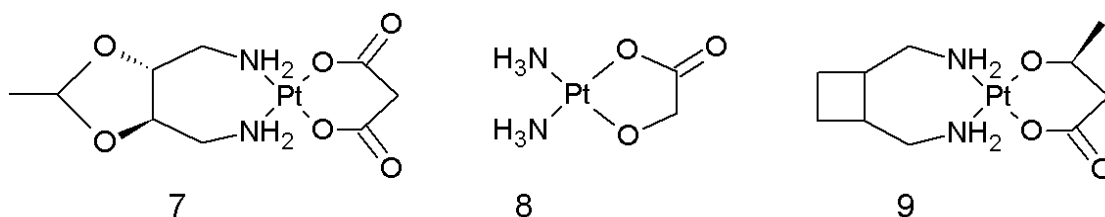


Figure 6. heptaplatin (7), nedaplatin (8) and lobaplatin (9).

The mode of action of cisplatin includes hydrolysis of the complex within the cell, where chloride concentration is lower than in the blood, which led to the very reactive mono-aqua complex $[Pt(NH_3)_2(OH_2)Cl]^+$ (Figure 7). This activated species is able to react with DNA and bind to the guanine side (N7). After second hydrolysis, the complex binds to the guanine moiety and forms intrastrand crosslinks which result in deformation of DNA.²⁵ Deformed DNA does not have its function any more and can not be repaired because the repair mechanisms are affected in cancer cells. That leads to apoptosis of the cell.

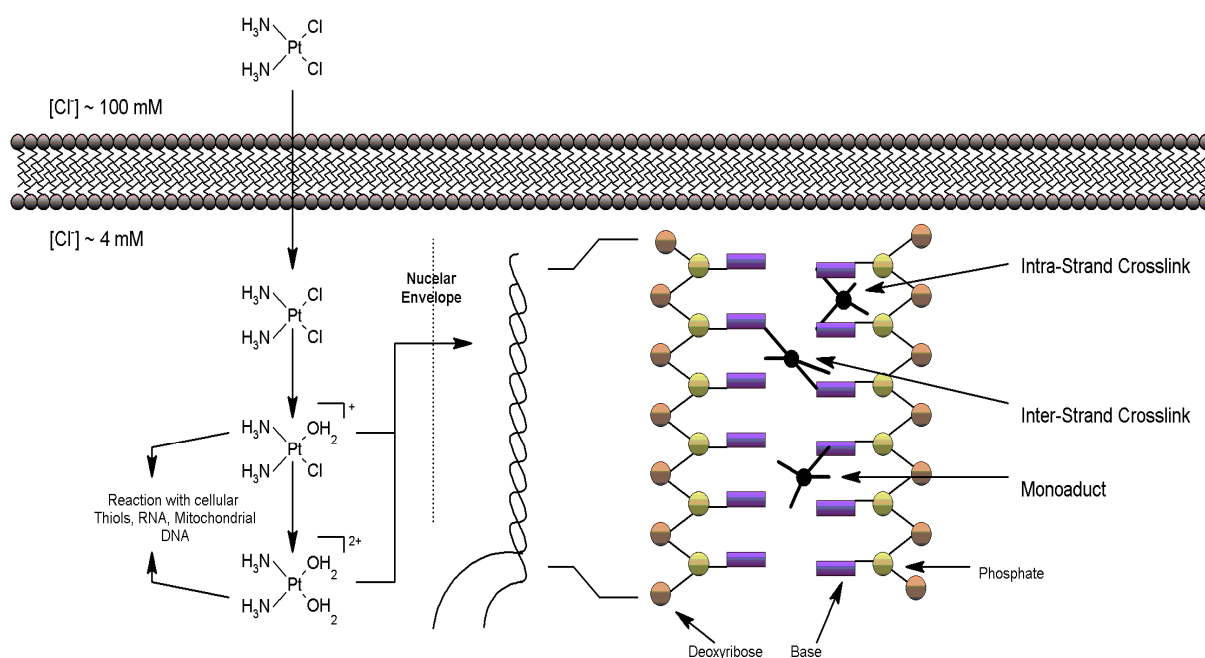


Figure 7. Schematic view of the cisplatin adduct formation: after entering the cell, chloride ligands of cisplatin are replaced by water molecules generating a positively charged aquated species. This aqua complex reacts with nucleophilic sites on intracellular macromolecules to form protein, RNA and DNA

adducts. Three possibilities of DNA adducts are possible: monofunctional adducts, intra- and inter-strand crosslinks with the platinum atom coordinated to the N7 position of guanine or adenine.²⁵

1.2.2 New metal complexes against cancer

The known disadvantages of cisplatin and its analogues and also the lack of efficiency against many tumours has triggered the interest in development of non platinum anticancer drugs. Other metal complexes should have a different mode of action which could stretch out the spectrum of possible treatments (Figure 8). Promising complexes with ruthenium, gallium and titanium have already been tested in clinical phase I and II trials.²⁶ The antitumor activity of gallium salts has already been described in 1971.²⁷ Similar behaviour of Ga(III) to Fe(III) which allows transport by transferrin, synergistic effects with other antineoplastic agents and lipophilic ligands bioavailability of some gallium compounds e.g. KP46 make them worthy of further investigation.²⁸ The octahedral titanium complexes, namely budotitane and titanocene dichloride have also shown very good results in preclinical trials²⁹ but unfortunately they did not show remarkable activity in clinical studies. This fact can be explained by the low solubility and instability of them under physiological conditions.³⁰

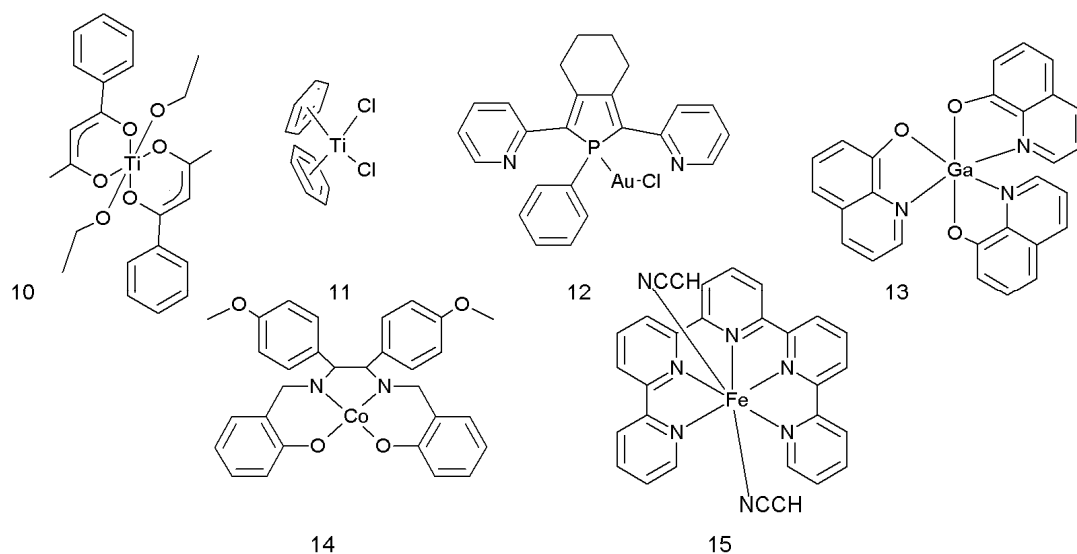


Figure 8. Some of potential antitumor non platinum drugs: budotitane (**10**), metallocene titanocene dichloride (**11**), gold phosphol complex (**12**), KP46 tris(8-quinolinato)gallium(III) (**13**), cobalt salen complex (**14**), iron complex with pentadentate pyridyl ligand (**15**).

Also other metals, such as copper, iron and cobalt showed interesting antitumour properties and research on this field is growing. As mentioned before, the mode of action varies between different metals. For example iron compounds do not bind to DNA. The oxidation state of iron can change between II and III within a cell.³¹ Due to this process reactive oxygen species can be generated and they lead to oxidative damage of DNA.³² The inhibition of cyclooxygenases is the most probable mode of action for some hexacarbonyldicobalt complexes³³ and the antiproliferative effects of gold complexes could be explained by inhibition of thioredoxin reductase.³⁴ Some of iron, cobalt and gold complexes in preclinical studies are shown in Figure 8. As this work deals with the synthesis and characterization of ruthenium complexes, the ruthenium anticancer agents will be discussed in more detail.

1.2.3 Ruthenium complexes as promising alternative to Cisplatin

Nowadays ruthenium complexes seem to be the most promising alternatives to platinum complexes in the research field of metal-based anticancer compounds.³⁵⁻³⁸ Ruthenium complexes possess at least two important features, which are distinct from those of platinum(II)-based anticancer drugs. The first is the octahedral geometry of the ruthenium complexes mainly in the oxidation states 2+ and 3+ (the platinum(II) complexes are square-planar). The second is the possible electron-transfer for Ru^{II}/Ru^{III} couples accessible under physiological conditions.^{38,39} The change of oxidation state from Pt^{IV} to Pt^{II} results in the change of the coordination number. A large benefit of working with ruthenium is also its well-studied chemistry, which allows for a projection of the future compound and synthesis of innovative but also stable under different conditions drugs. The possibility to tune different properties of ruthenium, such as redox potential, substitution rate or ligand affinity, and increasing knowledge about the biological activity of ruthenium complexes makes this metal worthy of investigation. The latest investigations have shown that the mode of action of ruthenium-based drugs differs from that of platinum chemotherapeutics.⁴⁰ Some of ruthenium compounds seem to exhibit activity against tumours that developed cisplatin resistance or where cisplatin was inactive. In addition, most of ruthenium complexes show lower toxic side effects than platinum compounds, making them good candidates for clinical trials.⁴¹ Other advantage of ruthenium drugs is the similarity of ruthenium and iron, which allows for the transport of ruthenium to the cell and internalization via transferrin receptor mediated

endocytosis.⁴²⁻⁴⁴ It has been reported that the number of transferrin receptors for normal cells is lower than for cancer cells.⁴⁵ This fact explains the high uptake of ruthenium complexes by cancer cells.

After the successful clinical trials of the ruthenium(III) complex (IndH)[*trans*-RuCl₄(Ind)₂], KP1019, which shows a remarkable tumor-inhibiting activity⁴⁶⁻⁴⁸ and (ImH)[*trans*-RuCl₄(Im)(DMSO)], NAMI-A (Figure 9), which is known for its high antimetastatic activity⁴⁹ a large variety of ruthenium complexes with azole heterocycles has been synthesized and investigated to improve their pharmacological characteristics.

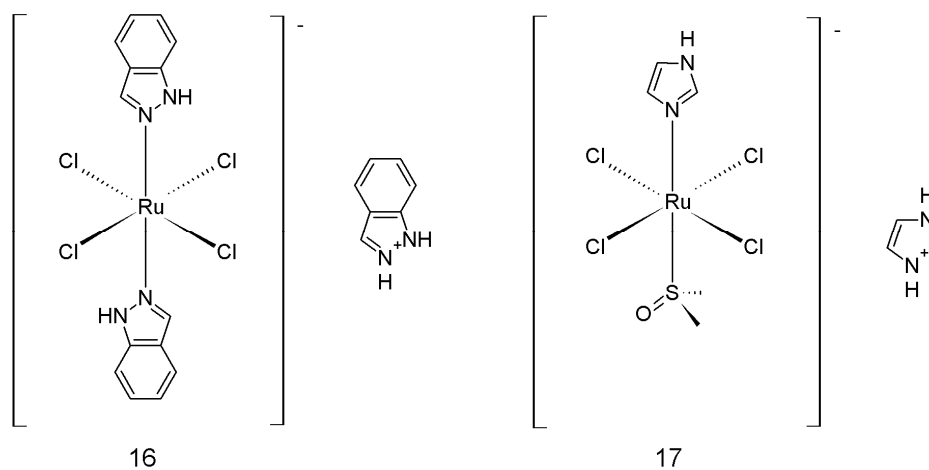


Figure 9. Ruthenium complexes in clinical trials: KP1019 (**16**) and NAMI A (**17**).

Recent investigations have shown that the replacement of the chlorido ligands with indazole ligands improves the antiproliferative activity and ruthenium(III) complexes with the general formula (HL)[RuCl₄L₂] (L = azole heterocycle) are well-known for their antitumor properties⁵⁰ (Figure 10).

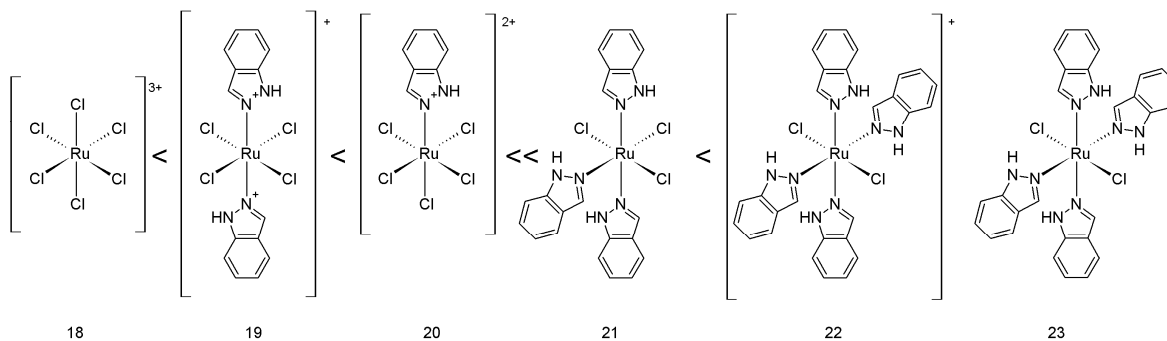


Figure 10. Potency of the indazole complexes in vitro against two human cell lines, CH1 (ovarian carcinoma) and SW480 (colon carcinoma). increasing in the following rank order (counterions omitted for clarity): $[\text{Ru}^{\text{III}}\text{Cl}_6]^{3-}$ (**18**) < $[\text{Ru}^{\text{III}}\text{Cl}_4(\text{ind})_2]^-$ (**19**) < $[\text{Ru}^{\text{III}}\text{Cl}_5(\text{ind})]^{2-}$ (**20**) << $[\text{Ru}^{\text{III}}\text{Cl}_3(\text{ind})_3]$ (**21**) < $[\text{Ru}^{\text{III}}\text{Cl}_2(\text{ind})_4]^+$ (**22**) = $[\text{Ru}^{\text{II}}\text{Cl}_2(\text{ind})_4]$ (**23**).⁵⁰

1.2.3 Modes of action of ruthenium drugs

Several studies have shown that many ruthenium compounds are cytotoxic in cell lines resistant to cisplatin.^{51,52} Those results suggest that the mode of action of ruthenium drugs differs from that of cisplatin. However, the DNA binding mode of ruthenium and the other effects of ruthenium drugs are very complex and still not understood very well. It is very probable that the activity of ruthenium involves many processes not connected to DNA adducts, which would explain the amounts of complex reaching DNA. The knowledge about the mechanism of the antitumour activity needs to be expanded as it is a useful tool to design new metalodrugs. Figure 12 shows the proposed mode of action of KP1019. This includes the transport into the cell with transferrin and reduction of Ru^{III} to Ru^{II} due to reductive conditions in the cancer tissue.^{53,54} The reductive environment of cancer cells is the consequence of oxygen and blood vessels deficiency in very fast growing tissue.⁵⁶ This 'activation by reduction' converts ruthenium complex into the aggressive drug which attacks DNA, proteins and mitochondria.

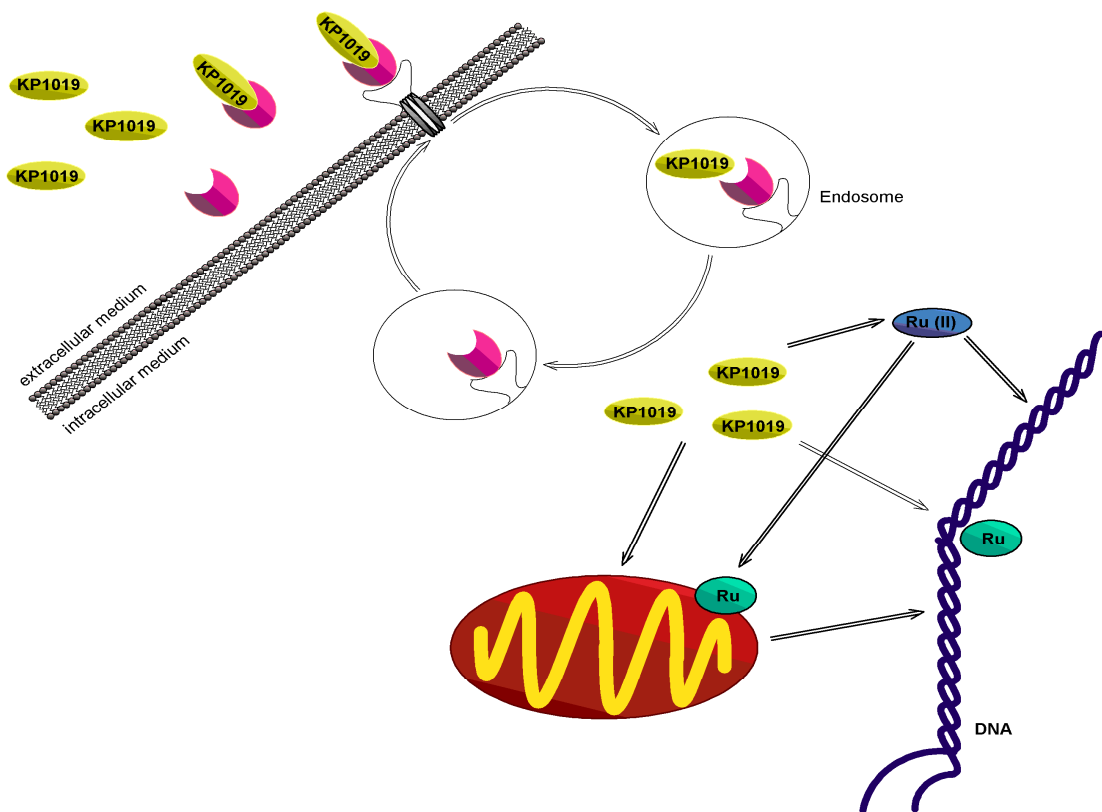


Figure 12. Proposed mode of action of KP1019.⁵⁵

Although the hypothesis seems to be applicable for KP1019 and few other ruthenium drugs, this theory can not be applied for the other drug candidates. A good example is NAMI-A and its anti-tumour activity.^{57,58} NAMI-A is very effective against lung metastases and the lung tissue is obviously the most oxygenated tissue.⁵⁹ The metastases of lung don't show any necrosis due to oxygen deficiency. Clearly the 'activation by reduction' can't be the main mode of action of NAMI-A. The metastatic removal of NAMI-A is shown in Figure 12. Due to the action of NAMI-A the tumour mass remains the same, but the distant metastases can be reduced by almost 100%.

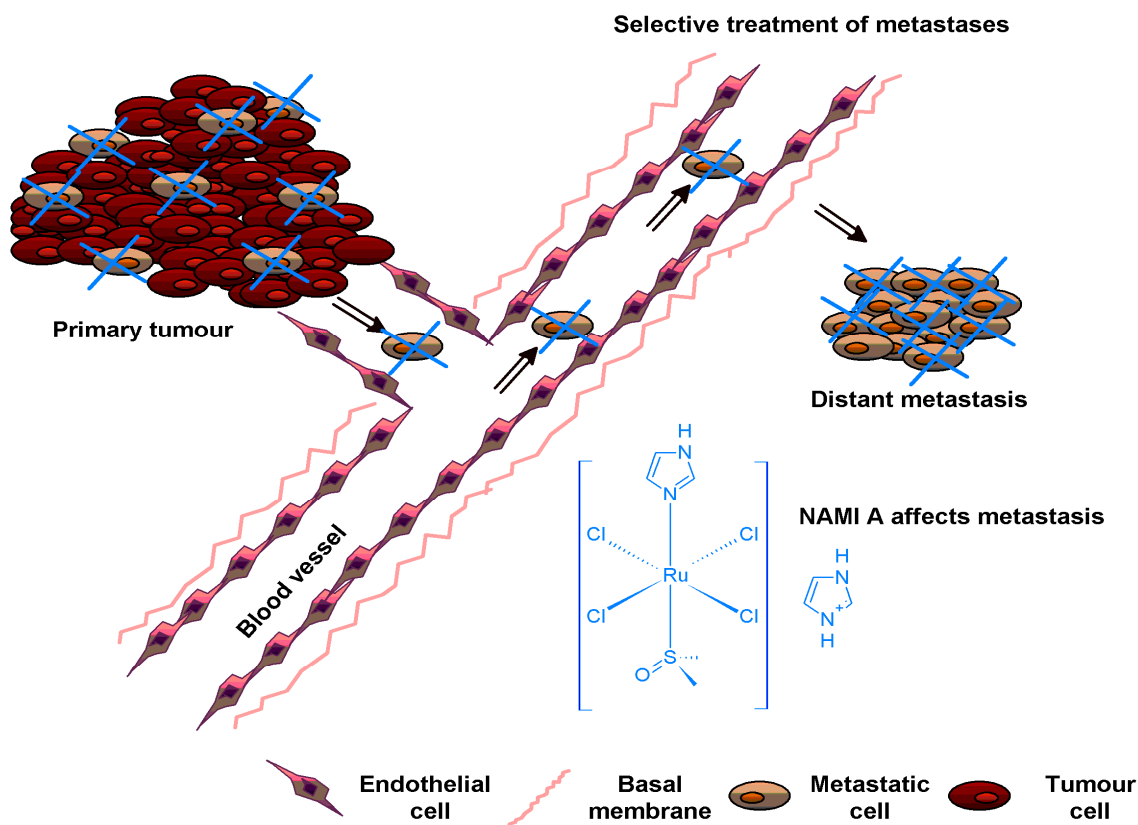


Figure 12. Selective metastatic removal by NAMI-A. NAMI-A reduces weakly primary tumour (where metastases represent a subpopulation) and removes almost total distant metastases (where metastatic cells represent almost 100% of the total cells).⁵⁹

DNA binding

The main proposed mode of action for many ruthenium drugs is binding to DNA. Several publications support this theory and provide the evidence for the covalent binding of ruthenium compounds to DNA.^{40,60-63} Thus, the favoured binding properties remain still unknown. The investigation of the ruthenium(III) complex salt (IndH)[*trans*-RuCl₄(Ind)₂] demonstrated that this complex interacts with DNA forming cross-links or induces strand breaks. Also formation of H₂O₂ and inhibition of both processes by *N*-acetylcysteine was observed. In case of NAMI the binding to DNA was more specific than by other ruthenium drugs.^{49,64} The bifunctional intrastrands with NAMI are capable of terminating RNA synthesis *in vitro*, while the propensity of other ruthenium compounds to form such adducts is markedly lower. Comparing with (IndH)[*trans*-RuCl₄(Ind)₂], the explanation of this fact could be bigger steric barrier

present in indazole complex. The affection of DNA conformation is in case of NAMI most effective. A similar behaviour in other DMSO complexes of ruthenium suggests the altered DNA binding mode in comparison to cisplatin and it is probably responsible for altered cytostatic activity of this class of ruthenium compounds in tumour cells. DNA modifications trigger many other processes, such as damage recognition by proteins and enzymes, repair of this damage, various signaling processes, apoptosis and necrosis. Those processes are also different in case of ruthenium complexes comparing to platinum drugs.

Inhibition of Topoisomerase

Topoisomerase is an important target for many anticancer drugs. The double helical nature of DNA leads to the overwound during the replication which could cause tension and stop the replication. The function of Topoisomerase is to overcome this problem, breaking the DNA helix.⁶⁵ This break allows DNA to be untangled and after the replication the broken bond is formed again. During this process chemical composition and connectivity of the DNA remains the same. There are two types of Topoisomerase: I and II. The first one cuts only one strand of a DNA double helix, whereas the other one both of them. The studies of (HIm)[*trans*-RuCl₄(Im)₂], (IndH)[*trans*-RuCl₄(Ind)₂], [Ru(C₆H₆)(DMSO)Cl₂] and its derivatives have shown that these complexes inhibit the activity of topoisomerase II by forming a ternary cleavage complex of DNA-drug-topoisomerase.⁶⁶⁻⁶⁸ These studies do not provide a clear evidence of poisoning the topoisomerase by ruthenium complexes but at least a part of their anticancer activity can be assigned to this behaviour.

Mitochondrial membrane damage

The damage of the mitochondrial membrane is believed to be another possible mode of action of ruthenium drugs. This leads to induction of apoptosis through the potential and by caspase-dependent cleavage of poly-(ADP-ribose)-polymerase (PARP). Especially under influence of (IndH)[*trans*-RuCl₄(Ind)₂] comes to depolarisation of the membrane potential.⁴⁷ This process is inhibited by *N*-acetylcysteine. *N*-acetylcysteine reduces the population of depolarized mitochondrial membranes and prevent cleavage by poly-(ADP-ribose)-polymerase.

Interference with type IV collagenolytic activity

The observable differences between the activity of NAMI-A and other ruthenium drugs lead to the conclusion that the most important mechanism of the antimetastatic activity of this drug does not necessarily involve DNA adducts. The proposed mode of action is in this case the interference with type IV collagenolytic activity, followed by reduction of metastatic potential of tumor.⁴⁰

1.3 Nitric oxide

The discovery that nitric oxide is one of the most important physiological regulators⁶⁹ had a stimulating effect on the coordination and biological chemistry of this non-innocent ligand. NO plays an important role in many different biological processes, such as neurotransmission, blood pressure control, antioxidant action and immunological responses.⁷⁰ It influences the activity of transcription factors, modulates upstream signaling cascades, mRNA stability and translation, and processes the primary gene products. Most of those processes are controlled with cGMP-dependent protein kinases. The activation of sGC, formation of cGMP, and concomitant protein phosphorylation are considered the main physiological signaling pathway of NO. The cGMP activates various protein kinases, phosphodiesterases and ion channels, which modify cell functions⁷¹ (Figure 13). This may lead to protein modifications and activation of mechanisms of NO-mediated apoptosis, which includes not only DNA damage, but also inhibition of mitochondrial respiration.⁷² Cyclic guanosine monophosphate (cGMP) is a secondary messenger, which activates these proteins. It is synthesised by guanylate cyclase (GC). Soluble GC is a primary receptor for NO. It possesses a heme and binding of NO to that heme causes activation of protein and production of cGMP.⁷¹ Nitric oxide is produced in a cell due to conversion of L-arginine to L-citrulline. The enzyme responsible for this conversion is nitric oxide synthase. There are three forms of NOS: Neuronal NOS (nNOS, NOS type I), inducible NOS (NOS type II) and endothelial NOS (eNOS, NOS type III). Two of them are calcium ions and calmodulin dependent enzymes. The third form is activated by proinflammatory stimuli.⁷³

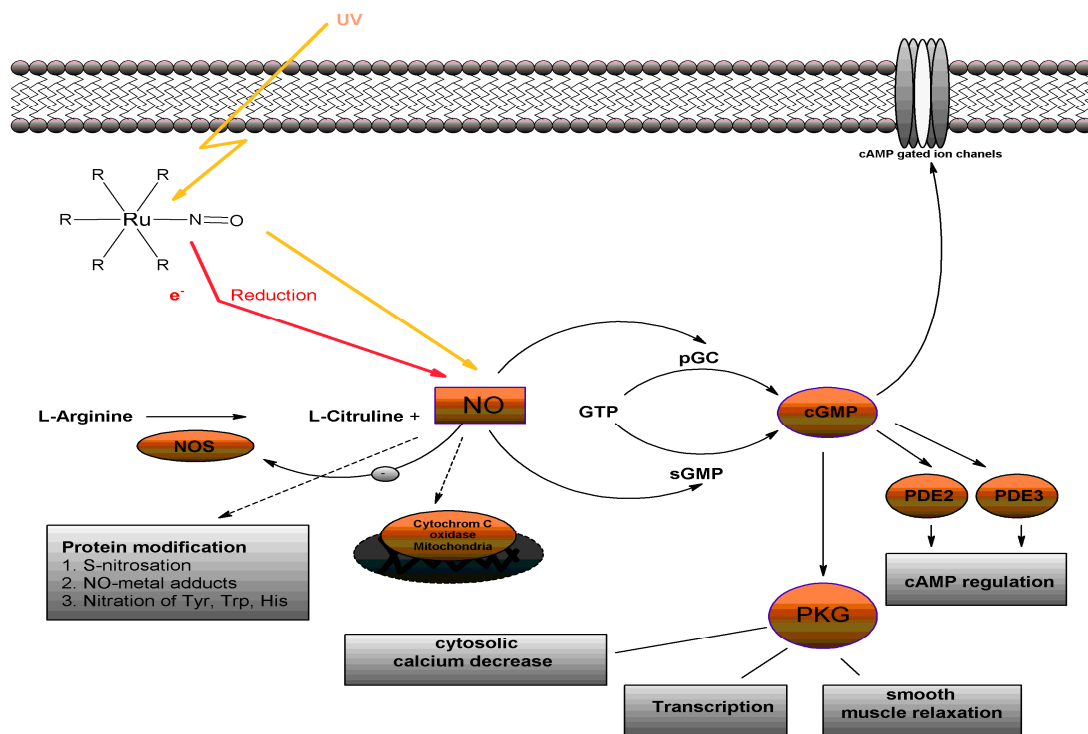


Figure 13. Schematic view of nitric oxide generation and signaling. Nitric oxide, generated by NOS, activates soluble guanylate cyclase (sGC) and guanylate cyclase (pGC), inhibits nitric oxide synthase and cytochrome c oxidase. cGMP activates cGMP-dependent protein kinases (PKG). The concentration of cGMP is controlled by phosphodiesterases (PDE). Nitric oxide affects also some of proteins (nitric oxide–metal adduct formation, S-nitrosation, nitration).⁷³

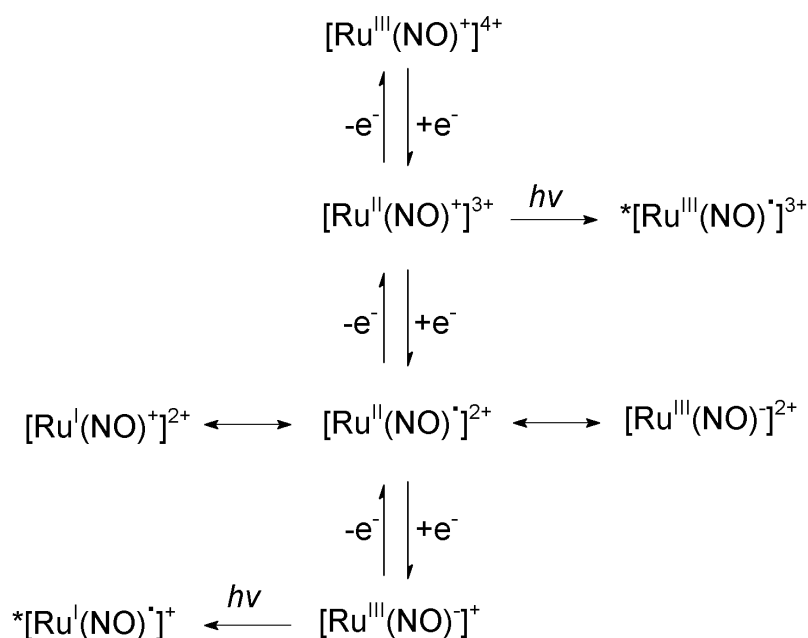
1.3.1 NO as non-innocent ligand

The control of NO concentration, which is needed to obtain the required effect, could be achieved with carriers, e.g., metal complexes. The controlled NO-releasing or scavenging complexes are, therefore, of great interest for medical purposes. The best example of the use of metal nitrosyl complex for medical approach is sodium nitroprusside⁷⁴ (Figure 14). The administered complex releases NO in circulation, which activates a cascade of biochemical reactions and causes in result vascular smooth muscle relaxation. The drug is used in cases of acute hypertensive emergency. Although sodium nitroprusside is widely used, there are problems associated with its breakdown, followed with the release of cyanide.

1.4 Ruthenium NO-complexes

1.4.1 Electronic structure alternatives

Ruthenium, as the heavier homologue of iron has high affinity towards NO.⁷² The mentioned variability of ruthenium in oxidation states combined with the nitrosyl as a ligand allows for many combinations (Scheme 1),⁷⁷ especially when other potent ligands are present.



Scheme 1. Alternative $\text{Ru}^x(\text{NO})^n$ oxidation state combinations for various charged forms.⁷⁷

Using the Enemark–Feltham notation⁷⁸ $\{\text{RuNO}\}^y$, where the number of valence electrons of the metal and of the p^* orbitals of NO are combined (as “y”) because of the problems to define meaningful oxidation states, we can compare the behaviour and stability of Ru-NO pairs. The available oxidation states under physiological conditions are Ru^{II} and Ru^{III} . Nitric oxide as ligand has three possible forms, the nitrosonium cation NO^+ , nitric oxide (“nitrosyl”) NO^\cdot , and the nitroxide anion NO^- . The most stable configuration is $\{\text{RuNO}\}^6$ including strongly π accepting nitrosonium cation and low-spin d^6 metal center. Due to the one electron reduction this configuration changes to labile $\{\text{RuNO}\}^7$ which involves NO radical molecule. This form is not stable and most of complexes reported to have this configuration were chemically or spectroelectrochemically generated forms, which could not be isolated

and were only characterised by EPR and/or IR vibrational spectroscopy.⁷⁹⁻⁸² The characteristic NO wave number in IR for $\{\text{RuNO}\}^6$ between 1900 and 1800 cm^{-1} shifts by about 250-300 cm^{-1} to lower region in case of $\{\text{RuNO}\}^7$.

1.4.2 NO release in Ruthenium complexes

The release of NO in ruthenium complexes can be achieved by one-electron reduction^{83,84} or by photolysis.⁸⁵⁻⁸⁷ The metal-centre effective charge, which changes with the reduction, is a very important factor for the stability of the Ru–NO bond, which is also affected by the ligand in trans position to NO via trans-effect and trans-influence. Generally, the NO-release in ruthenium-nitrosyl complexes is dependent on the trans effect⁸⁸ of the ligands which are bound trans to NO.

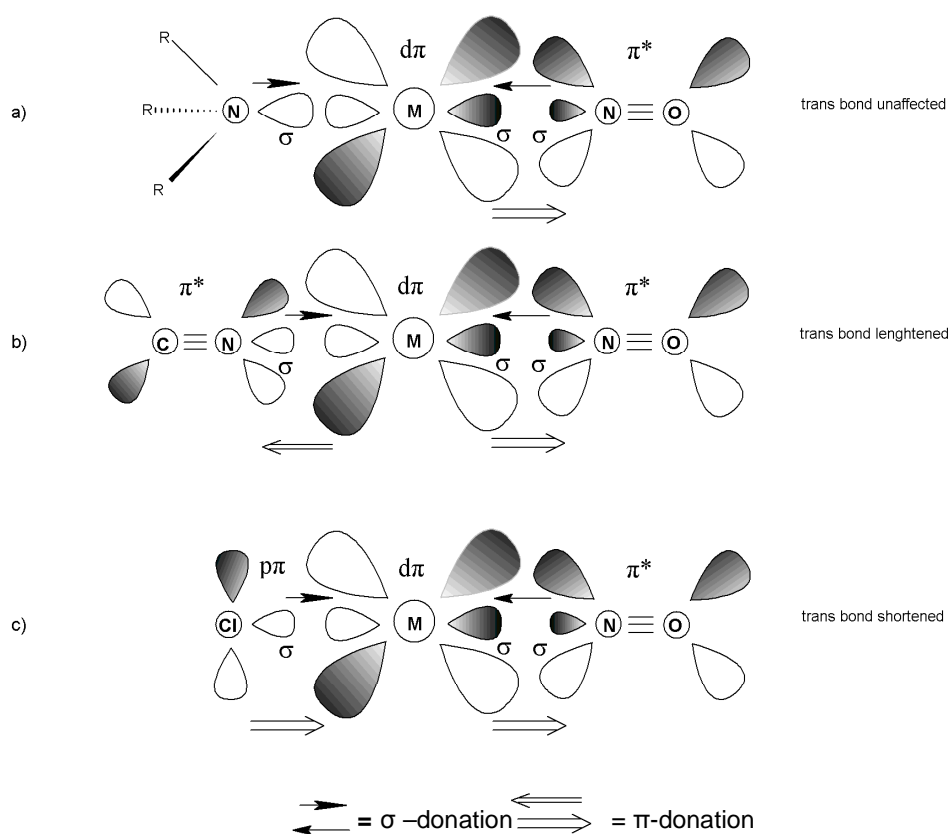


Figure 16. Simplified orbital representations of the bonding in linear metal nitrosyl complexes with different types of *trans* ligand. (a) σ -Donor NH_3/NR_3 ligand; (b) σ -donor– π -acceptor CN^- ligand; (c) σ -donor– π -donor Cl^- ligand.⁸⁸

In the reduction pathway, NO^+ can be reduced with one electron transfer to nitric oxide NO^0 or with two electron transfer to nitroxyl anion NO^- . Both of them have low

affinity to Ru center, facilitating their release. The NO free complex after reduction can react with NO₂ in plasma,⁸⁹ yielding the nitro complex. Considering the reductive conditions in cancer cells, the nitro complex can be reduced to NO⁺ with formation of the starting compound.⁹⁰⁻⁹² Additionally, the [Ru^{II}NO⁺]³⁺/[Ru^{II}NO⁰]²⁺ redox couple is accessible under physiological conditions. The complexes trans-[Ru^{II}(NO⁺)(NH₃)₄(P(OEt)₃)](PF₆)₃ and trans-[Ru^{II}(NO⁺)(NH₃)₄(4-pic)](BF₄)₃ (Figure 17) with E NO⁺/NO⁰ (V vs. NHE) equal 0.142 and -0.008 are good examples for NO complexes with reduction potentials in this range.⁹³

In the photolysis pathway, [Ru^{III}NO⁺]³⁺ converts to [Ru^{III}NO]³⁺ under light irradiation, followed by release of NO.^{85,87} The nitro compounds of Ru are also potentially photoactive.⁹⁴ They produce NO₂⁻ in first photolysis step, which can be splitted into NO and O⁻ in the second step. Several different Ru complexes were reported to be photoactive NO donors. These are mainly ruthenium porphyrins e.g. [Ru(TPP)(NO)(Cl)] (Figure 17) and [Ru(OEP)(NO)(Cl)], which release NO after exposure to 366 nm light.⁹⁵ However, many ruthenium nitrosyl complexes have no absorption bands in visible region and several strategies have been proposed to release NO via photolysis in phototherapeutic window with 600–1100 nm light.

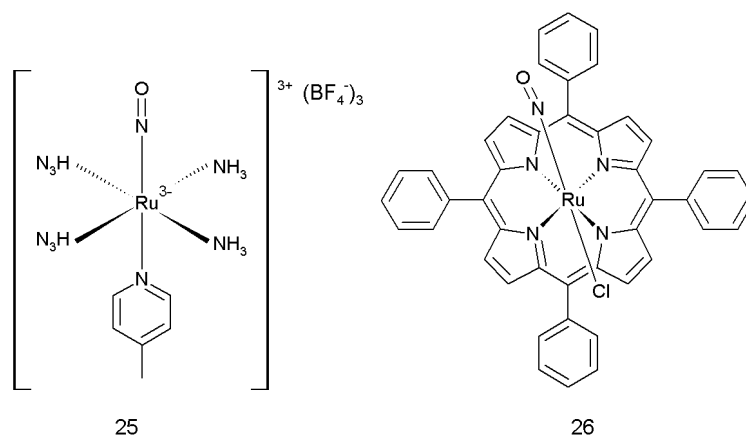


Figure 17. Examples of redox active trans-[Ru^{II}(NO⁺)(NH₃)₄(4-pic)](BF₄)₃ (**25**) and photoactive [Ru(TPP)(NO)(Cl)] (**26**) ruthenium nitrosyl complexes.

The research activity on ruthenium-nitrosyl complexes with their promising properties, like electron transfer activity, photochemical response along with chemical stability is permanently increasing.

1.4.3 Antiproliferative activity

As mentioned before selective use of the nitrosyl complexes can be very effective against cancer. However, NO in in vitro can act in both ways inhibiting cancer cell growth and inducing apoptosis or stimulating cell proliferation. The mode of action depends here on the concentration. Low concentrations are stimulating and promoting tumour growth,⁹⁶ whereas high concentration of NO leads to cell death.⁹⁷ This fact has to be taken into account to design NO complexes with good NO-releasing properties.

Several ruthenium nitrosyl compounds have been synthesized and their in vitro activity has been investigated. Some of them, as for example cis-[Ru^{II}(NO⁺)(dppp)(L)Cl₂]PF₆ (dppp = 1,3-bis(diphenylphosphino) propane; L = py, 4-pic, 4-phenylpyridine, or dmsO) have been analyzed in vitro using human breast carcinoma MDA-MB-231 tumor cell line. The obtained IC₅₀ values were 19.0, 7.4, 7.1 and 12.1 μM and were much lower than those of cisplatin (63 μM) under the same conditions.⁹⁸ The table shows some results of the in vitro studies of NO compounds.⁹⁹

Table 1. IC₅₀ values of ruthenium nitrosyl complexes in cancer cells.⁹⁹

NO complex	Cells	IC ₅₀ , μM
cis-[Ru ^{II} (NO ⁺)(dppp)(py)Cl ₂]PF ₆	MDA-MB-231	19.0
cis-[Ru ^{II} (NO ⁺)(dppp)(4-pic)Cl ₂]PF ₆	MDA-MB-231	7.4
cis-[Ru ^{II} (NO ⁺)(dppp)(4-phen)Cl ₂]PF ₆	MDA-MB-231	7.1
cis-[Ru ^{II} (NO ⁺)(dppp)(dmsO)Cl ₂]PF ₆	MDA-MB-231	12.1
trans-[Ru ^{II} (NO ⁺)(NH ₃) ₄ (isn)](BF ₄) ₃	B16F10-Nex2	1.0
trans-[Ru ^{II} (NO ⁺)(NH ₃) ₄ (4-pic)](BF ₄) ₃	B16F10-Nex2	6.0
trans-[Ru ^{II} (NO ⁺)(NH ₃) ₄ (nic)](BF ₄) ₃	B16F10-Nex2	20.0
trans-[Ru ^{II} (NO ⁺)(NH ₃) ₄ (P(OEt) ₃)](PF ₆) ₃	B16F10-Nex2	33.0

MDA-MB-231 = human breast carcinoma; B16F10-Nex2 = murine melanoma subclone Nex2.

1.4.4 Ruthenium nitrosyl complexes withazole heterocycles

As already mentioned ruthenium complexes withazole heterocycles have shown promising antitumour properties. The best examples are successful clinical trials of KP1019 and NAMI-A. The prodrug KP1019 is active as an anticancer agent in preclinical models of colon cancer and other malignancies and also in the clinical

setting in refractory solid tumors including metastatic disease. Due to the possibility of enhancing the antitumour activity and the reported properties of NAMI A attributed to its high affinity to NO,^{100,101} the interest in synthesizing ruthenium nitrosyl complexes with azole heterocycles has grown. It was suggested that NAMI A captures NO lowering its concentration within a cell and in this way it controls the metastasis. A series of ruthenium complexes with the general formula (cation)⁺[cis-RuCl₄(NO)(Hazole)]⁻, (cation)⁺[trans-RuCl₄(NO)(Hazole)]⁻ and *trans*-[RuCl₃(Hazole)₂(NO)] (Figure 18) has been synthesized and characterized.^{102,103} Also their antitumour activity has been tested.

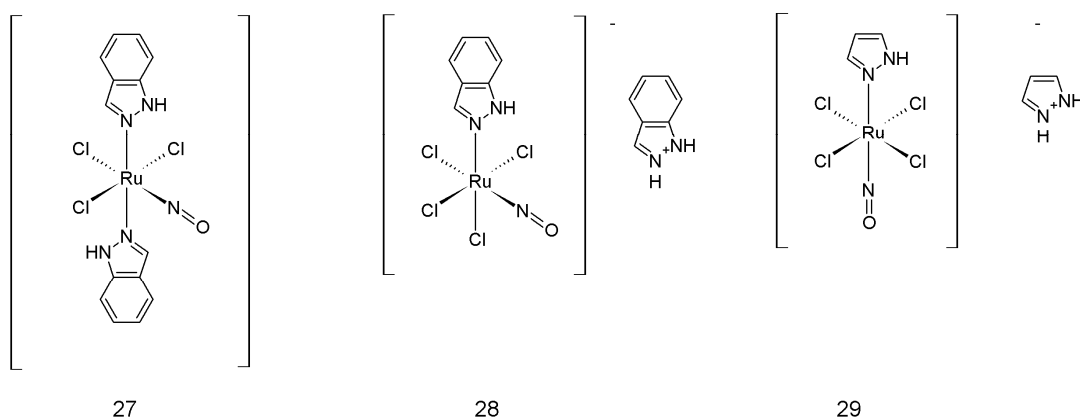


Figure 18. *trans*-[RuCl₃(Hind)₂(NO)] (**27**) (H₂ind)⁺[cis-RuCl₄(NO)(Hind)]⁻ (**28**), (H₂pz)⁺[cis-RuCl₄(NO)(Hpz)]⁻ (**29**).

The cytotoxic potency of *trans* and *cis* complexes with one azole heterocycle has been elucidated in the human cancer cell lines A549, CH1, and SW480. The impact of *cis/trans* isomerism on cytotoxic potency was not distinct: for example the *trans*-configured ruthenium complex is about 2 times more potent than its *cis* analogue, based upon IC₅₀ values. Although the reported antiproliferative activity of those compounds was good, no evidence of the NO-releasing has been found for complexes with one and two azole heterocycles.

Table 2. Inhibition of cancer cell growth by ruthenium nitrosyl compounds with one coordinated azole heterocycle in three human cancer cell lines with 50% inhibitory concentrations (means \pm standard deviations), obtained by the MTT assay (exposure Time: 96 h)¹⁰²

compd	IC ₅₀ , μ M		
	A549	CH1	SW480
(H ₂ ind)[cis-RuCl ₄ (NO)(Hind)]·0.25CHCl ₃	14 \pm 3	2.7 \pm 0.6	2.6 \pm 0.3
(H ₂ ind)[trans-RuCl ₄ (NO)-(Hind)]·CHCl ₃	8.0 \pm 1.3	1.3 \pm 0.3	1.1 \pm 0.3
(H ₂ bzim)[cis-RuCl ₄ (NO)(Hbzim)]	7.6 \pm 2.6	0.83 \pm 0.17	1.8 \pm 0.1
(H ₂ im)[cis-RuCl ₄ (NO)(Him)]·0.1CHCl ₃	35 \pm 13	4.0 \pm 1.1	3.7 \pm 0.5
KP1019	n.d.	44 \pm 11	79 \pm 5

Considering these results, of particular interest is the synthesis of ruthenium nitrosyl complexes with four azole heterocycles. As mentioned before, the higher azole-to-chloride ratio decreases the reduction potential of those compounds, which results in higher antiproliferative activity.⁵⁰ This is a reason which makes these complexes of potential interest. Another one is that having the four coordinated azoles in the equatorial plane around ruthenium, the only possibility for the coordination of NO is one or two axial positions. By exploring the trans effect⁸⁸ and its impact on the stability of the trans metal-ligand bond, the ligand in the trans position to NO can be varied to weak an Ru-NO bond. In this way the release of NO from the complex can be easier achieved by one-electron reduction or by photolysis.

1.5 References

- [1] From the WHO,
http://www.who.int/gho/mortality_burden_disease/causes_death/2008/en/index.html
- [2] From Statistik Austria,
http://statcube.at/statistik.at/ext/superweb/loadDatabase.do?db=degestorbene_ext
- [3] From Globocan 2008, Cancer specific incidence and mortality Worldwide in 2008, <http://globocan.iarc.fr/factsheets/populations/factsheet.asp?uno=900>
- [4] From the WHO,
http://www.who.int/healthinfo/global_burden_disease/2004_report_update/en/
- [5] J. Carl Barrett, *Environ. Health Perspect.*, **1993**, 100, 9-20.
- [6] D. Hanahan, R. A. Weinberg, *Cell*, **2000**, 7, 57-70.
- [7] V. Caligur, *BioFiles*, **2008**, 3(5), 18.
- [8] U. Sankpal, H. Pius, M. Khan, M. Shukoor, P. Maliakal, C. Lee, M. Abdelrahim, S. Connelly, R. Basha, *Tumor Biol.*, **2012**, 33, 1265-1274
- [9] From the ATC,
http://www.whocc.no/atc_ddd_index/?code=L01&showdescription=yes
- [10] P. Singh Sisodiya, *Int. J. Res. Dev. Pharm Life Sci.*, **2013**, 2, 2, 293-308.
- [11] H. A. J. Gelderblom, M. J. A. De Jonge, A. Sparreboom, J. Verweij, *Invest. New. Drugs*, **1999**, 17(4), 401-415.
- [12] W. Chen, J. Qiu, Y. M. Shen, *J Drug Del. Ther.*, **2012**, 6(5), 230-237.
- [13] A. Bamias, D. Cunningham, A. R. Norman, F. Y. Ahmed, M. Watson, A. S. Hill, M. C. Nicolson, M. E. O'Brien, T. C. Evans, V. Nicolson, *Cancer*, **1996**, 77(10), 1978-85.
- [14] D M Jolliffe, *J R Soc Med*, **1993**, 86, 287.
- [15] M. Peyrone, *Ann. Chem. Pharm*, **1884**, 51, 1-29.
- [16] B. Rosenberg, L. Van Camp, T. Krigas, *Nature*, **1965**, 205, 698-699.
- [17] B. Rosenberg, L. Van Camp, E. B. Grimley, A. J. Thomson, *J. Biol. Chem.*, **1967**, 242, 1347-1352.
- [18] B. Rosenberg, L. Van Camp, J. E. Trosko, V. H. Mansour, *Nature*, **1969**, 222, 385-386.

- [19] D. J. Higby, H. J. Jr Wallace, D. J. Albert, J. F. Holland, *Cancer* **1974**, 33, 1219–1225.
- [20] Ana-Maria Florea, D. Büsselberg, *Cancers*, **2011**, 3, 1351-1371.
- [21] U. Frey, J. D. Ranford, P. J. Sadler, *Inorg. Chem.*, **1993**, 32, 1333–1340.
- [22] S. C. Sweetman, *Martindale: The complete drug reference*, Pharmaceutical Press, London, *35th edn*, **2007**.
- [23] L. Kelland, *Nat. Rev. Cancer*, **2007**, 7, 573–584.
- [24] N. J. Wheate, S. Walker, G. E. Craig, R. Oun, *Dalton Trans.*, **2010**, 39, 8113–8127.
- [25] M. Kartalou, J. M. Essigmann, *Mutat. Res.*, **2001**, 478, 1–21.
- [26] I. Ott, R. Gust, *Arch. Pharm. Chem. Life Sci.*, **2007**, 340, 117 – 126.
- [27] M. M. Hart, C. F. Smith, S. T. Yancey, R. H. Adamson, *J. Nat. Cancer Inst.*, **1971**, 47, 1121–1127.
- [28] P. Collery, B. Keppler, C. Madoulet, B. Desoize, *Crit. Rev. Oncol. Hematol.*, **2002**, 42, 283–296.
- [29] F. Caruso, M. Rossi, *Mini Rev. Med. Chem.*, **2004**, 4, 49–60.
- [30] E. Melendez, *Crit. Rev. Oncol. Hematol.* **2002**, 42, 309–315.
- [31] D. Osella, M. Ferrali, P. Zanello, F. Laschi, M. Fontani, C. Nervi, G. Cavigiolio, *Inorg. Chim. Act.* **2000**, 306, 42–48.
- [32] G. Tabbì, C. Cassino, G. Cavigiolio, D. Colangelo, A. Ghiglia, I. Viano, D. Osella, *J. Med. Chem.*, **2002**, 45, 5786–5796.
- [33] I. Ott, B. Kircher, P. Schumacher, K. Schmidt, R. Gust, *J. Med. Chem.* **2005**, 48, 622–629.
- [34] S. Gromer, L. D. Arscott, C. H. Williams, R. H. Schirmer, K. Becker, *J. Biol. Chem.*, **1998**, 273, 20096–20101.
- [35] B. K. Keppler, W. Rupp, U. M. Juhl, H. Endres, R. Niebl, W. Balzer, *Inorg. Chem.*, **1987**, 26, 4366
- [36] W. H. Ang and P. J. Dyson, *Eur. J. Inorg. Chem.*, **2006**, 20, 4003–4018.
- [37] P. C. A. Bruijninx and P. J. Sadler, *Curr. Opin. Chem. Biol.*, **2008**, 12, 197–206.
- [38] E. Reisner, V. B. Arion, B. K. Keppler, A. J. L. Pombeiro, *Inorg. Chim. Acta*, **2008**, 361, 1569–1583.
- [39] D. Chatterjee, A. Mitra and G. S. De, *Platinum Met. Rev.*, **2006**, 50, 2–12.
- [40] V. Brabec and O. Novakova, *Drug Resist. Updates*, **2006**, 9, 111-122.

- [41] G. Sava, I. Capozzi, K. Clerici, G. Gagliardi, E. Alessio, G. Mestroni, *Clin. Exp. Metastas.*, **1998**, 16, 371–379.
- [42] L. Messori, F. Kratz and E. Alessio, *Met.-Based Drugs*, **1996**, 3, 1-9.
- [43] L. Messori, F. Gonzalez, R. Vilchez Vilaplana, F. Piccioli, E. Alessio and B. K. Keppler, *Met.-Based Drugs* **2000**, 7, 335–342.
- [44] A. Bergamo, L. Messori, F. Piccioli, M. Cocchietto, G. Sava, *Invest. New Drugs*, **2003**, 21, 401 – 411.
- [45] E. Musgrove, C. Rugg, I. Taylor and D. Hedley, *J. Cell. Physiol.* **1984**, 118, 6–12.
- [46] S. Kapitza, M. A. Jakupec, M. Uhl, B. K. Keppler, B. Marian, *Cancer Lett.* **2005**, 226, 115–121.
- [47] S. Kapitza, M. Pongratz, M. A. Jakupec, P. Heffeter, W. Berger, L. Lackinger, B. K. Keppler, B. Marian, *J. Cancer Res. Clin. Oncol.*, **2005**, 131, 101–110.
- [48] C. G. Hartinger, M. A. Jakupec, S. Zorbas-Seifried, M. Groessl, A. Egger, W. Berger, H. Zorbas, P. J. Dyson, B. K. Keppler. *Chem. Biodiversity* **2008**, 5, 2140–2155.
- [49] G. Sava, S. Zorzet, C. Turrin, F. Vita, M. R. Soranzo, G. Zabucchi, M. Cocchietto, A. Bergamo, S. DiGiovone, G. Pezzoni, L. Sartor and S. Garbisa, *Clin. Cancer Res.*, **2003**, 9, 1898-1905.
- [50] M. A. Jakupec, E. Reisner, A. Eichinger, M. Pongratz, V. B. Arion, M. Galanski, Ch. G. Hartinger, B. K. Keppler, *J. Med. Chem.* **2005**, 48, 2831–2837.
- [51] M. M. Kasprzak, L. Szmigiero, E. Zyner, J. Ochocki, *J. Inorg. Biochem.*, **2011**, 105, 4, 518–524.
- [52] S. Fruhauf, W. J. Zeller, *Cancer Res.*, **1991**, 51, 2943-2948.
- [53] M. J. Clarke, S. Bitler, D. Rennert, M. Buchbinder, A. D. Kelman, *J. Inorg. Biochem.*, **1980**, 12, 79-87.
- [54] D. Frasca, J. Ciampa, J. Emerson, R. S. Umans, M. J. Clarke, *Met.-Based Drugs*, **1996**, 3, 197-209.
- [55] M. A. Jakupec, M. Galanski, V. B. Arion, C. G. Hartinger, B. K. Keppler, *Dalton Trans.*, **2008**, 183–194.
- [56] R. A. Gatenby, R. J. Gillies, *Nat. Rev. Cancer*, **2004**, 4, 891-899.
- [57] I. Bratsos, S. Jedner, T. Gianferrara, E. Alessio, *Chimia*, **2007**, 61, 692 – 697.

- [58] G. Sava, A. Bergamo, S. Zorzet, B. Gava, C. Casarsa, M. Cocchietto, A. Furlani, V. Scarcia, B. Serli, E. Iengo, E. Alessio, G. Mestroni, *Eur. J. Cancer*, **2002**, 38, 427 – 435.
- [59] A. Bergamo, G. Sava, *Dalton Trans.*, **2007**, 1267 – 1272.
- [60] M. J. Clarke, *Coord. Chem. Rev.*, **2003**, 236, 209–233.
- [61] M. J. Clarke, *Coord. Chem. Rev.*, **2002**, 232, 69–93.
- [62] P. Schluga, C. G. Hartinger, A. Egger, E. Reisner, M. Galanski, M. A. Jakupec, B. K. Keppler, *Dalton Trans.*, **2006**, 14, 1796-1802.
- [63] C. G. Hartinger, S. Zorbas-Seifried, M. A. Jakupec, B. Kynast, H. Zorbas, B. K. Keppler, *J. Inorg. Biochem.*, **2006**, 100, 891-904.
- [64] D. Pluim, R. C. A. M. van Waardenburg, J. H. Beijnen and J. H. M. Schellens, *Cancer Chemother. Pharmacol.*, 2004, **54**, 71-78.
- [65] J. M. Berger, S. J. Gamblin, S. C. Harrison, J. C. Wang, *Nature*, **1996**, 379, 225 – 232.
- [66] G. Feng, C. Hui, J. Liang-Nian, *Chem. Biodivers.*, **2008**, 5(10), 1962-79.
- [67] Y. N. Vashisht Gopal, D. Jayaraju, A. K. Kondapi, *Biochemistry*, **1999**, 38, 4382-4388.
- [68] Y. N. Vashisht Gopal, D. Jayaraju, A. K. Kondapi, *J. Biosci.*, **2001**, 26(2), 271–276.
- [69] D. E. Koshland, *Science* **1992**, 258, 1859–1971.
- [70] J. A. McCleverty *Chem. Rev.* **2004**, 104, 403–418
- [71] S. H. Francis, J. L. Busch, J. D. Corbin, *Pharmacol. Rev.* **2010**, 62, 525–563.
- [72] B. Bonavida, S. Khineche, S. Huerta-Yepe, H Garban. *Drug Resist. Updates* **2006**, 9, 157–173.
- [73] C. Villanueva, C. Giulivi, *Free Radic. Biol. Med.*, **2010**, 49, 307–316
- [74] A. R. Butler, I. L. Megson, *Chem. Rev.*, **2002**, 102, 1155-1165.
- [75] D. A. Wink, Y. Vodovotz, J. Laval, F. Laval, M. W. Dewhirst, J. B. Mitchell, *Carcinogenesis* **1998**, 19, 711–721.
- [76] H.-G. Bernstein, B. Bogerts, G. Keilhoff, *Schizophr. Res.*, **2005**, 78, 69– 86.
- [77] G. K. Lahiri, W. Kaim, *Dalton Trans.*, **2010**, 39, 4471-4478.
- [78] J. H. Enemark, R. D. Feltham, *Coord. Chem. Rev.*, **1974**, 13, 339-406.
- [79] M. Wanner, T. Scheiring, W. Kaim, L. D. Slep, L. M. Baraldo, J. A. Olabe, S. Z'ali's, E. J. Baerends, *Inorg. Chem.*, **2001**, 40, 5704-5707.
- [80] I.A. Bagatin, H. E. Toma, *Spectrosc. Lett.*, **1996**, 29(7), 1409-1416.

- [81] D. R. Lang, J. A. Davis, L. G. F. Lopes, A. A. Ferro, L. C. G. Vasconcellos, D.W. Franco, E. Tfouni, A.Wieraszko, M. J. Clarke, *Inorg. Chem.*, **2000**, *39*, 2294-2300.
- [82] B. R. McGarvey, A.A. Ferro, E. Tfouni, C.W. Brito Bezerra, I. Bagatin, D. W. Franco, *Inorg. Chem.*, **2000**, *39*, 3577-3581
- [83] P. G. Zanichelli, H. F. G. Estrela, R. C. Spadari-Bratfisch, D. M. Grassi-Kassisse, D. W. Franco. *Nitric Oxide-Biol. and Ch.*, **2007**, *16*, 189–196.
- [84] A. G. de Candia, P. Singh, W. Kaim, L. D. Slep, *Inorg. Chem.*, **2009**, *48*, 565-573.
- [85] E. Tfouni, M. Krieger, B.R. McGarvey, D.W. Franco, *Coord. Chem. Rev.* **2003**, *236*, 57–69.
- [86] J. Bordini, D. O. Novaes, I. E. Borissevitch, B. T. Owens, P. C. Ford, E. Tfouni, *Inorg. Chim. Acta* **2008**, *361*, 2252–2258.
- [87] R. M. Carlos, A. A. Ferro, H. A. S. Silva, M. G. Gomes, S. S. S. Borges, P. C. Ford, E. Tfouni, D. W. Franco. *Inorg. Chim. Acta* **2004**, *357*, 1381–1388.
- [88] B. J. Coe, S. J. Glenwright, *Coord. Chem. Rev.* **2000**, *203*, 5–80.
- [89] P.H. MacArthur, S. Shiva, M.T. Gladwin, *J. Chromatogr. B Analyt. Technol. Biomed. Life Sci.*, **2007**, *851*, 93–105.
- [90] R.Z. de Osti, D.W. Franco, *Polyhedron*, **2007**, *26*, 4746–4750.
- [91] P.G. Zanichelli, R.L. Sernaglia, D.W. Franco, *Langmuir*, **2006**, *22*, 203–208.
- [92] F.G. Doro, U.P. Rodrigues, E. Tfouni, *J. Colloid Interf. Sci.*, **2007**, *307*, 405–417.
- [93] L.G.F. Lopes, E.E. Castellano, A.G. Ferreira, C.U. Davanzo, M.J. Clarke, D.W. Franco, *Inorg. Chim. Acta*, **2005**, *358*, 2883–2890.
- [94] R.M. Carlos, D.R. Cardoso, E.E. Castellano, R.Z. Osti, A.J. Camargo, L.G. Macedo, D.W. Franco, *J. Am. Chem. Soc.*, **2004**, *126*, 2546–2555.
- [95] K.M. Miranda, X. Bu, I. Lorkovic, P.C. Ford, *Inorg. Chem.*, **1997**, *36*, 4838–4848.
- [96] L.J. Ignarro, *Nitric Oxide Biology and Pathobiology*, Academic Press, 2nd edn., London, **2000**.
- [97] G.C. Brown, *Bioenergetics*, **2001**, *1504*, 46–57.
- [98] C.C. Golfeto, G. Von Poelhsitz, H.S. Selistre-de-Araujo, M.P. de Araujo, J. Ellena, E.E. Castellano, L.G.L. Lopes, I.S. Moreira, and A.A. Batista, *J. Inorg. Biochem.*, **2010**, *104*, 489–495.

- [99] E. Tfouni, D. R. Truzzi, A. Tavares, A. J. Gomes, L. E. Figueiredo, D. W. Franco. *Nitric Oxide*, **2012**, 26, 38–53.
- [100] B. Serli, E. Zangrado, E. Lengo, G. Mestroni, L. Yellowlees, E. Alessio, *Inorg. Chem.*, **2002**, 41, 4033–4043.
- [101] Serli, B.; Zangrado, E.; Gianferrara, T.; Yellowlees, L.; Alessio, E. *Coord. Chem. Rev.*, **2003**, 245, 73–83.
- [102] G. E. Büchel, A. Gavriluta, M. Novak, S. M. Meier, M. A. Jakupec, O. Cuzan, C. Turta, J.-B. Tommasino, E. Jeanneau, G. Novitchi, D. Luneau, V. B. Arion, *Inorg. Chem.*, **2013**, 52, 6273-85.
- [103] L. Bucinský, G. E. Büchel, R. Ponec, P. Rapta, M. Breza, J. Kozísek, M. Gall, S. Biskupic, M. Fronc, K. Schiessl, O. Cuzan, D. Prodius, C. Turta, S. Shova, D. A. Zajac, Vladimir B. Arion, *Eur. J. Inorg. Chem.*, **2013**, 2505–2519.

2 General Part

Within this work the new ruthenium nitro and nitrosyl complexes and two novel precursors of them have been synthesized, characterized and tested for the ability to release NO. The results of these studies will be prepared for publication after tests for antiproliferative activity *in vitro*.

Abstract

The synthesis of new ruthenium nitro and nitrosyl complexes with closely relatedazole heterocycles namely indazole, pyrazole and 3,5-dimethylpyrazole, with the general formulas $\text{trans}[\text{Ru}(\text{NO}_2)_2(\text{HL})_4]$, $\text{trans}[\text{RuX}(\text{NO})(\text{HL})_4](\text{HL})$ (HL = azole heterocycle, $\text{X} = \text{Cl}^-$, OH^- , SO_4^{2-}) and ruthenium nitrosyl complex with three metal centers $\{[\text{Ru}(\text{NO})(\text{Hpz})(\text{pz})_3(\mu\text{-OH})]_2\text{Mg}\}$ as well as of new complexes $\text{trans}[\text{RuCl}_2(\text{Hpz})_4]$ and $[\text{Ru}_2\text{Cl}_5\text{O}](3,5\text{-dimepz})_4$ has been performed (Chart 1). These compounds were characterized by elemental analysis, NMR spectroscopy, IR spectroscopy, UV–vis spectroscopy, electrospray ionization mass spectrometry (ESI-MS), and X-ray crystallography. The electrochemical behavior has been studied in detail by cyclic voltammetry, and controlled potential electrolysis. In addition, the solubility in water, stability to hydrolysis and sensitivity to light irradiation was investigated.

Chart 1. Compounds reported in this work

(anion/cation/-)

	M	L₁	L₂	HL	Config	counterion	comp
1H-indazole	Ru	NO_2^-	NO_2^-	Hind	trans	-	1
	Ru	NO	OH	Hind	trans	Cl^-	2
	Ru	Cl^-	Cl^-	Hpz	trans	-	3
1H-pyrazole	Ru	NO	OH^-	Hpz	trans	-	4
	2Ru,Mg	NO	OH^-	Hpz	trans	-	5
	Ru	NO	SO_4^{2-}	Hpz	trans	SO_4^{2-}	6
3,5-dimethyl-2H-pyrazole	Ru	NO_2^-	NO_2^-	Hdimepz	trans	3,5- H_2dimepz	7
	Ru	NO	Cl^-	Hdimepz	trans	Cl^-	8
	2Ru	O^{2-}	Cl^-	Cl^{2-}	-	3,5- H_2dimepz	9
	Ru	NO	OH^-	Hpz	trans	SO_4^{2-}	10
	Ru	NO	Cl	Hpz	trans	Cl	11
	Ru	NO	Cl	Hind	trans	Cl	12

Experimental

Chemicals. RuCl₃ was purchased from Johnson Matthey. NaNO₂, NaBH₄, Mg(OH)₂, 1H-pyrazole (Hpz) and 3,5-dimethyl-2H-pyrazole were from Aldrich and Acros, while 1H-indazole (Hind) was from Polivalent-95. All these chemicals were used without further purification.

Synthesis of the Complexes.

trans-[RuCl₂(Hind)₄]¹ (**A**), *trans*-[RuCl₂(Hpz)₄]Cl¹ (**B**), *trans*-[RuCl₂(3,5-dimepz)₄]Cl² (**C**) were prepared according to published protocols.

[*trans*-Dinitrotetraindazolruthenium(II)] (1). A solution of NaNO₂ (0.2 g, 2.6 mmol) in H₂O (8 mL) was added to the mixture of **A** (0.6 g, 0.93 mmol) in acetone/CH₂Cl₂ 1:1 (100 ml). The solution was refluxed under stirring for 12 h, and cooled to room temperature. The organic phase was separated in a separatory funnel then washed with water (3 x 30 mL). The volume of the separated organic phase was reduced to ca. 40 mL. After 2 h the precipitated yellow crystals were filtered off, washed with acetone (5 mL), ethanol (10 mL) and diethyl ether (10 mL). The product was dried in vacuo at r.t. Yield: 0.14 g, 23.0%. X-ray diffraction quality single crystals were grown in CH₂Cl₂/hexane (solvent/vapor diffusion). ¹H NMR in DMSO-*d*₆: 13.32 (s, 4NH), 8.09 (s, 4H), 7.73 (d, 4H, *J* = 8.5 Hz), 7.61 (d, 4H, *J* = 8.5 Hz), 7.34 (t, 4H, *J* = 7.5 Hz), 7.13 (t, 4H, *J* = 7.5 Hz). Elem. anal. Calc. for C₂₈H₂₄N₁₀O₄Ru (*M*_r = 665.62 g/mol), %: C, 50.52; H, 3.63; N, 21.04; O, 9.61. Found, %: C, 50.61; H, 3.39; N, 21.12; O, 9.52. ESI-MS in MeOH (negative): *m/z* 665 [Ru(NO₂)₂(Hind)₄]⁻, 647, 556 541. IR, $\tilde{\nu}$, cm⁻¹: 3303, 3117, 1517, 1469, 1403, 1349, 1257, 1122, 1046, 1026, 755, 602. UV-vis (CH₂Cl₂), λ_{\max} , nm (ϵ , M⁻¹ cm⁻¹): 231 (18 108), 293 (17 513), 325 (21 281), 382 (1 108).

[*trans*-Hydroxidonitrosyltetraindazolruthenium]chloride (2). To a suspension of **1** (0.17 g, 0.25 mmol) in MeOH (4 mL) a 3 M HCl (2.5 ml) was added. The mixture was refluxed under argon for 40 min, and cooled to room temperature. Then the dark-orange solution was filtered and the volume was reduced to ca. 3 mL. The precipitate was filtered off and washed with water (10 mL). The product was recrystallized from

acetone (40 mL), washed with diethyl ether (10 mL) and dried in vacuo at r.t. Yield: 0.11 g, 62%. X-ray diffraction quality single crystals were grown in acetone. ^1H NMR in $\text{DMSO-}d_6$: 14.27 (s, 4NH), 8.56 (s, 4H), 7.89 (d, 4H, $J = 8.5$ Hz), 7.66 (d, 4H, $J = 8.5$ Hz), 7.56 (t, 4H, $J = 7.5$ Hz), 7.29 (t, 4H, $J = 7.5$ Hz). Elem. anal. Calc. for $\text{C}_{28}\text{H}_{25}\text{Cl}_2\text{N}_9\text{O}_2\text{Ru}\cdot\text{H}_2\text{O}$ ($M_r = 704.53$ g/mol), %: C, 47.40; H, 3.83; N, 17.77; O, 6.76; Found, %: C, 47.07; H, 3.62; N, 17.57; O, 6.25. ESI-MS in MeOH (positive): m/z 620 $[\text{Ru}(\text{NO})(\text{OH})(\text{Hind})_4]^+$, 484 $[\text{Ru}(\text{Hind})_3]^+$, 310 $[\text{Ru}(\text{NO})(\text{OH})(\text{Hind})_4]^{2+}$. IR, $\tilde{\nu}$, cm^{-1} : 3354, 1879 (NO), 1657, 1585, 1512, 1474, 1441, 1378, 1358, 1334, 1272, 1242, 1151, 1126, 1081, 1003, 964, 830, 784, 746, 656, 619. UV-vis (H_2O), λ_{max} , nm (ϵ , $\text{M}^{-1} \text{cm}^{-1}$): 257 (99 175), 365 (53 287), 482 (22 994).

[*trans*-Dichlorotetrapyrazolruthenium(II)] (3). To a solution of **B** (0.5 g, 1.04 mmol) in MeOH (25 mL) a portion of NaBH_4 (0.07 g, 1.72 mmol) was slowly added. The solution became dark-red and a red solid precipitated. After addition of a second portion of NaBH_4 (0.07 g, 1.72 mmol) the solid became orange and the suspension was stirred for 1 h. The product was filtered off, washed with water (5 mL), methanol (5 mL) and diethyl ether (5 mL), and then dried in vacuo at r.t. Yield: 0.37 g, 80%. X-ray diffraction quality single crystals were grown in acetone/hexane (solvent/vapor diffusion). ^1H NMR in $\text{DMSO-}d_6$: 12.09 (s, 4NH), 7.59 (s, 4H), 7.27 (s, 4H), 6.16 (s, 4H). Elem. anal. Calc. for $\text{C}_{12}\text{H}_{16}\text{Cl}_2\text{N}_8\text{Ru}$ ($M_r = 444.28$ g/mol), %: C, 32.44; H, 3.63; N, 25.22; Found, %: C, 32.60; H, 3.32; N, 25.11. ESI-MS in MeOH (positive): m/z 444 $[\text{Ru}(\text{Cl})_2(\text{Hpz})_4]^+$, 408 $[\text{Ru}(\text{Cl})(\text{Hpz})_4]^+$, IR, $\tilde{\nu}$, cm^{-1} : 3287, 1512, 1462, 1404, 1349, 1115, 1038, 849, 757, 599. UV-vis (CH_2Cl_2), λ_{max} , nm (ϵ , $\text{M}^{-1} \text{cm}^{-1}$): 317 (17 656), 394 (35).

[*trans*-Hydroxidonitrosyltetrapyrazolruthenium(II)] (4). NaNO_2 (0.05 g, 0.72 mmol) was dissolved in H_2O (3 mL) and added to the mixture of **3** (0.11 g, 0.25 mmol) in acetone/ CH_2Cl_2 1:1 (25 mL). The solution was refluxed under argon for 12 h, and cooled to room temperature. The organic phase was separated in a separatory funnel and washed with water (3 x 15 mL). The solvent was removed in vacuo and the solid was dried in vacuo at r.t. The NMR spectra showed a mixture of products. A few crystals of **4** were collected from the mixture. Yield: 5 mg, 2%. X-ray diffraction quality single crystals were grown in methanol (slow evaporation). ^1H NMR in $\text{DMSO-}d_6$: 7.84 (d, 4H), 7.24 (d, 4H), 6.35 (t, 4H), ESI-MS in MeOH (positive): m/z

391 [Ru(OH)(Hpz)₄]⁺. IR, $\tilde{\nu}$, cm⁻¹: 3121 (OH), 1841 (NO), 1642, 1517, 1481, 1405, 1362, 1323, 1252, 1192, 1164, 1066, 1002, 952, 923, 856, 820, 752, 690, 657, 617, 568.

{[Ru(NO)(Hpz)(pz)₃(μ -OH)]₂Mg} (5). A solution of NaNO₂ (0.08 g, 1.10 mmol) and Mg(OH)₂ (0.05 g, 0.81 mmol) in H₂O (6 mL) was added to the mixture of **3** (0.27 g, 0.61 mmol) in acetone/CH₂Cl₂ 1:1 (60 ml). The solution was refluxed under stirring for 12 h, and cooled to room temperature. The organic phase was separated in a separatory funnel and washed with water (3 x 30 mL). The solvent was removed in vacuo and the remaining solid was dissolved in a small amount of MeOH (10 mL). The solution was kept in the fridge overnight. The red crystalline solid was filtered off, washed with acetone, ethanol and diethyl ether and dried in vacuo at r.t. Yield: 0.13 g, 25.0%. X-ray diffraction quality single crystals were grown in acetone/hexane (solvent/vapor diffusion). Elem. anal. Calc. for C₂₄H₂₈MgN₁₈O₄Ru₂(C₃H₆O)_{0.1} (*M_r* = 859.04 g/mol), %: C, 33.74; H, 3.33; N, 29.15; O, 7.58. Found, %: C, 33.55; H, 3.17; N, 28.83; O, 7.87. ESI-MS in MeOH (positive): *m/z* 860 ([Ru(NO)(Hpz)(pz)₃(μ -OH)]₂Mg)⁺. IR, $\tilde{\nu}$, cm⁻¹: 3597 (OH), 1847 (NO), 1483, 1409, 1381, 1352, 1274, 1160, 1050, 955, 874, 749, 673, 627, 568. UV-vis (CH₂Cl₂), λ_{\max} , nm (ϵ , M⁻¹ cm⁻¹): 231 (37 881), 497 (183).

trans-[Sulfonylnitrosyltetrapyrazolruthenium]sulfate (6). To a solution of **5** (0.03 g, 0.035 mmol) and [Bu₄N][BF₄] (0.16 g, 0.49 mmol) in nitrogen-flushed acetone (5 mL) a 1 M H₂SO₄ (0.5 mL) was slowly added with formation of an orange solid. After further addition of 1 M H₂SO₄ (0.5 mL) the solid dissolved, giving an orange solution. An electrolysis at 0 V was performed in order to reduce the compound. The solution was kept in fridge overnight. The orange crystals were filtered off, washed with cold acetone (5 mL) and diethyl ether (10 mL) and dried in vacuo at r.t. Yield: 0.015 g, 39.5%. X-ray diffraction quality single crystals were grown in acetone. ¹H NMR in DMSO-*d*₆: 8.05 (s, 4H), 7.52 (s, 4H), 6.52 (s, 4H). Elem. anal. calc. for C₁₂H₁₆N₉O₇RuS_{1.5}·(H₂O)_{4.5}·(CH₃COCH₃)_{0.8} (*M_r* = 675.01 g/mol), %: C, 25.62; H, 4.44; N, 18.67; S, 7.13. Found, %: C, 25.46; H, 3.97; N, 18.51; S, 7.54. ESI-MS in MeOH (positive): *m/z* 500 [Ru(NO)(SO₄)(Hpz)₄]⁺, 431 [Ru(NO)(SO₄)(Hpz)₃]⁺. IR, $\tilde{\nu}$, cm⁻¹: 3116 (OH), 1920 (NO), 1486, 1411, 1366, 1126, 1076, 1028, 955, 899, 769, 656, 602, 575. UV-vis (H₂O), λ_{\max} , nm (ϵ , M⁻¹ cm⁻¹): 213 (10 613), 442 (353).

3,5-Dimethylpyrazolium[decachlorido- μ -oxidoruthenate] (7). To a suspension of 3,5-dimethylpyrazole (5.6 g, 58.2 mmol) in 8 M HCl (4 mL) a “concentrated Kralik solution” (20 mL) of RuCl₃ (5.6 mmol) was added. The dark-red solution was stirred for 10 min at r.t. and then refluxed for 0.5 h. The mixture was cooled to room temperature. Red crystalline solid was filtered off, washed with ethanol (10 mL) and diethyl ether (10 mL) and dried in vacuo at r.t. Yield: 1.24 g, 23.0%. X-ray diffraction quality single crystals were selected from the reaction mixture. ¹H NMR in DMSO-*d*₆: 6.30 (s, 2H), 2.51 (m, 6H, *J* = 1.8 Hz). Elem. anal. Calc. for C₂₀H₃₆Cl₁₀N₈ORu (*M*_r = 961.22 g/mol), %: C, 24.99; H, 3.77; N, 11.66; O, 1.66; Cl, 36.88. Found, %: C, 24.97; H, 3.57; N, 11.49; Cl, 37.08. IR, $\tilde{\nu}$, cm⁻¹: 3118, 2958, 1598, 1524, 1384, 1273, 1155, 1013, 842, 691, 618. UV-vis (H₂O), λ_{\max} , nm (ϵ , M⁻¹ cm⁻¹): 258 (83 974), 372 (44 230), 483 (19 230).

[*trans*-Dinitrotetra-3,5-dimethylpyrazoleruthenium(II)] (8). To a solution of C (0.4 g, 0.68 mmol) in nitrogen-flushed acetone (30 mL) [Bu₄N][BF₄] (0.16 g, 0.49 mmol) was added. An electrolysis at -0.15 V was performed in order to reduce the compound. After electrolysis NaNO₂ (0.4 g, 5.79 mmol) in H₂O (8 mL) was added and the solution was stirred at r.t. overnight. The yellow precipitate was recrystallized from dichloromethane (diffusion of hexane) and the product washed with cold acetone, diethyl ether, and dried in vacuo at r.t. Yield: 0.22 g, 57%. X-ray diffraction quality single crystals were grown in acetone. ¹H NMR in DMSO-*d*₆: 12.70 (s, 4H), 5.93 (s, 4H), 2.25 (s, 12H), 1.26 (s, 12H). Elem. anal. Calc. for C₂₀H₃₂N₁₀O₄Ru·0.15(CH₂Cl₂) (*M*_r = 577.6 g/mol), %: C, 40.99; H, 5.52; N, 23.72; O, 10.84; Found, %: C, 41.07; H, 5.30; N, 23.38; O, 10.72. ESI-MS in MeOH (positive): *m/z* 601 {[Ru(NO₂)₂(3,5Dimepz)₄]Na⁺}⁺. IR, $\tilde{\nu}$, cm⁻¹: 3127 (NO), 1571, 1326, 1262, 1171, 1026, 810, 667, 605. UV-vis (CH₂Cl₂), λ_{\max} , nm (ϵ , M⁻¹ cm⁻¹): 231 (448), 281 (128), 398 (48).

***trans*-[Chloronitrosyltetra-3,5-dimethylpyrazolruthenium]chloride (9).** To a suspension of **8** (0.1 g, 0.17 mmol) in MeOH (3 mL) 3 M HCl (1.5 mL) was added. The mixture was refluxed under argon at 65 °C for 40 min, and cooled to room temperature. Then the dark-orange solution was filtered and the solvent was removed in vacuo. The solid was dissolved in acetone (2 mL) and kept in a fridge

overnight. The pink crystalline solid was filtered off, washed with cold water and diethyl ether, and dried in vacuo at r.t. Yield: 0.065 g, 70%. X-ray diffraction quality single crystals were grown in acetone. ^1H NMR in $\text{DMSO-}d_6$: 12.70 (s, 4H), 5.93 (s, 4H), 2.25 (s, 12H), 1.26 (s, 12H). Elem. anal. Calc. for $\text{C}_{20}\text{H}_{32}\text{Cl}_2\text{N}_9\text{ORu}\cdot 2,7\text{H}_2\text{O}$ ($M_r = 670.6$ g/mol), %: C, 35.82; H, 5.62; N, 18.79; Found, %: C, 35.87; H, 5.36; N, 18.60. ESI-MS in MeOH (positive): m/z 550 $[\text{Ru}(\text{NO})\text{Cl}(\text{3,5Dimepz})_4]^+$, 454 $[\text{Ru}(\text{NO})\text{Cl}(\text{3,5Dimepz})_3]^+$, 358 $[\text{Ru}(\text{NO})\text{Cl}(\text{3,5Dimepz})_2]^+$, 275 and $[\text{Ru}(\text{NO})\text{Cl}(\text{3,5Dimepz})_4]^{2+}$. IR, $\tilde{\nu}$, cm^{-1} : 1888 (NO), 1632, 1572, 1406, 1373, 1277, 1177, 1148, 1065, 1024, 985, 818, 696, 654. UV-vis (H_2O), λ_{max} , nm (ϵ , $\text{M}^{-1} \text{cm}^{-1}$): 218 (83 974), 506 (228).

***trans*-[Dyroxidonorosyltetrapyrazolruthenium][hexaaquamagnesium]disulfate (10).** To a solution of **5** (0.03 g, 0.035 mmol) in acetone (5 mL) a 1 M H_2SO_4 (0.5 mL) was slowly added with formation of an orange solid, which was filtered off immediately and washed with acetone. The crude product was recrystallized from acetone/isopropanol 1:1 (5 mL). Red crystals were filtered off, washed with diethyl ether (10 mL) and dried in vacuo at r.t. Yield: 0.014 g, 79.0%. X-ray diffraction quality single crystals were grown in acetone. ^1H NMR in $\text{DMSO-}d_6$: 8.01 (s, 2H), 7.75 (s, 2H), 7.47 (s, 2H), 7.11 (s, 2H), 6.50 (s, 2H), 6.28 (s, 2H). Elem. anal. calc. for $\text{C}_{12}\text{H}_{29}\text{MgN}_9\text{O}_{15}\text{RuS}_2$ ($M_r = 728.9$ g/mol), %: C, 19.77; H, 4.01; N, 17.29; S, 8.79; O, 32.92. Found, %: C, 20.54; H, 3.48; N, 17.31; S, 9.25; O, 32.48. ESI-MS in MeOH (positive): m/z 421 $[\text{Ru}(\text{NO})(\text{OH})(\text{Hpz})_4]^+$. IR, $\tilde{\nu}$, cm^{-1} : 3129 (OH), 1878 (NO), 1548, 1476, 1411, 1361, 1132, 1058, 951, 857, 767, 568.

***trans*-[chloronorosyltetrapyrazolruthenium]chloride (11).** To a solution of **5** (0.05 g, 0.06 mmol) in acetone (5 mL) a 1 M HCl (2 mL) was slowly added. The solution changed color from pink to orange. The solvent was removed in vacuo and the remaining solid was dissolved in a small amount of MeOH (2 mL). The crude product was purified on sephadex column chromatography with MeOH as a solvent. The solvent was evaporated to a small volume, orange solid was filtered off, washed with diethyl ether (10 mL) and dried in vacuo at r.t. Yield: 0.03 g, 36.0%. ^1H NMR in $\text{DMSO-}d_6$: 8.17 (d, 4H, $J = 2.7$ Hz), 7.70 (s, 4H), 6.61 (t, 4H, $J = 2.5$ Hz). Elem. anal. calc. for $\text{C}_{12}\text{H}_{16}\text{Cl}_3\text{N}_9\text{Ru}\cdot 2,6\text{H}_2\text{O}$ ($M_r = 556.6$ g/mol), %: C, 25.90; H, 3.84; N, 22.65; O, 10.35. Found, %: C, 26.16; H, 3.55; N, 22.66; O, 10.57. ESI-MS in MeOH

(positive): m/z 420 $[\text{Ru}(\text{NO})(\text{OH})(\text{Hpz})_4]^+$, 370 $[\text{Ru}(\text{NO})(\text{Cl})(\text{Hpz})_3]^+$, 352 $[\text{Ru}(\text{NO})(\text{OH})(\text{Hpz})_3]^+$. IR, $\tilde{\nu}$, cm^{-1} : 3089 (OH), 2864, 1875 (NO), 1637, 1537, 1477, 1408, 1363, 1283, 1141, 1066, 949, 884, 761, 605. UV-vis (H_2O), λ_{max} , nm (ϵ , $\text{M}^{-1} \text{cm}^{-1}$): 213 (10 613), 442 (229).

[*trans*-chloronitrosyltetraindazolruthenium]chloride (12). To a suspension of **1** (0.17 g, 0.25 mmol) in MeOH (30 mL) a conc. HCl (2.5 ml) was added. The mixture was refluxed under argon for 1 h, and cooled to room temperature. Then the dark-orange solution was filtered and the volume was reduced to ca. 3 mL. The precipitate was filtered off. The product was recrystallized from isopropanol (40 mL), washed with diethyl ether (10 mL) and dried in vacuo at r.t. Yield: 0.85 g, 52%. ^1H NMR in $\text{DMSO}-d_6$: 14.44 (s, 4NH), 8.48 (s, 4H), 7.91 (d, 4H, $J = 8.8$ Hz), 7.66 (d, 4H, $J = 8.8$ Hz), 7.61 (s, 4H), 7.33 (s, 4H). Elem. anal. Calc. for $\text{C}_{28}\text{H}_{24}\text{Cl}_3\text{N}_9\text{ORu}\cdot 1.5\text{H}_2\text{O}$ ($M_r = 737.00$ g/mol), %: C, 45.63; H, 3.69; N, 17.10. Found, %: C, 45.54; H, 3.35; N, 17.09. ESI-MS in MeOH (positive): m/z 638 $[\text{Ru}(\text{NO})(\text{OH})(\text{Hind})_4]^+$, 520 $[\text{Ru}(\text{NO})(\text{Hind})_3]^+$, 402 $[\text{Ru}(\text{NO})(\text{Cl})(\text{Hind})_2]^+$. IR, $\tilde{\nu}$, cm^{-1} : 2658, 1925 (NO), 1629, 1584, 1515, 1476, 1439, 1359, 1335, 1288, 1239, 1146, 1088, 999, 966, 902, 840, 783, 737, 614. UV-vis (H_2O), λ_{max} , nm (ϵ , $\text{M}^{-1} \text{cm}^{-1}$): 257 (99 175), 365 (53 287), 482 (22 994).

Physical Measurements. IR spectroscopy, and ESI mass spectroscopy measurements were carried out as described previously.³ Elemental analyses were performed by the Microanalytical Service of the Faculty of Chemistry of the University of Vienna. IR spectra were measured by using an ATR unit with a Perkin-Elmer 370 FTIR 2000 instrument (4000–400 cm^{-1}). UV-vis spectra were recorded on a Perkin-Elmer Lambda 20 UV-vis spectrophotometer using samples dissolved in water, methanol or dichloromethane. The ^1H NMR spectra were recorded at 400.13 MHz on a Bruker DPX400 and at 500.32 MHz on a Bruker DPX500. Chemical shifts for ^1H were referenced to residual ^1H present in deuterated dimethyl sulfoxide. Electrospray ionization mass spectrometry was carried out with a Bruker Esquire3000 instrument (Bruker Daltonics, Bremen, Germany) by using methanol as solvent.

Electrochemistry. The electrochemical measurements were carried out as reported previously.³ Cyclic voltammetry measurements were performed at room temperature using an AMEL 7050 all-in one potentiostat. For a cyclic voltammetry (CV) a 3 mm

GC (glassy carbon electrode) working electrode, a Pt auxiliary electrode and a SCE (saturated calomel electrode) reference electrode were used. The compartment of auxiliary electrode was separated from the compartment. Same electrodes were used for coulometry. The potentials were measured in 0.1 M [*n*-Bu₄N][BF₄]/ in acetone or CH₂Cl₂ using [Fe(*η*⁵-C₅H₅)₂] (*E*_{1/2}) +0.53 V or +0.58 V vs NHE in acetone or CH₂Cl₂, respectively) as internal standards. The concentrations amounted 1.5–2.5 mM. The redox potentials were first examined by CV to confirm the reversibility of each couple. The single-electron transfer for the Ru^{III}/Ru^{II} redox couple has been confirmed by coulometric measurements (consumption of one mol equiv. of electrons). The ferrocene was measured at the end of the experiment after electrolysis.

Crystallographic Structure determination. X-ray diffraction measurements of ruthenium complexes were performed on a Bruker X8 APEXII CCD and Bruker D8 Venture diffractometer both equipped with Cryoflex I (X8) and II (D8) cooler device and on an Oxford-Diffraction XCALIBUR equipped with an Oxford Cryosystem cooler device. Measured frames, exposure time and detector distance for the compounds **1-5**, **7** and **10** are shown in Table 1. The single crystals of the compounds **6**, **8** and **9** were positioned at 65 mm from detector. The compounds were measured over 1° or 2°, 0.5°, 0.25° scan width.

Table 1. Collected frames, exposure time and detector distance for **1-5**, **7** and **10**.

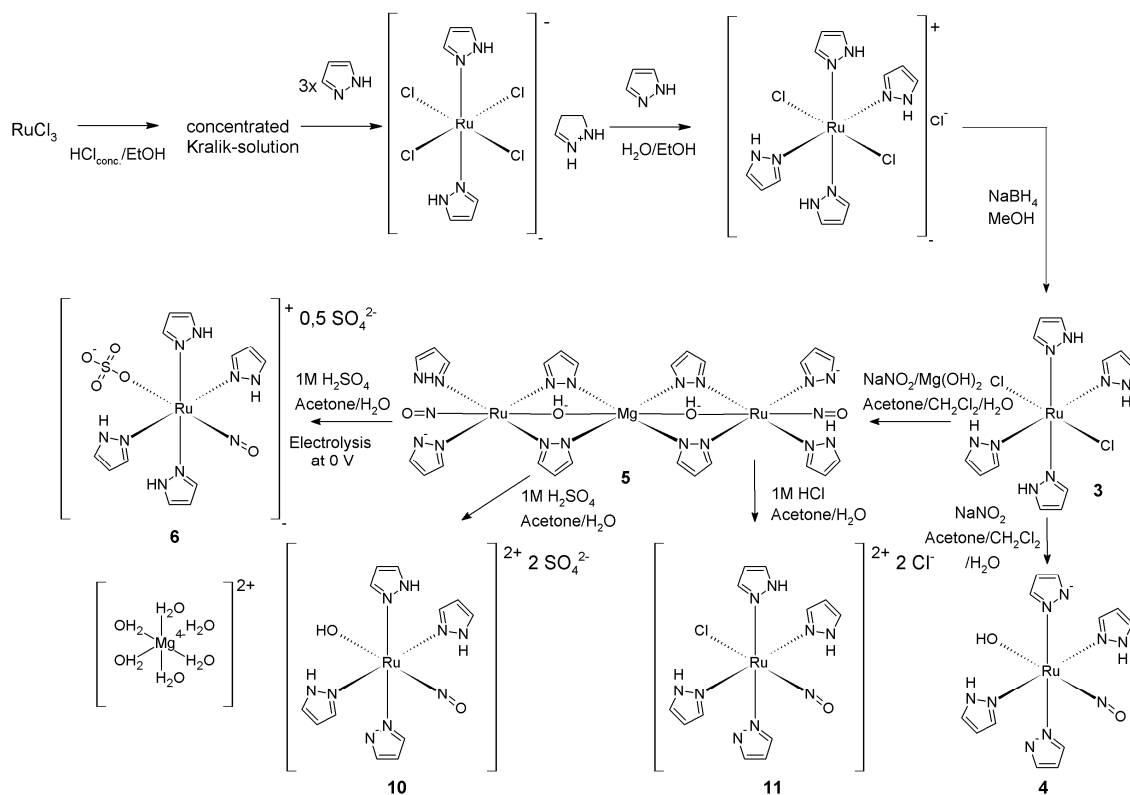
compound	frames	exposure time (s)	detector distance (mm)
1	763	30	35
2	1872	2	40
3	541	40	40
4	350	60	40
5	367	60	40
7	1640	20	40
10	879	15	50

The data for ruthenium complexes were processed using SAINT software and the CrysAlis RED package. The structures were solved by direct methods and refined by full-matrix least-squares techniques. All non-hydrogen atoms were refined with

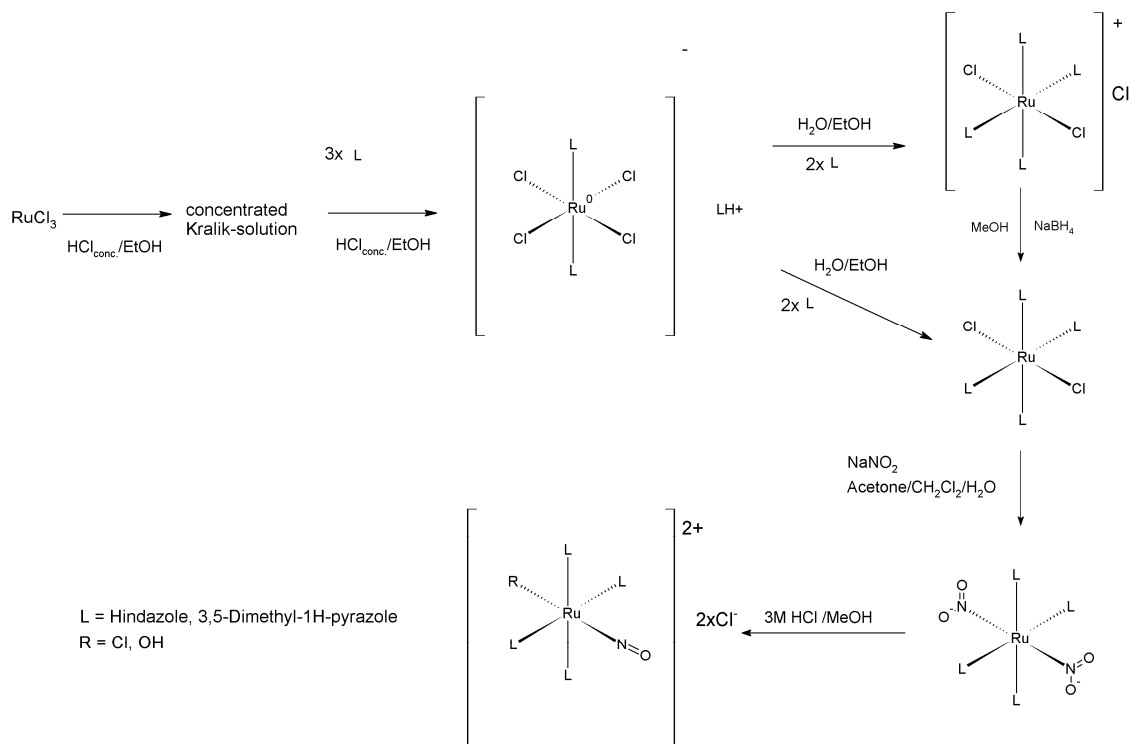
anisotropic displacement parameters. H atoms were inserted in calculated positions and refined with a riding model. The following software programs and computer were used structure solution, SHELXS-97^{4,5}; refinement, SHELXL-97 molecular diagrams, ORTEP-3⁶, Intel CoreDuo. Drawings were made with ORTEP.^{7,8}

Results and discussion

Synthesis and Characterisation of Ruthenium Complexes. The ruthenium nitro complex **1** was prepared in a two phase liquid-liquid system by reacting **A** in acetone/CH₂Cl₂ with NaNO₂ dissolved in water under reflux for 12 h. The following nitrosyl complex **2** was obtained in 62% yield by reaction of the **1** with 3 M HCl under reflux for 40 min. Similar complex **12** with Cl⁻ ligand instead of the OH⁻ was obtained using conc. HCl. The ruthenium nitrosyl complex **5** was prepared in a similar way as complex **1** using reduced complex **3** with addition of Mg(OH)₂ to reaction mixture. In the absence of Mg(OH)₂ the reaction led to a mixture of products and the complex **4** crystallized from this mixture. The starting compound **3** for the synthesis of **4** and **5** was obtained by reduction of **B** with NaBH₄ in methanol. The reaction of **5** with H₂SO₄ in acetone led to complexes **6** (after controlled electrolysis) and **10**. Using HCl instead of H₂SO₄ led to the complex **11**. For the preparation of the complex **8** compound **C** was reduced electrochemically at -0.15 V. To the in situ generated complex *trans*-[RuCl₂(3,5-dimepz)₄] in acetone, NaNO₂ was added and the mixture was stirred under argon at R.T. for 12 h leading to the nitro complex **8** with a good yield of 57%. The nitrosyl complex **9** was prepared in the same way as **2** using the nitro complex **8**. Complex **7** was prepared by addition of the 'concentrated Kralik solution' to 3,5-dimethylpyrazole in 8 M HCl and heating for 30 min. The synthesis of pyrazole complexes **3-6**, **10** and **11** is shown in Scheme 1. The general overview of the synthesis pathway leading to the complexes **1**, **2**, **8**, **9** and **12** is shown in Scheme 2.



Scheme 1. General overview of reaction pathway leading to complexes **3-6**, **10**, **11**.



Scheme 2. General overview of reaction pathway leading to complexes **1**, **2**, **8**, **9**, **12**.

ESI-MS. The formation of complexes was confirmed by electrospray ionisation mass spectra (ESI-MS, positive mode) in methanol or acetonitrile. Nitro complex **1** showed peaks with m/z values of 665, 647, 556 and 541. The signal with m/z value of 665 may be assigned to $[\text{Ru}(\text{NO}_2)_2(\text{Hind})_4]^-$, whereas the other signals could not be assigned. The other nitro complex **8** showed peak with m/z 601 assigned to $\{[\text{Ru}(\text{NO}_2)_2(3,5\text{Dimepz})_4]\text{Na}^+\}^+$. The nitrosyl compound **5** displayed a strong peak at m/z 860 corresponding to $\{[\text{Ru}(\text{NO})(\text{Hpz})(\text{pz})_3(\mu\text{-OH})]_2\text{Mg}\}^+$ and the sulfonyl-nitrosyl complex showed a peak at m/z 501 corresponding to $[\text{Ru}(\text{SO}_4)(\text{NO})(\text{pz})_4]^+$. The nitrosyl complex **9** with 3,5-dimethylpyrazole fragmented in ESI-MS with formation of ions $[\text{Ru}(\text{NO})\text{Cl}(3,5\text{Dimepz})_4]^+$, $[\text{Ru}(\text{NO})\text{Cl}(3,5\text{Dimepz})_3]^+$, $[\text{Ru}(\text{NO})\text{Cl}(3,5\text{Dimepz})_2]^+$ and $[\text{Ru}(\text{NO})\text{Cl}(3,5\text{Dimepz})_4]^{2+}$, with m/z values 550, 454, 358 and 275, respectively. **10** showed a peak at m/z 421 corresponding to $[\text{Ru}(\text{OH})(\text{NO})(\text{pz})_4]^+$. Complex **2** showed a signal with m/z 620, 484 and 310, which can be assigned to the $[\text{Ru}(\text{NO})(\text{OH})(\text{Hind})_4]^+$, $[\text{Ru}(\text{NO})(\text{OH})(\text{Hind})_3]^+$ and $[\text{Ru}(\text{NO})(\text{OH})(\text{Hind})_2]^+$, respectively. **12** displayed signals with m/z 638, 520 and 402, which can be assigned to the $[\text{Ru}(\text{NO})(\text{OH})(\text{Hind})_4]^+$, $[\text{Ru}(\text{NO})(\text{Hind})_3]^+$ and $[\text{Ru}(\text{NO})(\text{OH})(\text{Hind})_4]^{2+}$, respectively. MS evidence for the the formation of the complex **7** has not be obtained because of the high ion charge (4+) of the complex, which gives a mass peak with the m/z value of 146. In this region it is very difficult to detect a good signal.

Both nitro complexes **1** and **8** are poorly soluble in water and methanol and very good soluble in DMSO and CH_2Cl_2 . The neutral character of ruthenium(II) complexes also explains a poor solubility of complex **3** in solvents like water and methanol. Poor solubility in water makes those complexes unsuitable for the cytotoxicity tests in cancer cell lines. All of the synthesized nitrosyl complexes except **5** are soluble in water. The complex **5** with three metal centers, two nitrosyl and the hydroxyl groups is poorly soluble in water. The complex **7** shows very good aqueous solubility (50 mg/mL).

UV-vis spectroscopy. Stability of complexes in water was investigated by UV-vis measurements over time. For the complex **2** the stability under light irradiation was studied. Complex is stable in water and methanol in the absence of light irradiation. After light irradiation the complex undergoes solvolysis (Figure 1).

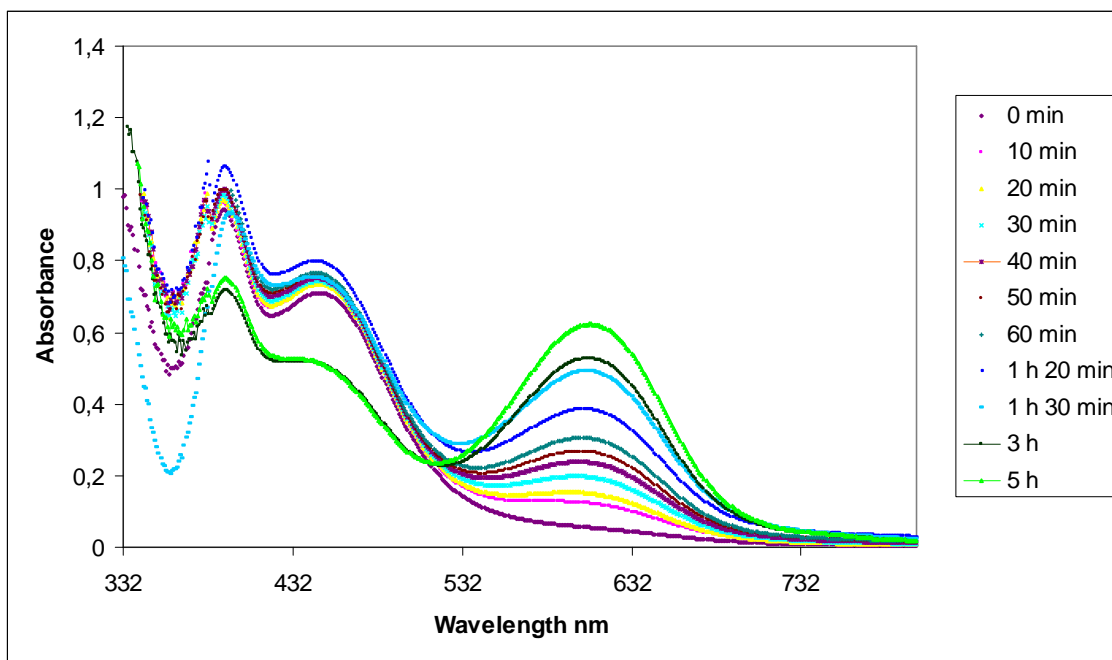


Figure 1. Solvolysis of *trans*-[Ru(OH)(NO)(Hind)₄]Cl₂ (**2**) in MeOH under light irradiation.

At the beginning only the bands at 390 and 443 nm are present. After 10 min of light irradiation a new band at 606 nm appeared and the absorbance of this wave is continuously growing with the time. This phenomenon could be explained with the change of the ligand. The bond between NO and Ru could be broken and the NO exchanged with OH. The process results in change of the color of the solution from orange to blue.

The complex **7** has also shown interesting properties. At pH values < 7 the complex is stable and no change in UV-vis spectra was observed. At pH 7 the complex undergoes changes and strong band at 480 nm disappeared over time (Figure 2). After 24 h the absorbance at 480 nm disappeared completely and a new band at 637 nm appeared. A possible reason for this behavior is hydrolysis of the complex.

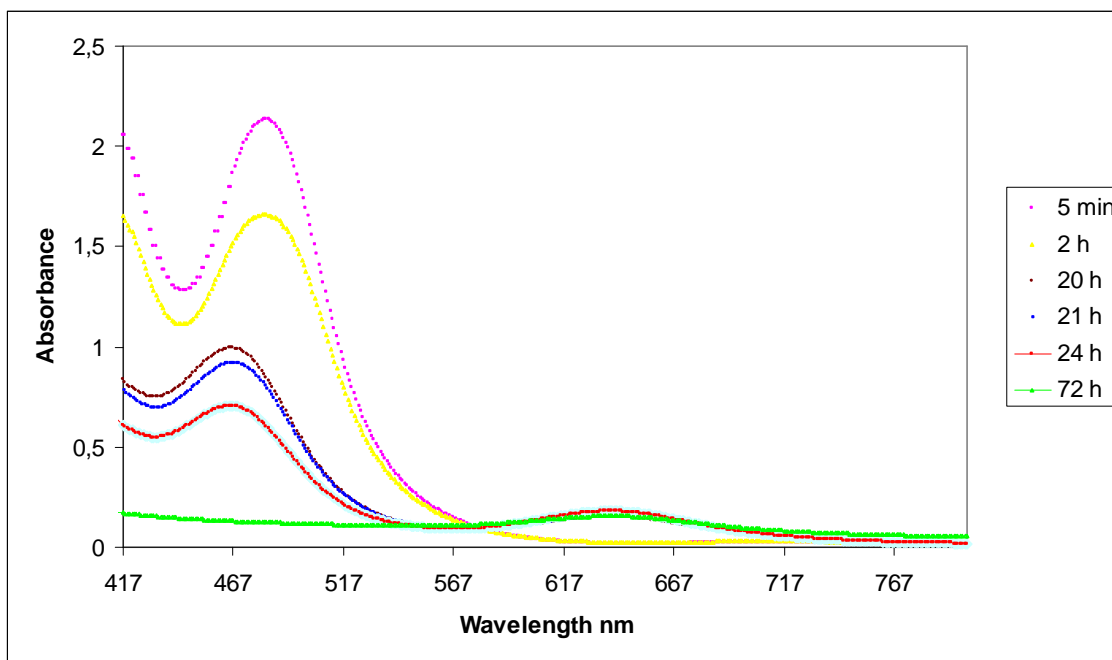


Figure 2. Time dependent UV-vis spectra of $[\text{Ru}_2\text{Cl}_5\text{O}](3,5\text{-dimepz})_4$ (**7**) in water.

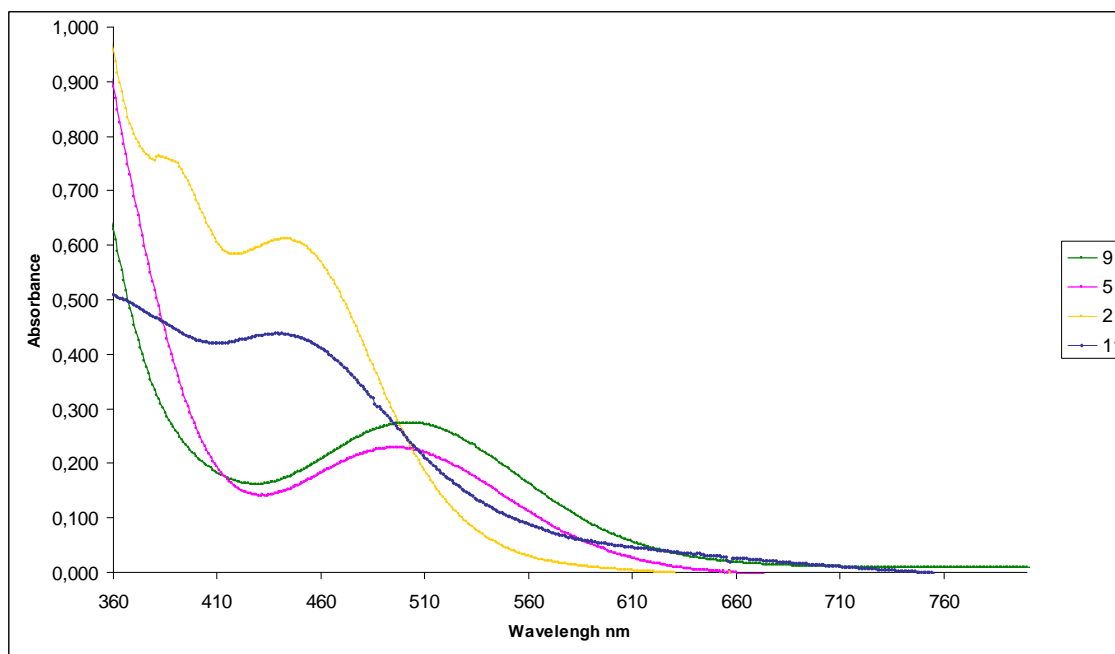


Figure 3. UV-vis spectra of the complexes $\text{trans-}[\text{RuCl}(3,5\text{-dimepz})_4(\text{NO})]\text{Cl}_2$ (**9**) $\{[\text{Ru}(\text{NO})(\text{Hpz})(\text{pz})_3(\mu\text{-OH})]_2\text{Mg}\}$ (**5**) $\text{trans-}[\text{Ru}(\text{OH})(\text{NO})(\text{Hind})_4]\text{Cl}_2$ (**2**) and $\text{trans-}[\text{Ru}(\text{Cl})(\text{NO})(\text{Hpz})_4]\text{Cl}_2$ (**11**) showing the d-d transitions.

The intensive colors of the nitrosyl complexes result from the d-d transitions in visible region of the UV-vis spectra. The absorption bands assigned to d-d transitions are

shown in Figure 3. Complexes **5** and **9** display absorption bands around 500 nm and have both pink color. Complexes **2**, **6** and **11** are orange and absorb at 482 (**2**) and 442 nm (**6**, **11**).

¹H NMR Spectroscopy. The measured ¹H NMR spectra of the compounds indicate S = 0 ground state. The lack of unusual shift and line broadening characteristic for paramagnetic complexes indicates a diamagnetic character of the ruthenium complexes. Only in case of complex **7** confirmation of ground state was not possible because only the counterion has protons. The ¹H NMR spectra display the same signal sets for metal-free and coordinated azoles. The spectra of **2** show signals at 14.27 ppm (s, 4NH), the signal at 8.56 ppm assigned to the neighboring proton (s, 4H) and four signals from aromatic protons 7.89 ppm (d, 4H, J = 8.5 Hz), 7.66 ppm (d, 4H, J = 8.5 Hz), 7.56 ppm (t, 4H, J = 7.5 Hz) and 7.29 ppm (t, 4H, J = 7.5 Hz). Figure 4 shows changes in the ¹H NMR spectra during the synthesis of **2**. The starting compound H₂ind[*trans*-Ru(NO)₂(Hind)₂] shows signals from the counterion H₂ind⁺ between 7 and 8.5 ppm and upfield signals from coordinated indazole at 4.45, -5.84 and -10.88 ppm. The other three complexes, namely *trans*-[RuCl₂(Hind)₄] (**A**), *trans*-[Ru(NO₂)₂(Hind)₄]Cl₂ (**1**) and *trans*-[Ru(OH)(NO)(Hind)₄]Cl₂ (**2**) are all diamagnetic and the coordinated indazole ligands display signals in lower field region. The proton signal shifts after substitution of NO₂ and further after reduction to NO are obvious in case of the proton bound to the nitrogen. The signal of this proton is upfield shifted.

The ¹H NMR spectra of the nitrosyl compounds **2**, **4**, **6** and **7** suggest the proposed diamagnetic {M(NO)}⁶ configuration of the Ru-(NO) entity.

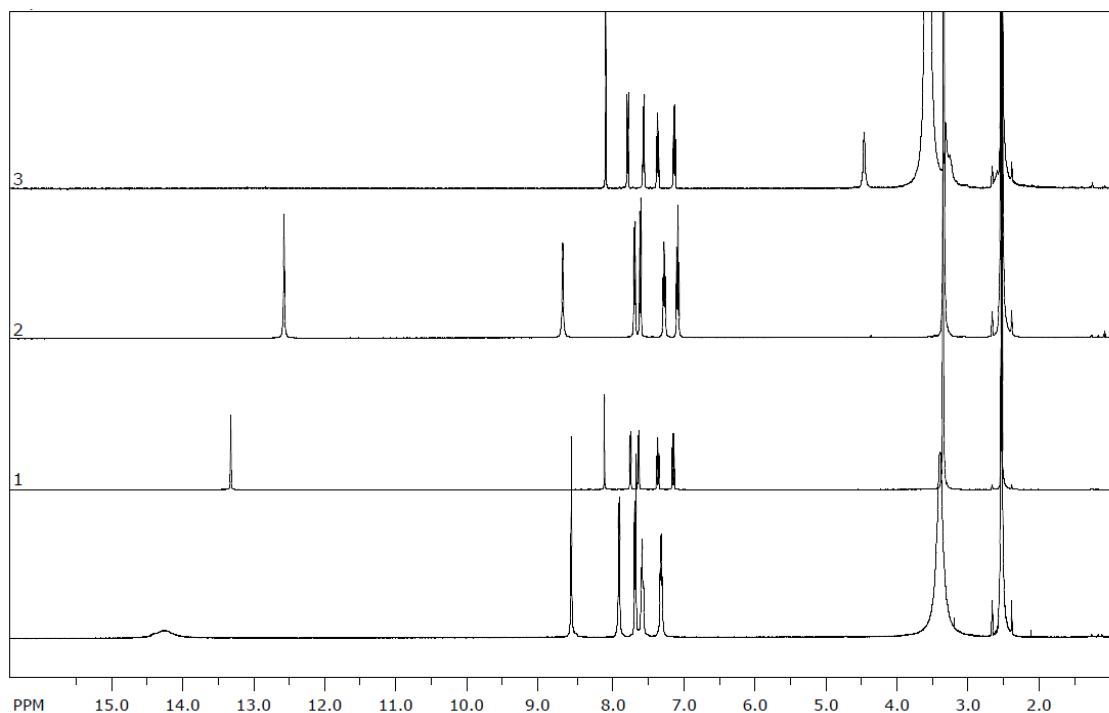


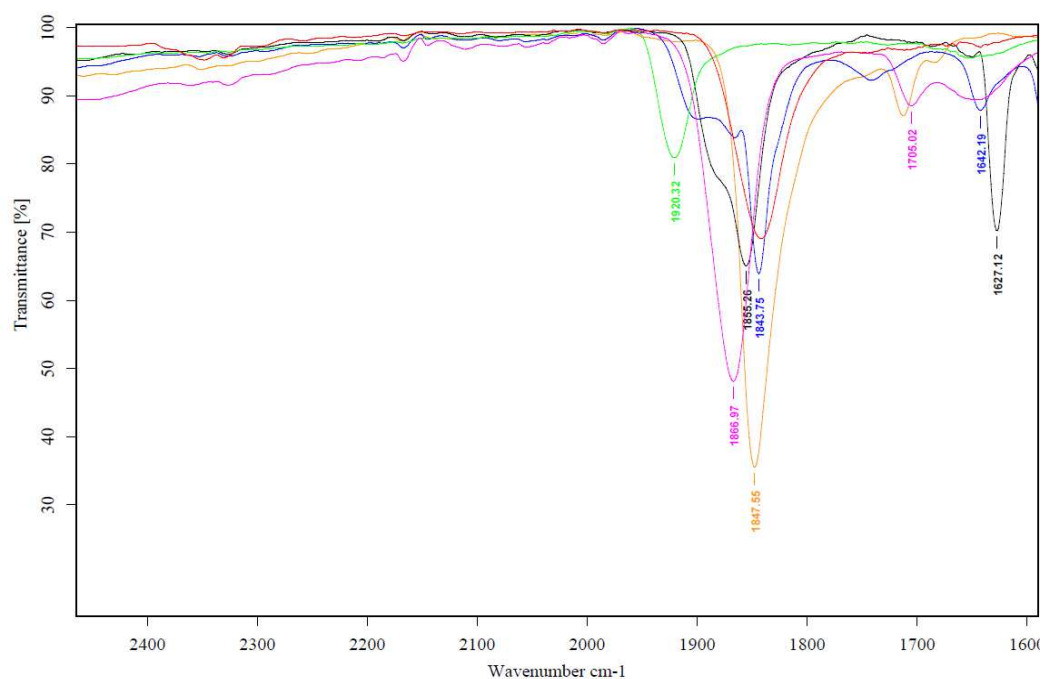
Figure 4 ^1H NMR spectra (from the top) of $\text{Hind}[\text{trans-RuCl}_4(\text{Hind})_2]$, $\text{trans}[\text{RuCl}_2(\text{Hind})_4]$ (**A**), $\text{trans}[\text{Ru}(\text{NO}_2)_2(\text{Hind})_4]$ (**1**) and $\text{trans}[\text{Ru}(\text{OH})(\text{NO})(\text{Hind})_4]\text{Cl}_2$ (**2**).

IR spectroscopy. The infrared spectra of the two nitro complexes were not easy to interpret. Three typical bands should occur for the metal-nitro complex, a symmetric (ν_s) and an asymmetric stretching (ν_{as}), along with a bending vibration ($\delta\nu$)⁹. Complex **1** displays a peak centered around 1354 cm^{-1} , which is typical for a symmetric NO_2 stretch (ν_s), while that at 1225 cm^{-1} is typical for an asymmetric NO_2 stretch (ν_{as}). The peaks at 830 cm^{-1} and 736 cm^{-1} are assigned to ONO scissoring modes. The second nitro complex shows a symmetric NO_2 stretch (ν_s) at 1262 cm^{-1} and an asymmetric NO_2 stretch (ν_{as}) at 1025 cm^{-1} . The ONO scissoring modes occur at 810 cm^{-1} and 667 cm^{-1} .

IR spectroscopy was a very important method for the characterization of ruthenium-nitrosyl compounds. A very intense NO stretching vibration in the region between 1826 cm^{-1} and 1925 cm^{-1} was observed for the complexes **2**, **4**, **5**, **6**, **9**, **12**. Those wavenumbers indicate the nitrosonium or nitrosyl character of the NO ligand.¹⁰ NO^+ shows stretching vibration at 2377 cm^{-1} .¹¹ The characteristic vibration bands for each complex are shown in Table 2 and in Figure 5.

Table 2. Data for the $\nu_{\text{NO}}(\text{cm}^{-1})$ of nitrosyl compounds

complex	$\nu_{\text{NO}}(\text{cm}^{-1})$
<i>trans</i> -[Ru(OH)(NO)(Hind) ₄]Cl ₂ (2)	1855
<i>trans</i> -[RuCl(3,5-dimepz) ₄ (NO)]Cl ₂ (9)	1888
<i>trans</i> -[Ru(SO ₄)(NO)(Hpz) ₄](SO ₄) _{0,5} (6)	1920
{[Ru(NO)(Hpz)(pz) ₃ (μ -OH)] ₂ Mg} (5)	1847
<i>trans</i> -[Ru(OH)(NO)(Hpz) ₄] (4)	1841
<i>trans</i> -[Ru(OH)(NO)(Hind) ₄]Cl ₂ (2)	1925

**Figure 5.** The $\nu_{\text{NO}}(\text{cm}^{-1})$ stretching bands of nitrosyl compounds **2** (black), **4** (red), **5** (orange), **6** (green), **9** (blue) and **10** (pink).

X-ray Crystallography. The results of X-ray diffraction study of the nitro compounds **1** and **8** are shown in Figure 6. Selected bond lengths and angles are shown in Table 3. The complexes **1** and **8** crystallized in the monoclinic space group *C2/c* and orthorhombic space group *Pbcn*, respectively. The ruthenium(II) center is six-coordinate, and as expected, four indazole and four 3,5-dimethylpyrazole ligands are bound to the metal via nitrogen atoms in equatorial positions and two nitro groups in axial positions. The Ru-N5 of 2.108(2) Å (**1**) and 2.049(4) Å (**2**) are typical for other ruthenium-nitro complexes.^{12,13,14} The Ru-N1 of 2.071(2) Å (**1**) and 2.094(3) Å (**8**) in **1**

and **8** are similar with those of other ruthenium indazole and 3,5-dimethylpyrazole complexes.^{1,2} The coordination geometry can be described as octahedral.

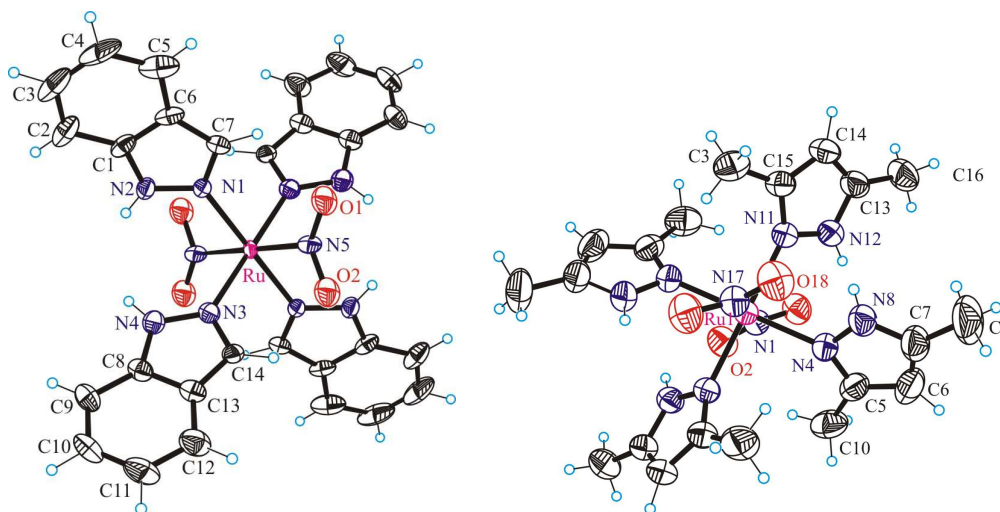


Figure 6. ORTEP view of one independent molecule of *trans*-[Ru(NO₂)₂(Hind)₄] (**1**) (left) and *trans*-[Ru(NO₂)₂(3,5-1H-pz)₄] (**8**) (right), showing the atom-numbering scheme. Thermal displacement ellipsoids are drawn at the 50% probability level.

For all of the nitrosyl complexes the linear coordination of NO to Ru was observed. The shortest distance Ru-NO was observed for *trans*-[Ru(NO)₂(Hind)₄]Cl₂ (**2**) with 1.702(11) Å and the longest for *trans*-[RuCl(3,5-dimepz)₄(NO)]Cl₂ (**9**) with 1.751(7) Å. The N-O bond was for all nitrosyl complexes similar and same distances were observed for other ruthenium-nitrosyl complexes.^{15,16,17} The distance between Ru and N from azole heterocycle was typical for coordination of azole.¹ All ruthenium-nitrosyl compounds have octahedral coordination geometry.

Table 3. Selected Bond Distances (Å) and Angles (deg) for **1, 2, 5, 6, 8, 9**.

	1	8	2	9	5	6
Ru-NO	-	-	1.702(11)	1.751(7)	1.743(2)	1.743(4)
Ru-NO ₂	2.108(2)	2.049(4)	-	-	-	-
Ru-N(azole)	2.071(2)	2.094(3)	2.078(3)	2.093(3)	2.077(2)	2.082(4)
N-O	1.139(7)	1.249(3)	1.364(12)	1.132(10)	1.153(3)	1.123(6)
Ru-N-O	122.13	122.1	171.0	179.99	176.13	174.68

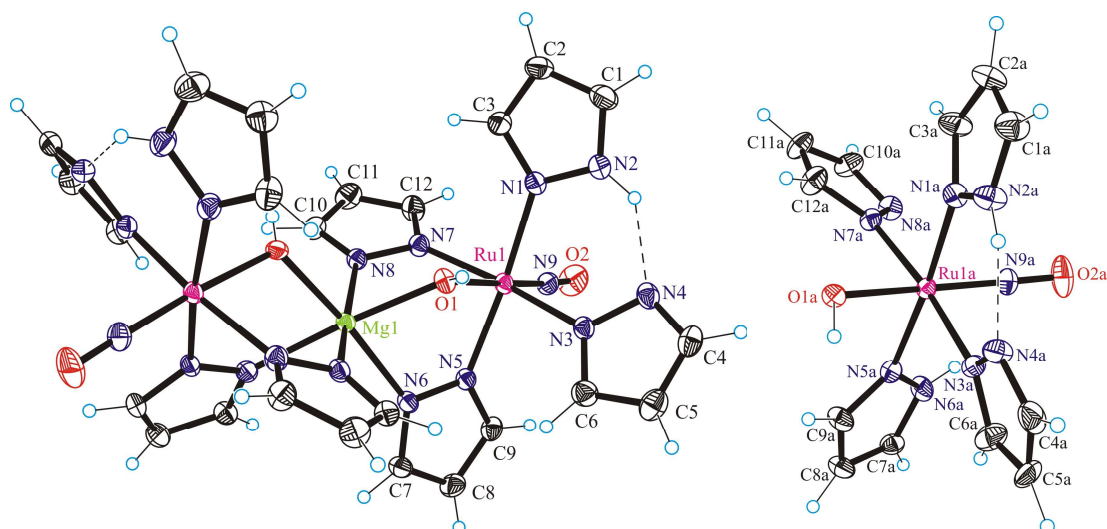


Figure 7. ORTEP view of the first independent molecule of $\{[\text{Ru}(\text{NO})(\text{Hpz})(\text{pz})_3(\mu\text{-OH})_2\text{Mg}]\}$ (**5**) (left) and $[\text{Ru}(\text{OH})(\text{NO})(\text{Hpz})_4]$ (**4**) (right) showing the atom-numbering scheme. Thermal displacement ellipsoids are drawn at the 50% probability level.

The results of X-ray diffraction studies of **5** showed a trinuclear complex with two Ru and one Mg center (Figure 7). The Ru-O1 and Mg-O1 distances are of 1.9629(16) Å and 2.0490(17) Å whereas the separation Mg-Ru is of 3.3886(3) Å. The Ru-O1 in mononuclear complex (**4**) is 1.952(3) Å. The complexes **4** and **5** crystallized in the monoclinic space group $C2/c$ and $P2_1/c$, respectively. The angle Ru-O-Mg is of 115.25°. The lack of counterion indicates deprotonation of nitrogen. Intramolecular hydrogen bonding between N2 and N4 are evident ($\text{N4}\cdots\text{H20}$ 1.882 Å).

Another compound with pyrazole ligands (**6**) crystallized also in the monoclinic space group $C2/c$ with Ru-O1 of 1.990(3) Å and O1-S1 of 1.453(3), respectively. Intramolecular hydrogen bonding between O from sulfate and H from pyrazole ($\text{O}\cdots\text{H}$ 1.909 Å, $\text{O}\cdots\text{H}$ 2.054 Å) stabilizes the position of the ligand. The refinement showed one sulfate counterion pro two complex ions (Figure 8).

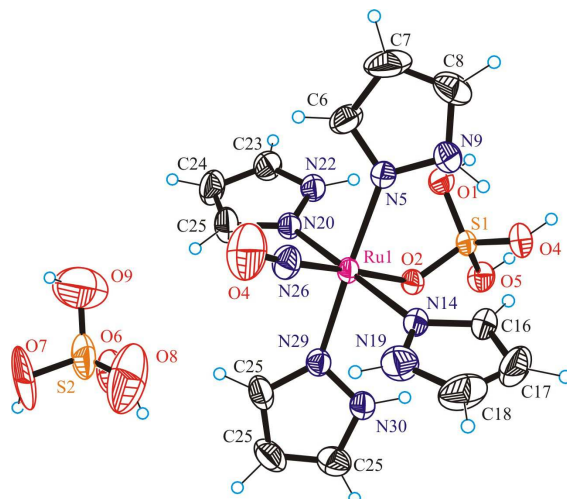


Figure 8. ORTEP view of the crystallographically independent molecule of *trans*-[Ru(SO₄)(NO)(Hpz)₄](SO₄)_{0.5} (**6**) showing the atom-numbering scheme. Thermal displacement ellipsoids are drawn at the 50% probability level.

The structure of **9** is shown in Figure 9. **9** crystallized in the tetragonal space group *P4/n*. The N1-Ru-N21 angle is 92.17° whereas the angle N1-Ru-Cl is of 87.19°. This deviation from the ideal octahedral coordination with 90° can be explained with the steric influence of the methyl groups of 3,5-dimethylpyrazole. Four azole ligands are bound to ruthenium in the equatorial plane, while one NO molecule and one Cl⁻ ligand occupy two axial positions. The structure consists of complex cations, two chloride anions and co-crystallized water molecules. The Ru-Cl bond of 2.139(2) Å is typical for other ruthenium nitrosyl compounds.

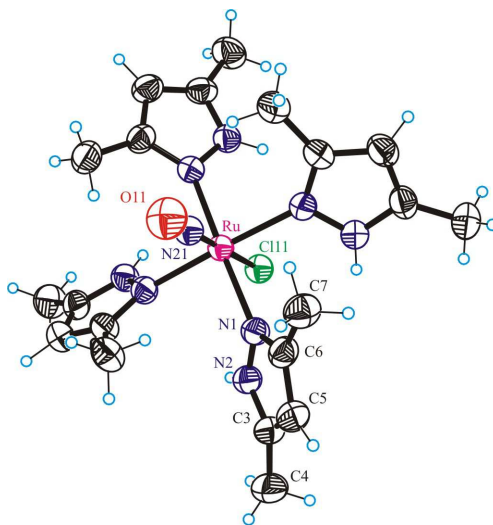


Figure 9. ORTEP view of one crystallographically independent cation of *trans*-[Ru(3,5dimepz)₄(NO)]Cl (**9**), showing the atom-numbering scheme. Thermal displacement ellipsoids are drawn at the 50% probability level.

The molecular structure of **2** is shown in Figure 10. The complex crystallized in the monoclinic space group $P21/m$. Besides four indazole ligands, the two remaining axial binding sites are occupied by a nitrosyl ligand and a hydroxyl group. The structure consists of complex cations, chloride anions and co-crystallized acetone molecules. The Ru-N-O angle is of $171.0(9)^\circ$.

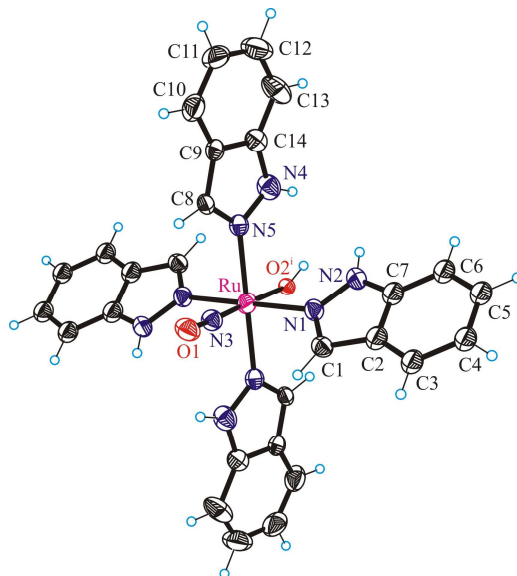


Figure 10. ORTEP view of one crystallographically independent cation of $\text{trans-[Ru(OH)(NO)(Hind)}_4\text{]Cl}_2$ (**2**), showing the atom-numbering scheme. Thermal displacement ellipsoids are drawn at the 50% probability level.

The structure of **10** is shown in Figure 11. The structure consists of two complex cations namely $\text{trans-[Ru(OH)(NO)(Hpz)}_4\text{]}^{2+}$ and $[\text{Mg(H}_2\text{O)}_6]^{2+}$ and two sulfate anions. **10** crystallized in the monoclinic space group $P2/c$ with Ru-O1 of $1.990(3)$ Å and Ru-N1 of $1.453(3)$ Å, respectively.

Table 4. Crystal Data and Details of Data Collection for **1, 2, 3, 4, 5, 6, 7, 8, 9, 10.**

Compound	1	2	3	4	5	6	7	8	9	10
empirical formula	C ₂₈ H ₂₄ N ₁₀ O ₄ Ru	C ₂₈ H ₂₅ Cl ₂ N ₉ O ₂ Ru·H ₂ O	C ₁₂ H ₁₆ Cl ₂ N ₈ Ru	C ₁₂ H ₁₆ N ₉ O ₂ Ru	C ₂₄ H ₂₈ Mg N ₁₈ O ₄ Ru ₂ ·0.1(C 3H ₆ O)	C ₁₂ H ₁₆ N ₉ O ₇ Ru S _{1.5} ·4.5(H ₂ O) ·0.8(CH ₃ COCH 3)	C ₂₀ H ₃₆ Cl ₁₀ N ₆ O Ru	C ₂₀ H ₃₂ N ₁₀ O ₄ Ru ·0.15(CH ₂ Cl ₂)	C ₂₀ H ₃₂ Cl ₂ N ₉ OR ·4.5H ₂ O	C ₁₂ H ₂₉ MgN ₉ O 15RuS ₂
fw	665.62	704.53	444.28	419.38	864.85	675.01	860.15	590.34	667.57	728.9
space group	C _{2/c}	P2 _{1/n}	C _{2/c}	P2 _{1/c}	C _{2/c}	C _{2/c}	P-1	P _{bcn}	P _{4/n}	P2/c
a, Å	40.289	10.443	13.822	18.284	12.736	31.953	8.4096	15.433	14.380	16.8196(7)
b, Å	7.019	8.455	9.183	10.805	16.113	7.800	11.0163	11.0916	14.380	11.0763
c, Å	28.498	20.55	14.006	17.603	16.325	19.316	11.1216	15.6678	9.235	16.8580
α, deg	90.00	90.00	90.00	90.00	90.00	90.00	89.691	90.00	90.00	90.00
β, deg	134.98	96.46	116.785	109.75	98.98	98.76	68.921	90	90.00	90.4950
γ, deg	90.00	90.00	90.00	90.00	90.00	90.00	69.709	90.00	90.00	90.00
V, Å³	5700.2	1799	1587	3273	3309	4758	893.31	2682	1910	3140.51
Z	8	2	4	8	4	7		4	2	4
λ, Å	0.71073	0.71073	0.71073	0.71073	0.71073	0.71073	0.71073	0.71073	0.71073	0.71073
Calcd, g cm⁻³	1.551	1.491	1.860	1.698	1.724	1.562	1.418	1.430	1.303	1.728
Crystal size, mm	0.04 x 0.04 x 0.30	0.28 x 0.22 x 0.20	0.2 x 0.2 x 0.09	0.01 x 0.04 x 0.06	0.06 x 0.08 x 0.1	-	0.5 x 0.05 x 0.04	0.12 x 0.19 x 0.26	0.01 x 0.12 x 0.19	0.15 x 0.11 x 0.08
T, K	100	100	100	100	100	293	120	293	293	100
μ, mm⁻¹	0.60	0.635	1.336	0.98	0.99	0.843	1.600	0.629	0.539	0.746
R1^a	0.0492	0.0497	0.0233	0.0353	0.0328	0.0584	0.0625	0.0385	0.0581	0.0317
wR2^b	0.1311	0.1241	0.0548	0.0747	0.0770	0.0536	0.1798	0.0434	0.0608	0.0714
GOF^c	1.021	1.003	1.071	1.0130	1.0150	0.9564	1.0510	1.0914	1.0027	1.044

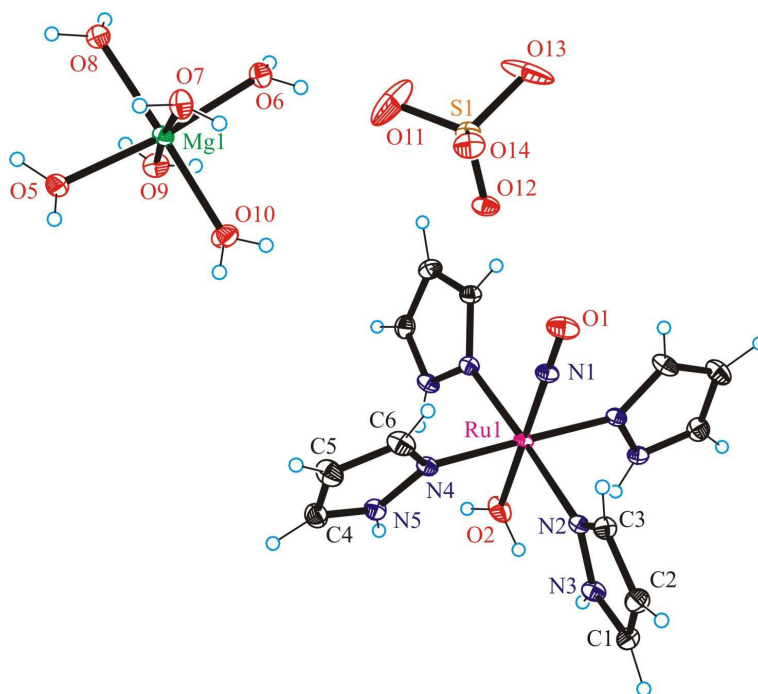


Figure 11. ORTEP view of one crystallographically independent molecule of trans-[Ru(OH)(NO)(Hpz)₄][Mg(H₂O)₆](SO₄)₂ (**10**), showing the atom-numbering scheme. Thermal displacement ellipsoids are drawn at the 50% probability level.

The crystal structure of **3** consists of a neutral complex with four pyrazole ligands (Figure 12). As expected due to reduction no chloride counterion is present. The complex crystallized in the monoclinic space group *C2/c*. The Ru-Cl1 is of 2.4474(4) Å, whereas the Ru-N1 bond is of 2.0748(15) Å.

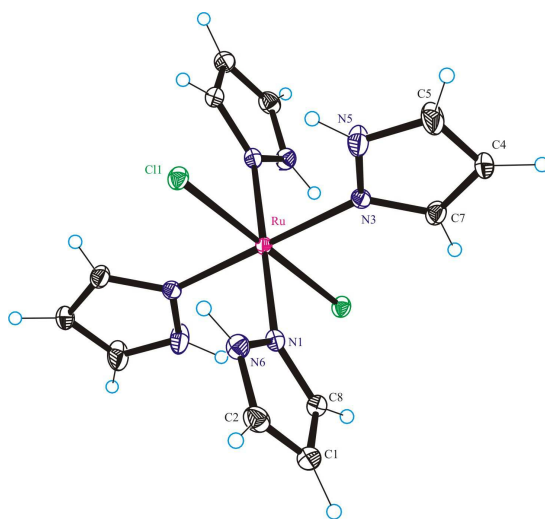


Figure 12. ORTEP view of one independent molecule of trans-[RuCl₂(Hpz)₄] (**3**), showing the atom-numbering scheme. Thermal displacement ellipsoids are drawn at the 50% probability level.

The complex **7** crystallized in the triclinic centrosymmetric space group $P-1$. The structure of **7** consists of a binuclear complex with two Ru centers (Figure 13) bridged by an oxygen atom. The distance Ru1-O1 is 1.787 Å and the angle Ru-O1-Ru is linear. Five remaining coordination positions at each Ru are occupied with chloride ligands. The Ru1-Cl1 bond of 2.366 Å is typical for other Ru chloride-species. The resulting charge 4+ of the complex is balanced by four protonated 3,5-dimethylpyrazoles.

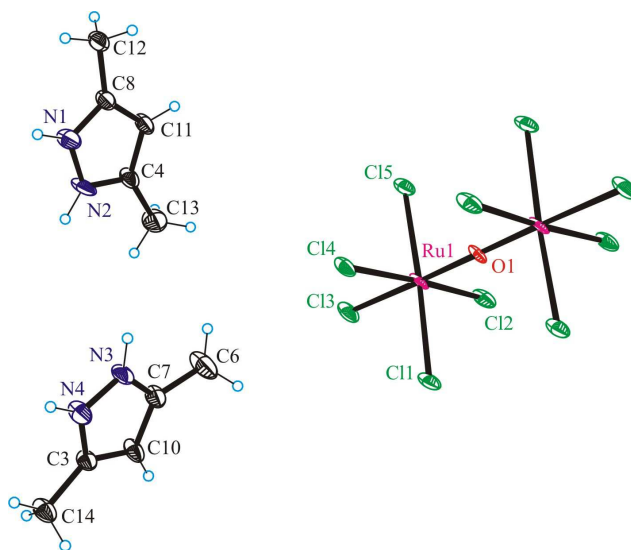


Figure 13. ORTEP view of one crystallographically independent molecule of $[\text{Ru}_2\text{Cl}_5\text{O}](3,5\text{-dimepz})_4$ (**7**), showing the atom-numbering scheme. Thermal displacement ellipsoids are drawn at the 50% probability level.

Electrochemistry

All of the synthesized compounds were investigated by electrochemical methods. The goal was to find out if the complexes are able to release nitrosyl after reduction and, whether the reduction potentials are accessible for biological reducing agents. Also the confirmation of the oxidation state of ruthenium was important. The comparison of electrochemical behaviour of nitro and nitrosyl complexes was also of interest.

The cyclic voltammograms (CVs) of the two nitro complexes **1** and **8** (Figures 14 and 15) in CH_2Cl_2 show a single-electron oxidation wave, I^{ox} assigned to $\text{Ru}^{\text{II}} \rightarrow \text{Ru}^{\text{III}}$ process. The redox potential values for the $\text{Ru}^{\text{II}}/\text{Ru}^{\text{III}}$ redox couple are 1.35 for **1** and

0.97 V for **8** (Table 4). In the case of indazole complex **1** we observed a quasi-reversible oxidation wave and in case of 3,5-dimethylpyrazole complex **8** the wave is reversible. These results were confirmed by electrolysis. The electrolysis of the first complex at 1.7 V was an irreversible process with two-electron transfer and the oxidation of **8** at 1.2 V was reversible and proceeded with one electron transfer. The second oxidation wave I^{ox2} at 2.1 V for **1** and at 2.2 V for **8** was assigned to oxidation of Ru^{III} to Ru^{IV} and it was an irreversible wave with $I_{p_{ox}}$ (μA) around 70 μA . The current ratio I_{p2}/I_{p1} between the two waves is 1.75.

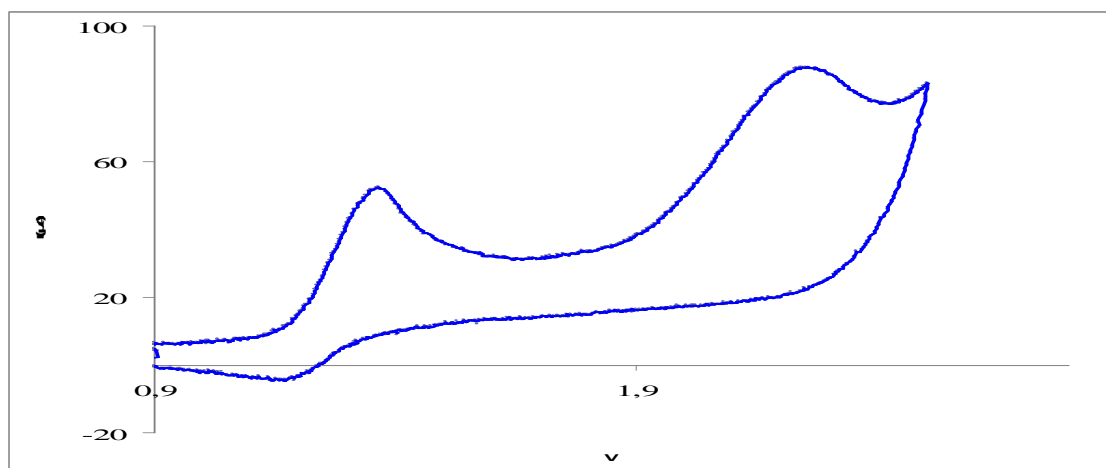


Figure 14. Cyclic voltammogram of $trans-[Ru(NO_2)_2(Hind)_4]$ at 0.10 V s^{-1} . The first wave is assigned to the Ru^{II}/Ru^{III} redox couple and the second wave to Ru^{III}/Ru^{IV} redox couple.

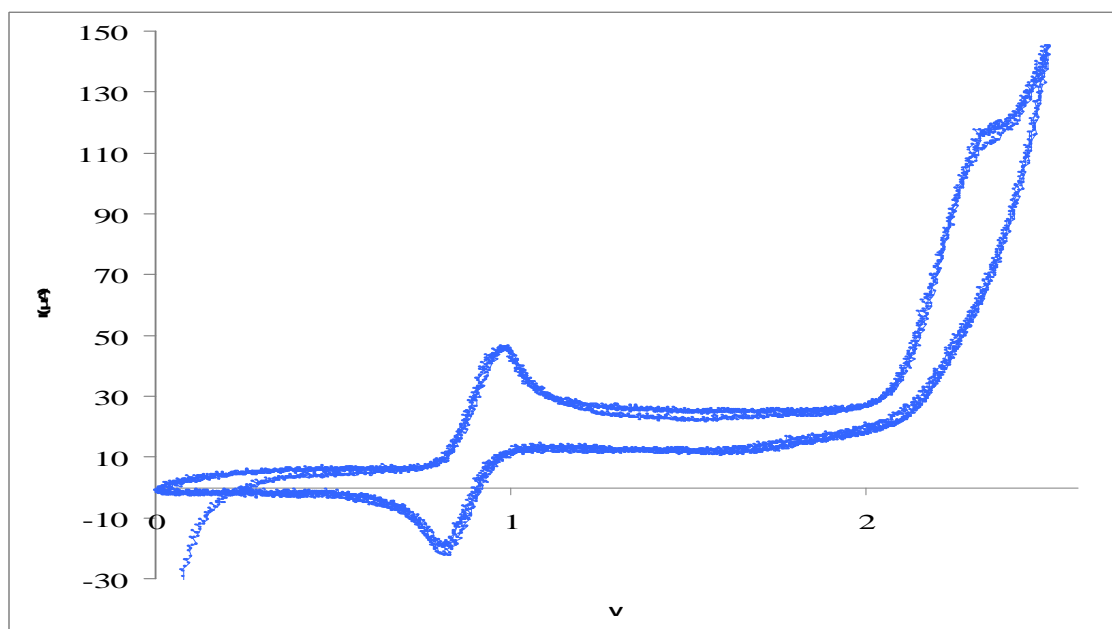


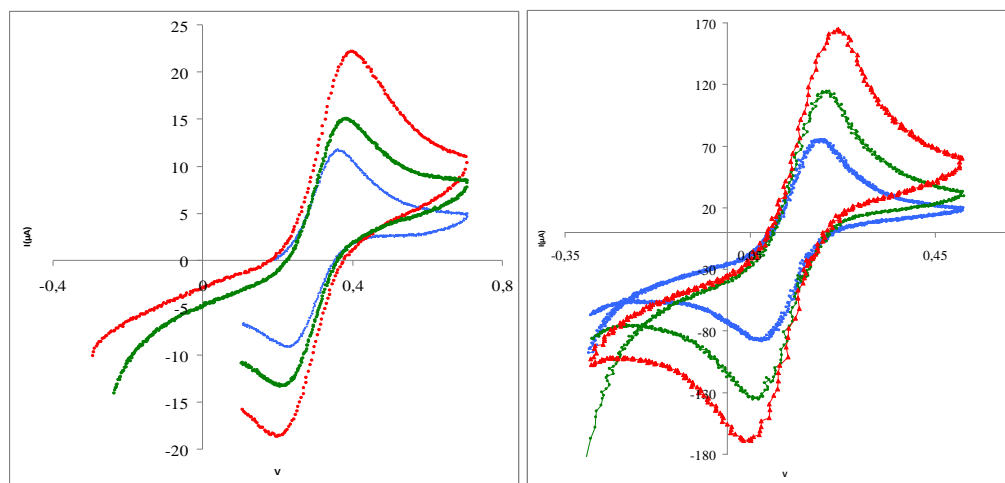
Figure 15. Cyclic voltammogram of $trans-[Ru(NO_2)_2(3,5-dimepz)_4]$ at 0.10 V s^{-1} . The first wave is assigned to the Ru^{II}/Ru^{III} redox couple and the second wave to Ru^{III}/Ru^{IV} redox couple.

Table 4. Cyclic voltammetric data for complex **1** and **8** and their corresponding estimated redox Potentials.

	$E_{p_{ox}}$ (V)	$E_{1/2}$ (V)	$i_{p_{ox}}$ (μ A)
<i>trans</i> -[Ru(NO ₂) ₂ (Hind) ₄] (1)	1.35	1.275	40.0
<i>trans</i> -[Ru(NO ₂) ₂ (3,5Dimepz) ₄] (8)	0.97	0.89	45.92

The multi-scan of CV curve of **1** at 100 mV/s showed a decrease of the current characteristic for an area phenomenon at the electrode whereas the $i_p = f(Vv)$ and multi-scan CV at 100 mV/s indicate a diffusion controlled process for **8**. In this case passivation of the conductive area, probably due to indazole ligand, takes place. The peak ratio between I^{ox1} and I^{ox2} was equal to 1.75 for the complex **1**.

The electrochemical studies of the nitrosyl compounds **2**, **5**, **6** and **9** in acetone electrolyte solution revealed a single-electron reduction wave, I^{red} assigned to $Ru^{III} \rightarrow Ru^{II}$ process (Figure 16). Except for **5**, all of the waves have reversible character and the reduction potential reached the values between 0.39 V and 0.18 V for the complexes **2**, **6** and **9** (Table 5). The reduction potential of **6** was negative at - 0.6 V and the wave is quasi-reversible.



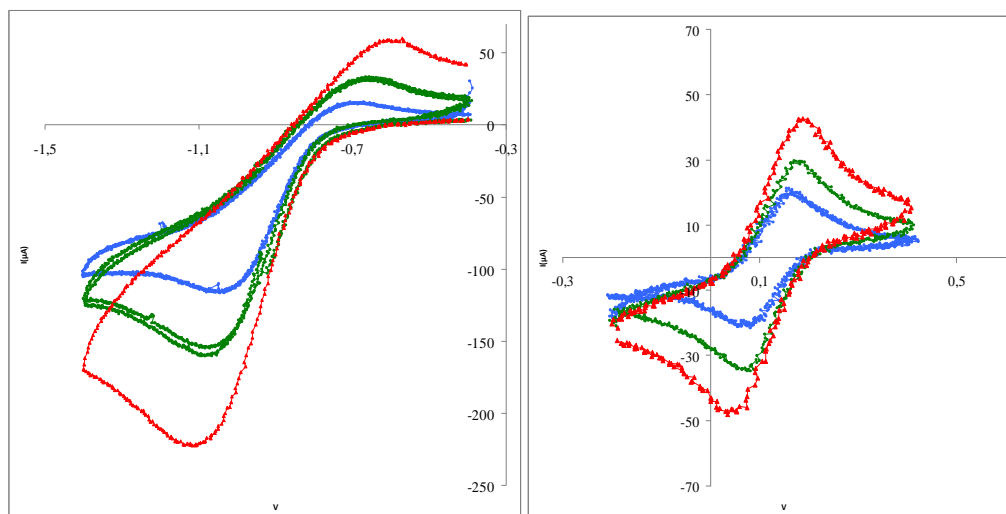


Figure 16. Cyclic voltammograms of 2 mM solutions of *trans*-[Ru(OH)(NO)(Hind)₄]Cl₂ (**2**), *trans*-[Ru(SO₄)(NO)(Hpz)₄](SO₄)_{0.5} (**6**), {[Ru(NO)(Hpz)(pz)₃(μ-OH)]₂Mg} (**5**) and *trans*-[RuCl(3,5-dimepz)₄(NO)]Cl₂ (**9**) in acetone with 0.1 M [*n*-Bu₄N][BF₄] at a glassy carbon electrode at a scan rate of 0.05 (blue), 0.10 (green) and 0.20 V s⁻¹ (red). The waves are assigned to the Ru^{III}/Ru^{II} redox couple.

Table 5. Cyclic voltammetric data for **1** and **8** and their corresponding redox potentials.

	E_pred (V)	E_{1/2} (V)	I_pred (µA)
<i>trans</i> -[Ru(OH)(NO)(Hind) ₄]Cl ₂ (2)	0,387	0,215	16,34
<i>trans</i> -[RuCl(3,5-dimepz) ₄ (NO)]Cl ₂ (9)	0,18	0,12	34,83
<i>trans</i> -[Ru(SO ₄)(NO)(Hpz) ₄](SO ₄) _{0.5} (6)	0,21	0,13	149,6*
{[Ru(NO)(Hpz)(pz) ₃ (μ-OH)] ₂ Mg} (5)	-	-	-

The electrolysis of **2** was performed at 0 V. The reduction was an irreversible process with one-electron transfer. After reduction the wave from the starting compound was not present. The complex **6** was electrolyzed at - 0.15 V. Q was equal to 96560 C and, considering the concentration, it results in one-electron transfer. The reduction was a reversible process. After reduction the same wave was detected. Thus the reduction took place in acidic condition after the in situ generation of the complex and it is not directly comparable with the other complexes. In case of **9** a very complicated new wave has occurred after reduction at - 0.15 V. The reduction was an irreversible process. The observed process can be understood as a two-step reaction. After first reduction the transient product A⁻ reacts spontaneously to B⁻, which has a similar reduction potential as A and transfers to B²⁻ (Figure 17). Electrolysis of **5** was also an

irreversible two-electron transfer process, which was expected due to cyclic voltammometric measurements.

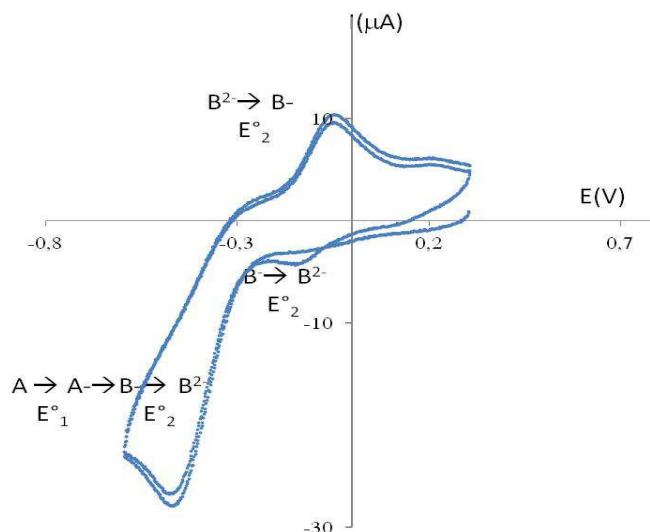
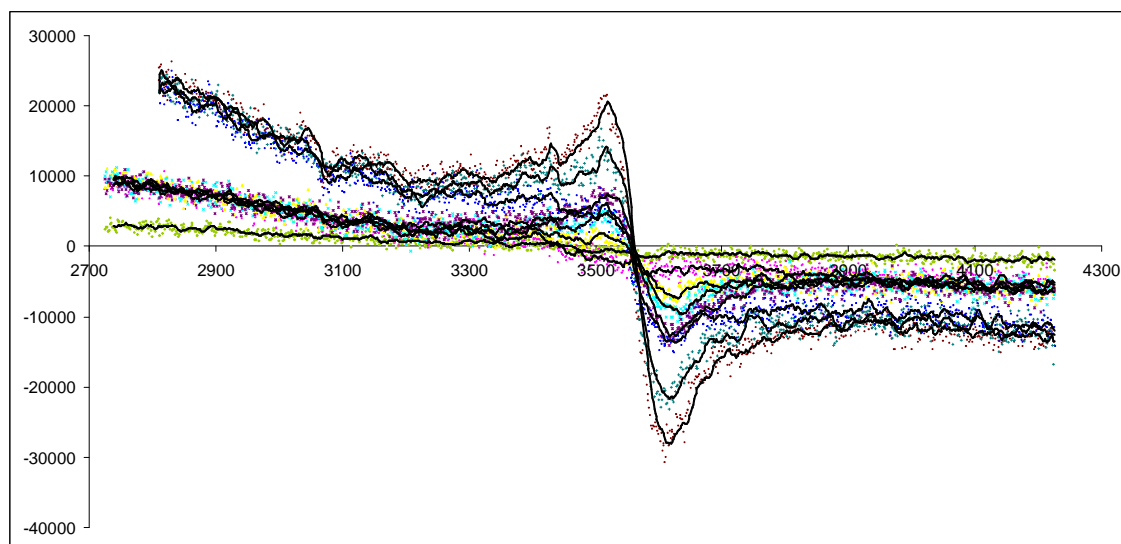


Figure 17. Cyclic voltammogram of trans-[RuCl(3,5-dimepz)₄(NO)]Cl at 0.10 V s⁻¹ after electrolysis.

The measured reduction potentials for the nitrosyl compounds are all lying in the area accessible under biological conditions. That means it is possible to reduce the complex within a cell bridging the NO release.

EPR spectroscopy

The electrolysis of the complexes **2**, **6** and **9** was monitored using electron paramagnetic resonance (EPR). The potential was reduced stepwise from 0 V to -0,5 V. All of the measured complexes were EPR silent before electrolysis.



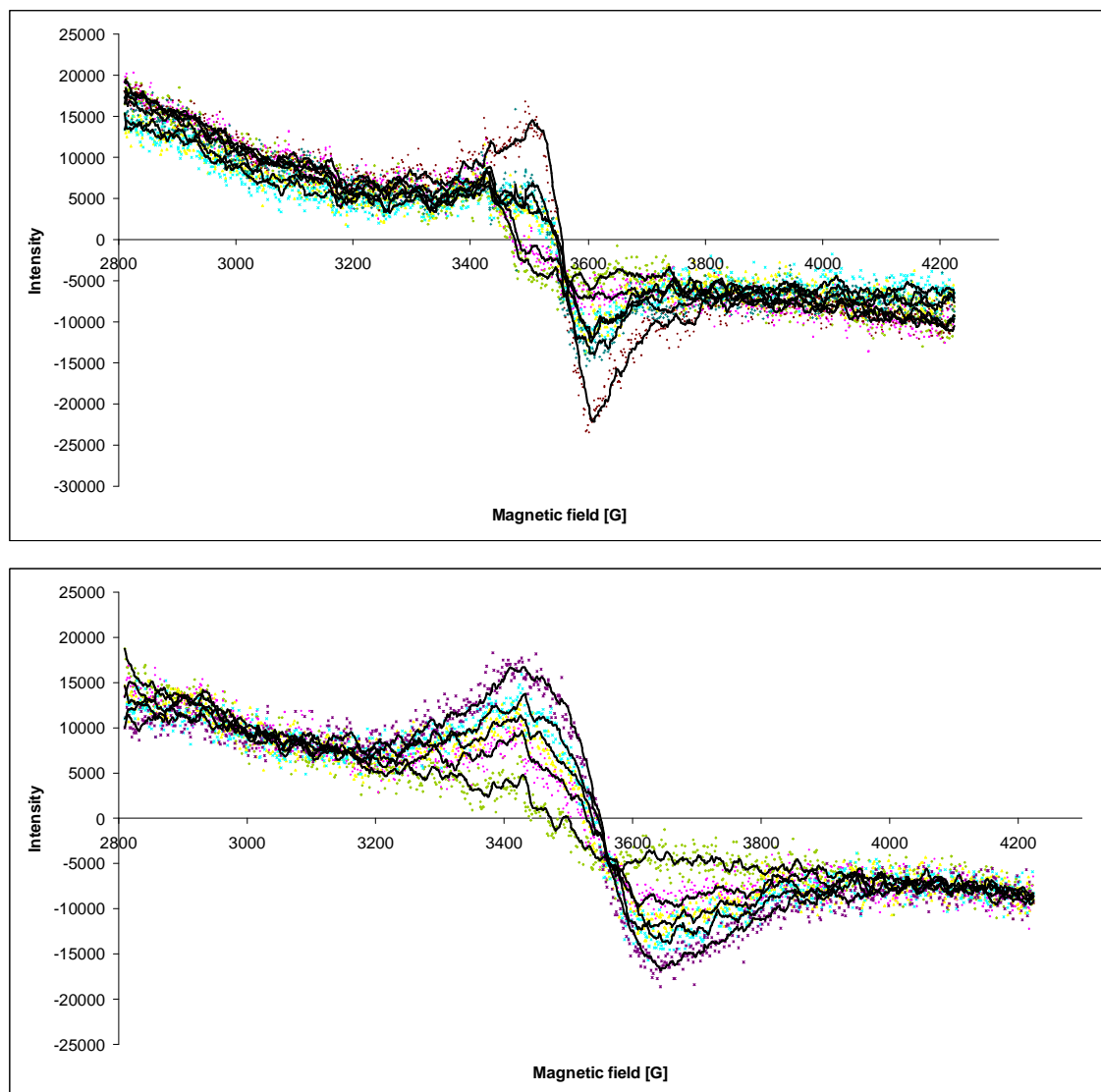


Figure 18. Changes in EPR spectra of *trans*-[Ru(OH)(NO)(Hind)₄]Cl₂ (**2**) (top), *trans*-[RuCl(3,5-dimepz)₄(NO)]Cl₂ (**9**) and *trans*-[Ru(SO₄)(NO)(Hpz)₄](SO₄)_{0.5} (**6**) (bottom) at 293 K during the controlled electrolysis from 0 V to -0.5 V.

During the electrolysis a broad signal appeared and grew proportional to the dropping potential (Figure 18). The spectra provide a proof of the paramagnetic nature of the reduced species. The exact characterisation of the signal was not possible because of the signal broadening at room temperature.

Complex **2** was also measured using EPR at low temperature (120 K). The complex was EPR silent before reduction and after reduction a typical Ru-NO signal was detected (Figure 19).^{18,19} These results indicate the formulation {Ru(NO)}⁶ containing Ru^{II} ($S = 0$) bonded to NO⁺ ($S = 0$) or NO⁰ ($S = \frac{1}{2}$) for the not reduced complex. Ru

and NO are coupled antiferromagnetically or through a closed-shell interaction to Ru^{III} ($S = \frac{1}{2}$). The Ru^{II} with NO⁺ ($S = 0$) or the antiferromagnetic closed-shell interaction of Ru^{III} ($S = \frac{1}{2}$) with NO⁰ ($S = \frac{1}{2}$) radical results in low-spin configuration of the complex. Reduction of the complex results in {Ru(NO)}⁷ species which has an unpaired electron, accompanied by EPR activity²⁰.

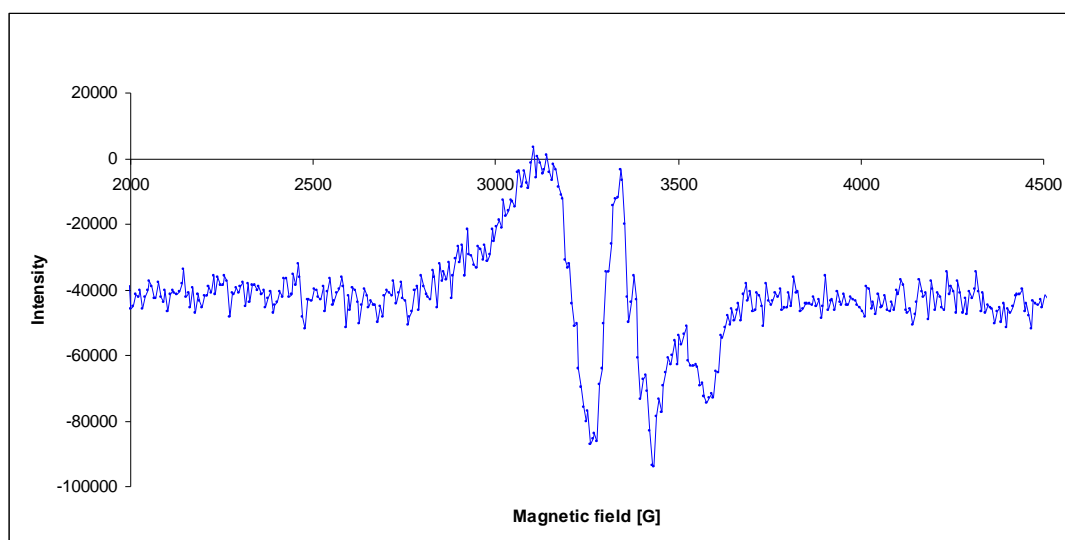


Figure 19. EPR spectra of trans-[Ru(OH)(NO)(Hind)₄]Cl₂ (**2**) (top) at 120 K in acetone.

Final remarks

Nitrosylation of ruthenium(II) complexes with fourazole heterocycles resulted in formation of nitro or directly nitrosyl complexes, which are potential anticancer agents and NO donors. The electrochemical studies confirm the possible release of nitrosyl due to one-electron reduction. Also the EPR spectra of the reduced complex **2** indicate the presence of radical NO. The nitrosyl complexes showed light sensitivity so that the release of nitrosyl could be also achieved with light irradiation. After the successful clinical trials of KP1019^{21,22,23} and NAMI-A²⁴, we can expect encouraging properties of the new potential antitumour drugs. The synthesized complexes have not only higher azole-to-chloride ratio, which increases the anticancer activity²⁵ but also reduction potentials accessible under biological conditions. Furthermore the non-innocent ligand NO is supposed to enhance the activity.²⁶ The complexes are water soluble and stable in solution, which makes them good candidates for cytotoxicity tests. The next step for these promising compounds should be *in vitro* experiments and GMP tests verifying the release of NO.

3 Supporting information

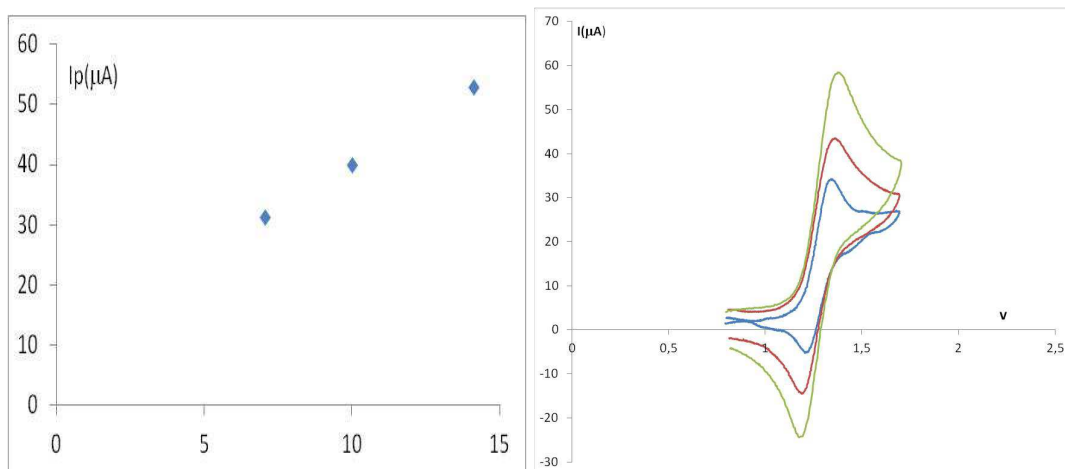


Figure 1. Plot showing the linearity of $I_p = f(v)$ (left side) and cyclic voltammogram (right side) of 2 mM solution in acetone with 0.1 M $[n\text{-Bu}_4\text{N}][\text{BF}_4]$ of $\text{trans}[\text{Ru}(\text{NO}_2)_2(\text{Hind})_4]$ (**3**) at a glassy carbon electrode at a scan rate of 0.05 (blue), 0.10 (red) and 0.20 V s^{-1} (green). The wave is assigned to the $\text{Ru}^{\text{II}}/\text{Ru}^{\text{III}}$ redox couple.

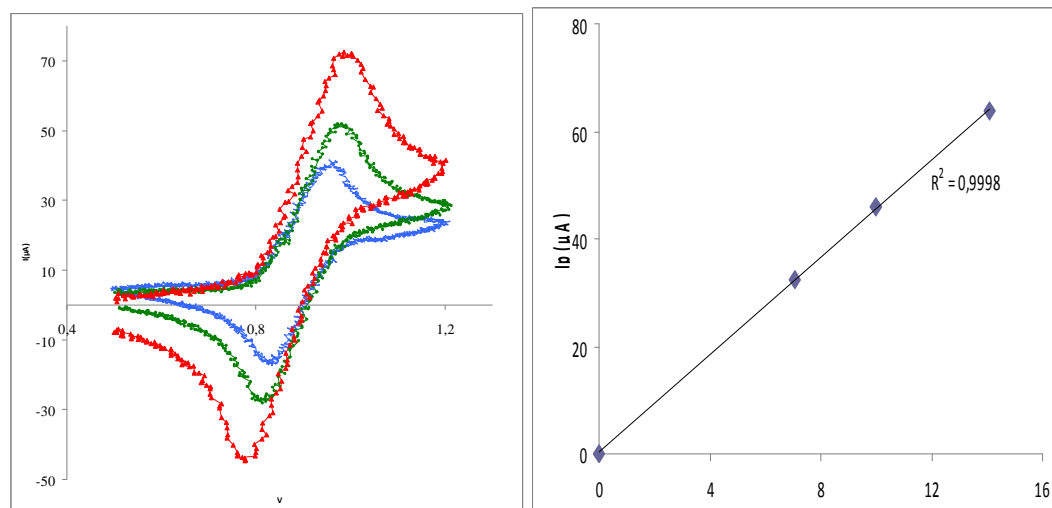


Figure 2. Plot showing the linearity of $I_p = f(v)$ (left) and cyclic voltammogram (right) of 2 mM solution of $\text{trans}[\text{Ru}(\text{NO}_2)_2(3,5\text{-dimepz})_4]$ (**8**) in acetone with 0.1 M $[n\text{-Bu}_4\text{N}][\text{BF}_4]$ at a glassy carbon electrode at a scan rate of 0.05 (blue), 0.10 (green) and 0.20 V s^{-1} (red). The wave is assigned to the $\text{Ru}^{\text{III}}/\text{Ru}^{\text{II}}$ redox couple.

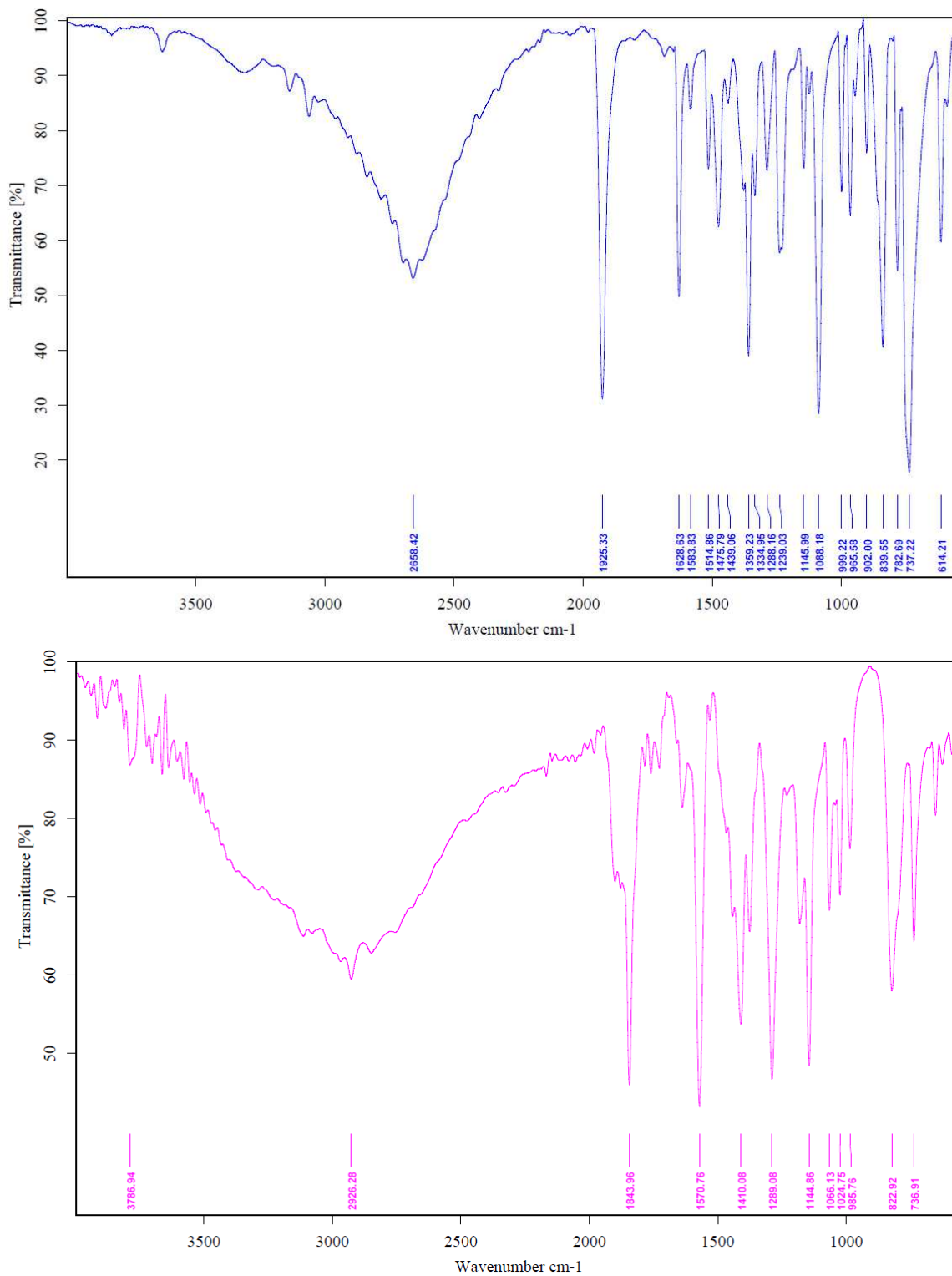


Figure 4. IR spectra of trans-[Ru(NO)₂(Hind)₄]Cl₂ (**2**) (top) and trans-[Ru(NO)Cl(Hdimepz)₄]Cl (**9**) (bottom).

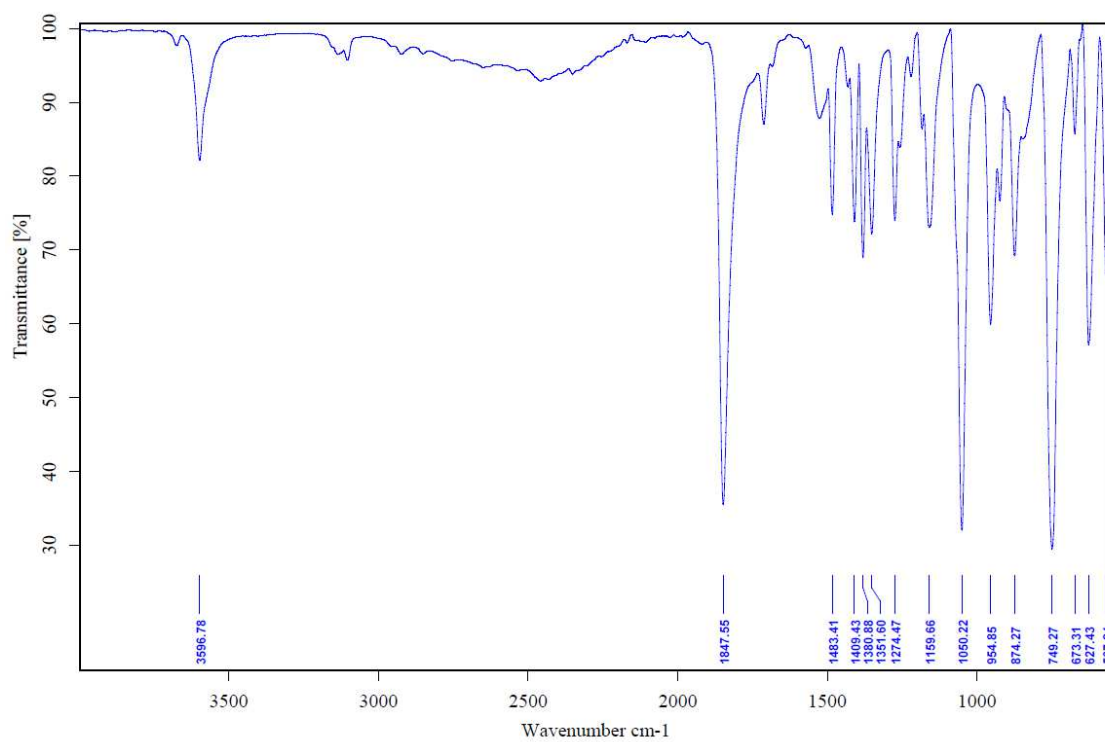
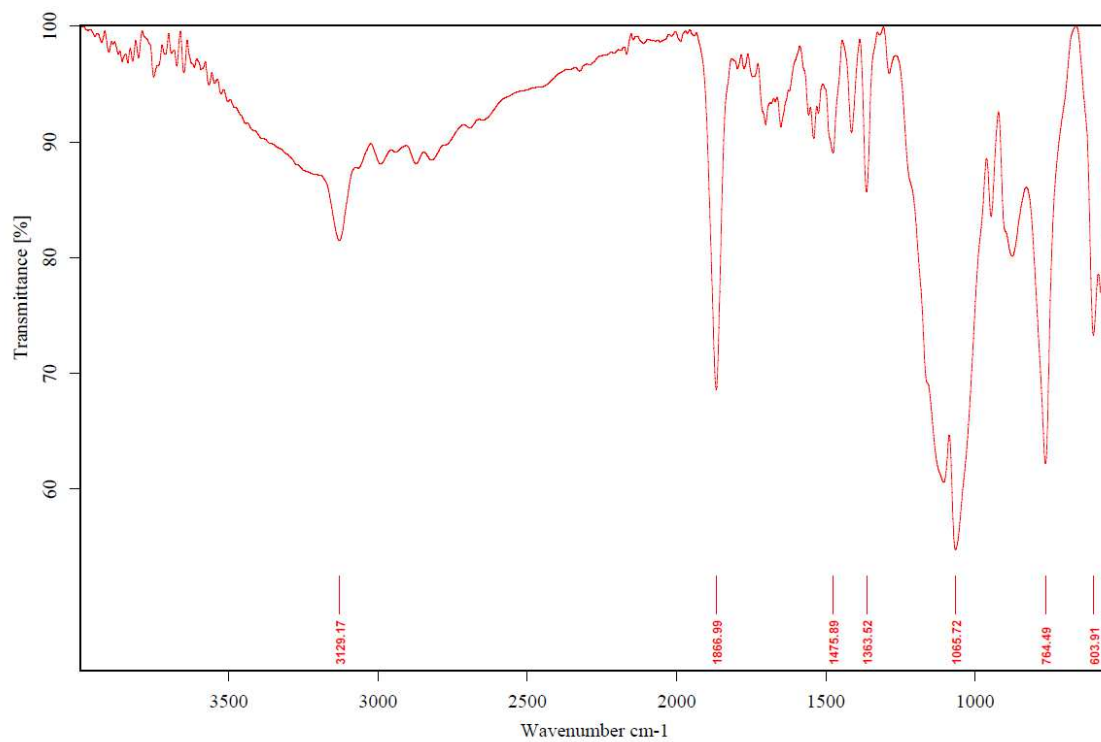


Figure 5. IR spectra of $\text{trans-[Ru(NO)(SO}_4\text{)(Hpz)}_4\text{]}\cdot 0.5\text{SO}_4$ (**6**) (top) and $\{[\text{Ru(NO)(Hpz)(pz)}_3(\mu\text{-OH})]_2\text{Mg}\}$ (**5**) (bottom).

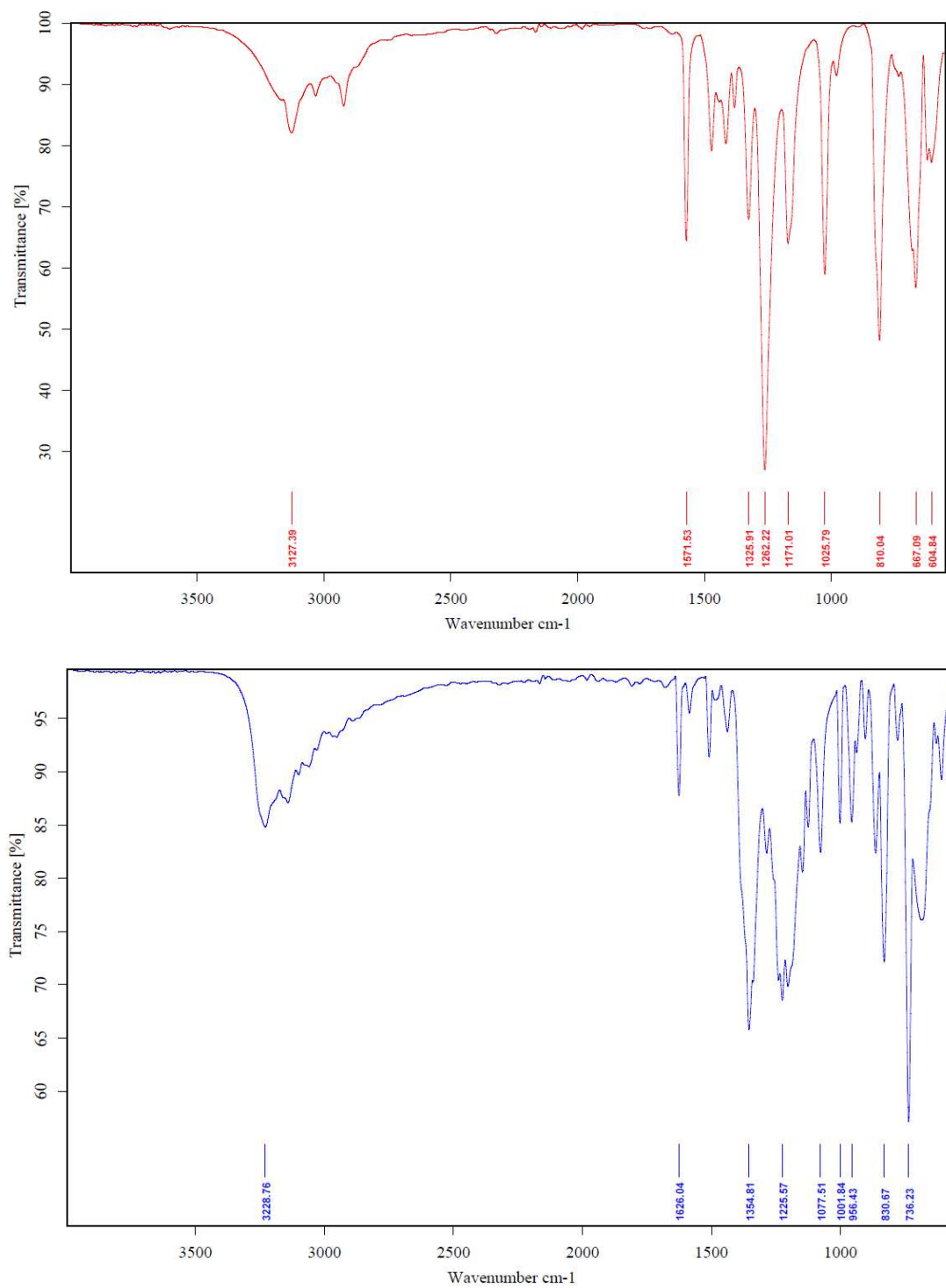


Figure 6. IR spectra of trans-[Ru(NO₂)₂(Hdimepz)₄] (**8**) (top) and trans-[Ru(NO₂)₂(Hind)₄] (**1**) (bottom).

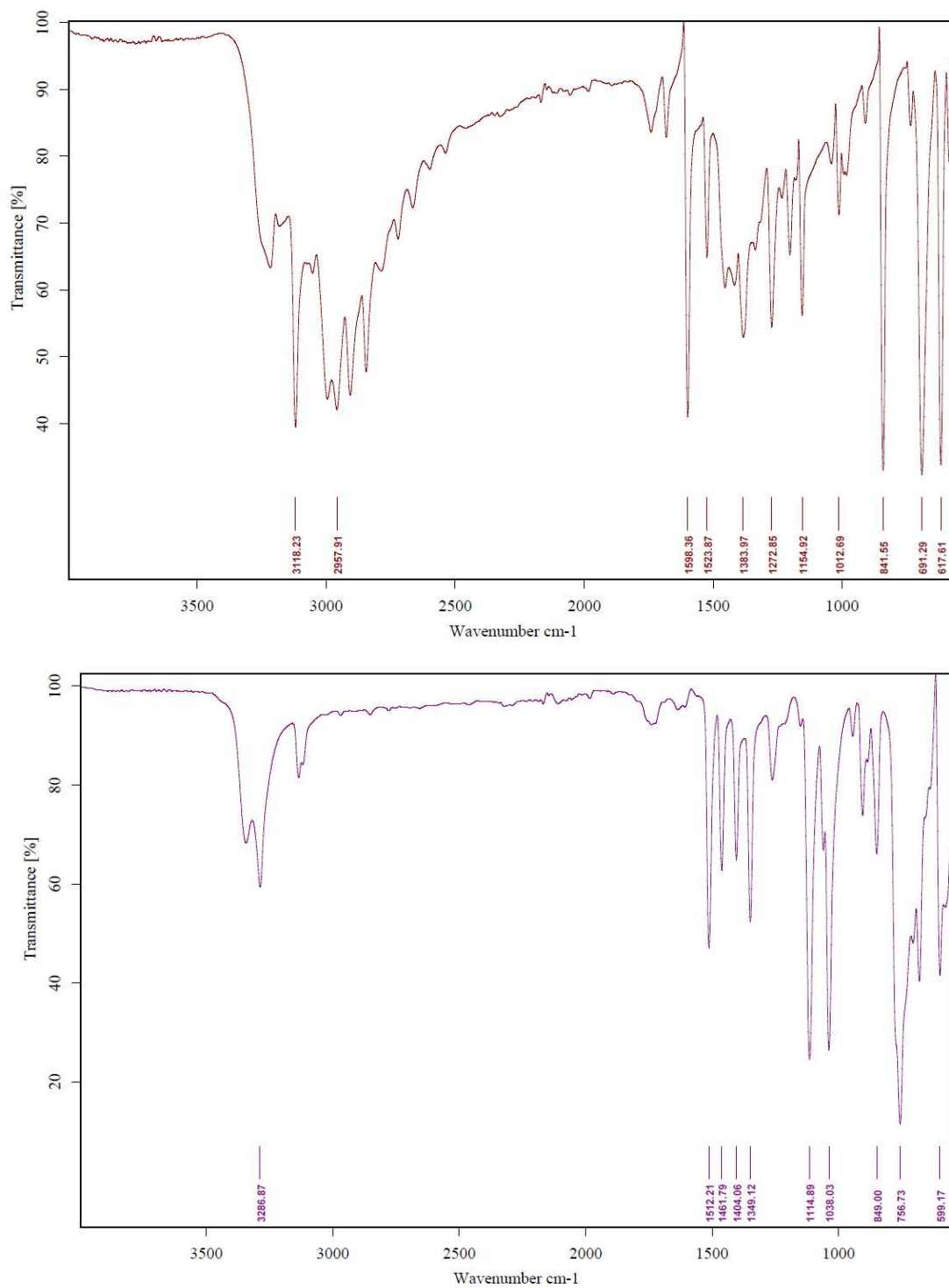


Figure 7. IR spectra of trans-[Ru(NO₂)₂(Hind)₄] (**7**) (top) and trans-[RuCl₂(Hpz)₄] (**3**) (bottom).

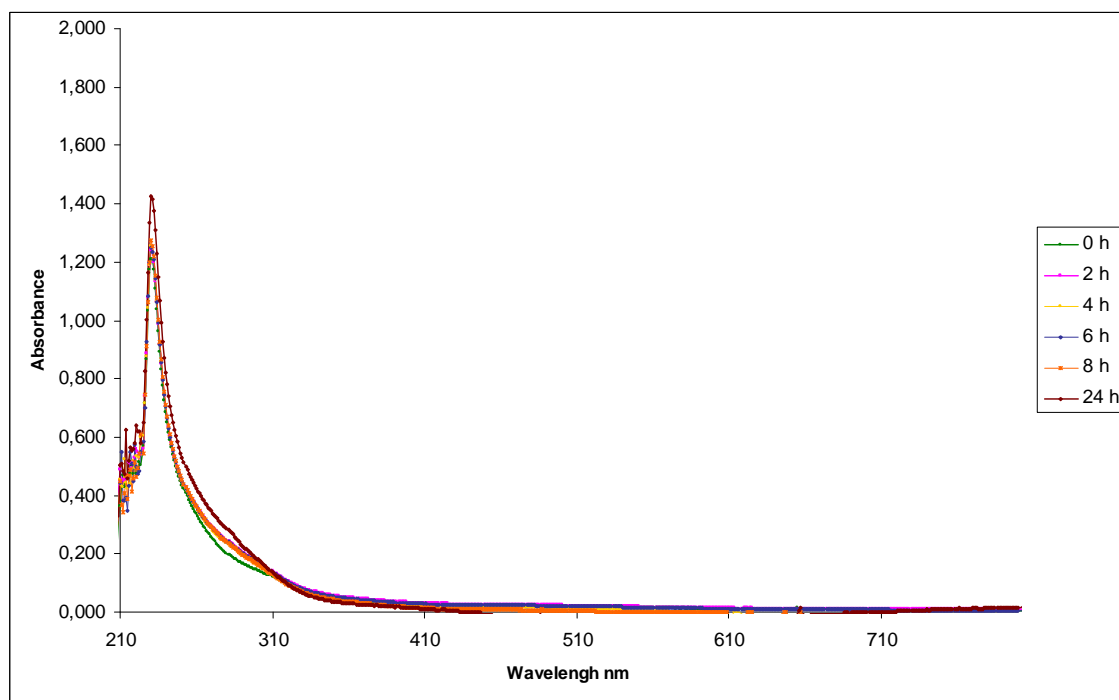
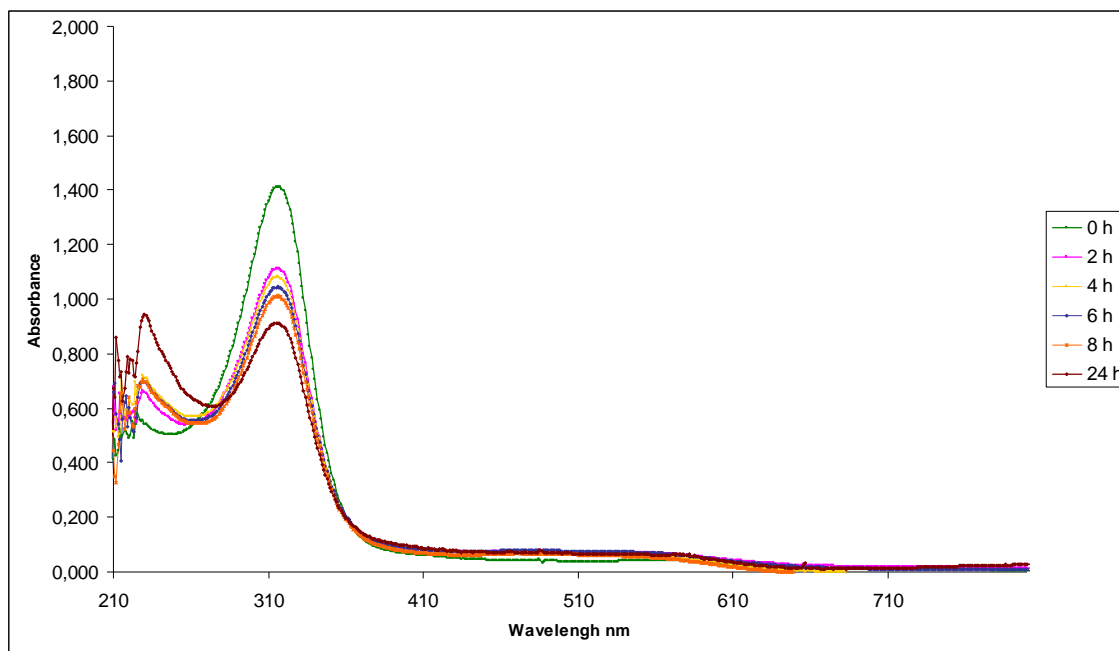


Figure 8. Time dependent UV-vis spectra of $\text{trans-}[\text{RuCl}_2(\text{Hpz})_4]$ (**3**) (top) and $\{[\text{Ru}(\text{NO})(\text{Hpz})(\text{pz})_3(\mu\text{-OH})_2]\}_2\text{Mg}$ (**5**) (bottom) in CH_2Cl_2 . The spectra were measured immediately after dissolution (green), after 2 h (pink), 4 h (yellow), 6 h (blue), 8 h (orange) and 24 h (violet).

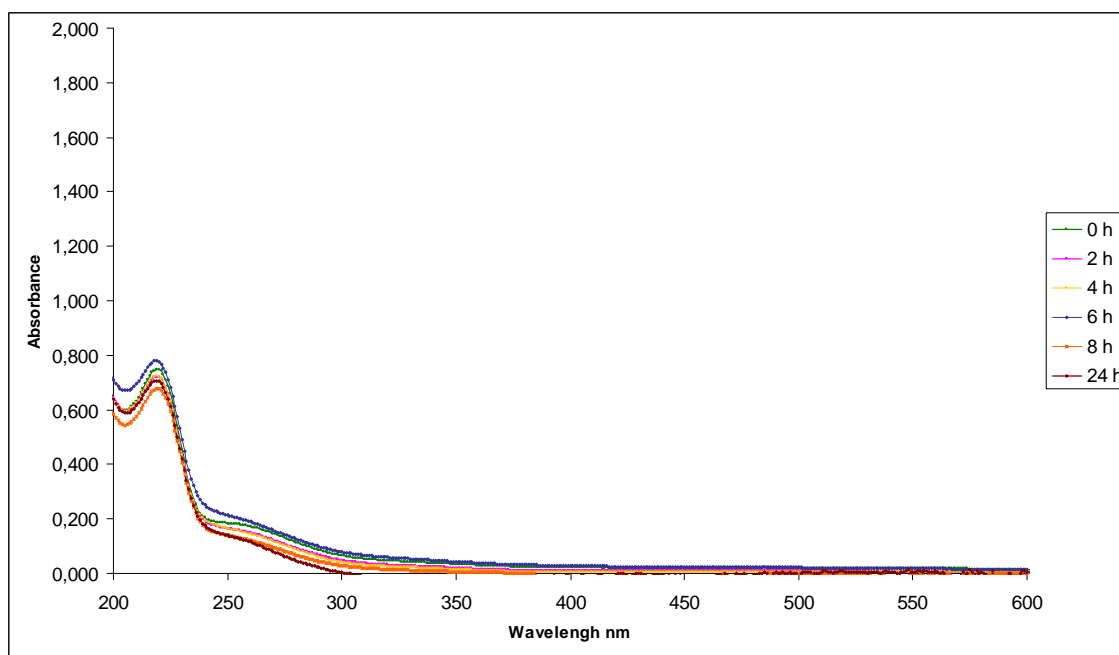
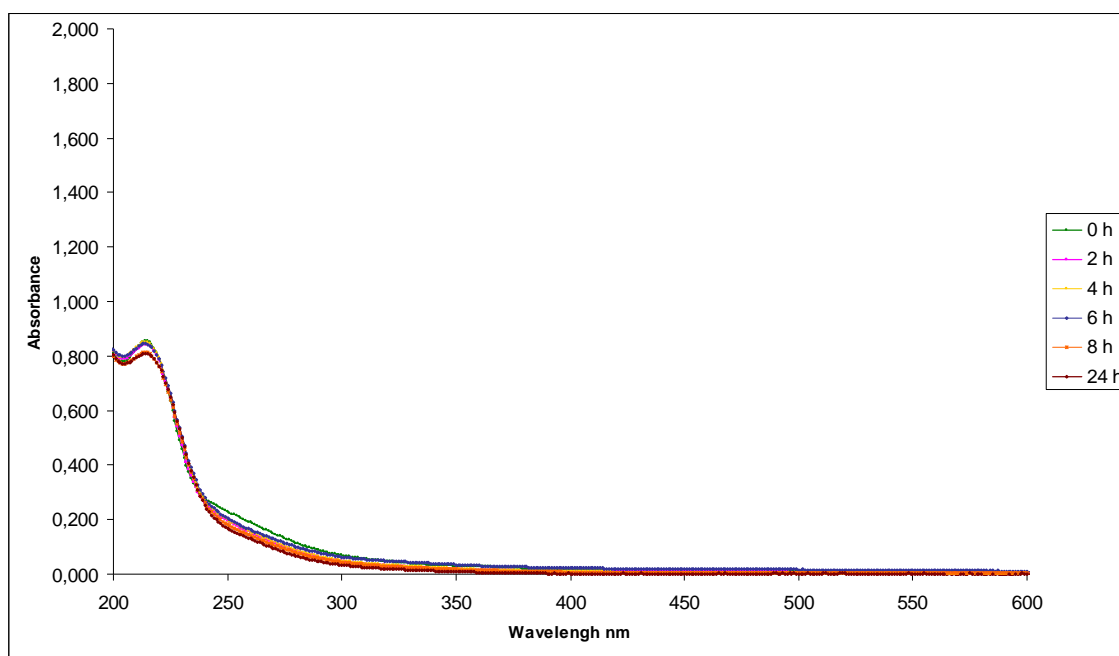


Figure 9. Time dependent UV-ivs spectra of trans-[Ru(NO)(SO₄)(Hpz)₄]_{0.5}SO₄ (**6**) (top) and trans-[RuCl(NO)(Hdimepz)₄]₄Cl (**9**) (bottom) in H₂O. The spectra were measured immediately after dissolution (green), after 2 h (pink), 4 h (yellow), 6 h (blue), 8 h (orange) and 24 h (violet).

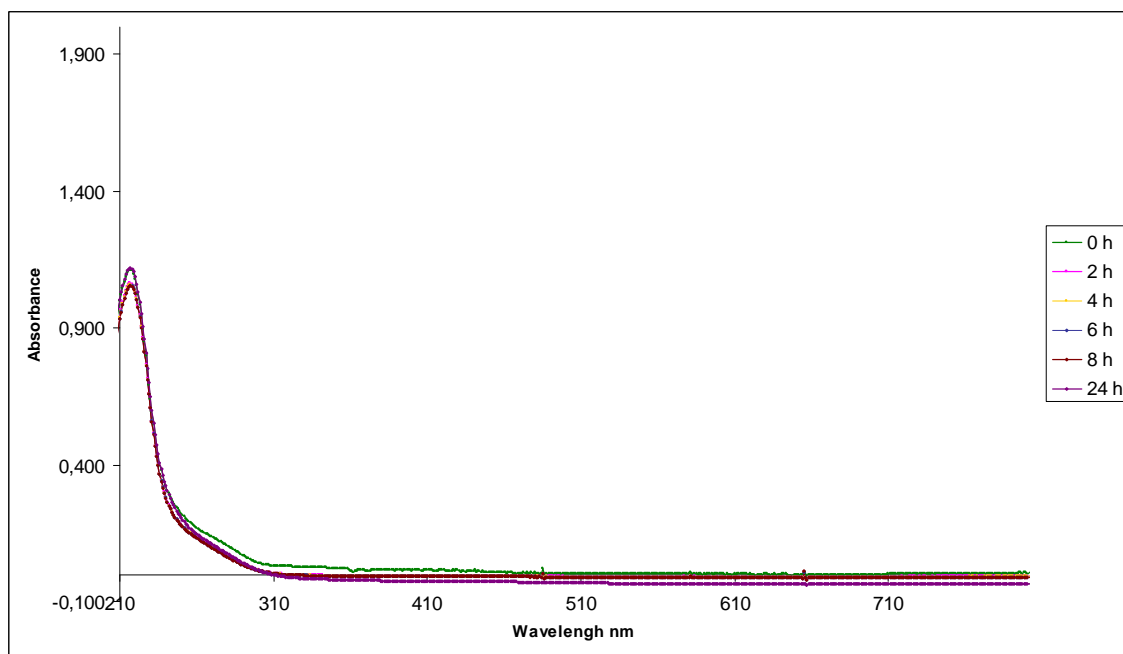
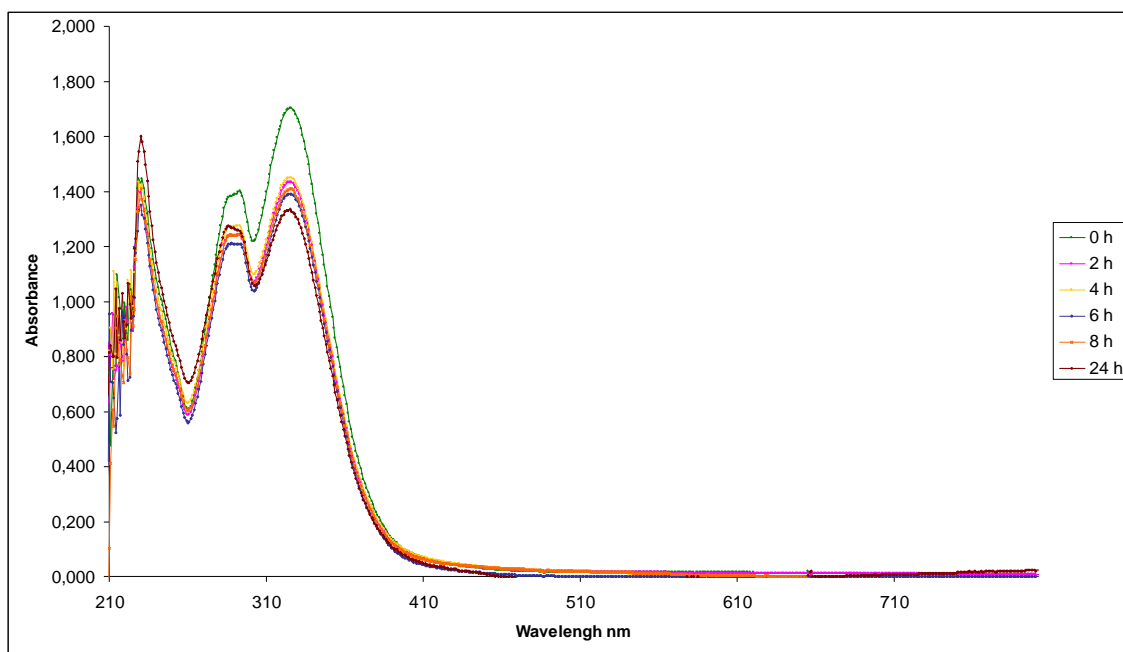


Figure 10. Time dependent UV-vis spectra of $\text{trans-}[\text{Ru}(\text{NO}_2)_2(\text{Hind})_4]$ (**1**) (top) in CH_2Cl_2 and $\text{trans-}[\text{Ru}(\text{Cl})(\text{NO})(\text{Hpz})_4]\text{Cl}_2$ (**11**) (bottom) in H_2O . The spectra were measured immediately after dissolution (green), after 2 h (pink), 4 h (yellow), 6 h (blue), 8 h (orange) and 24 h (violet).

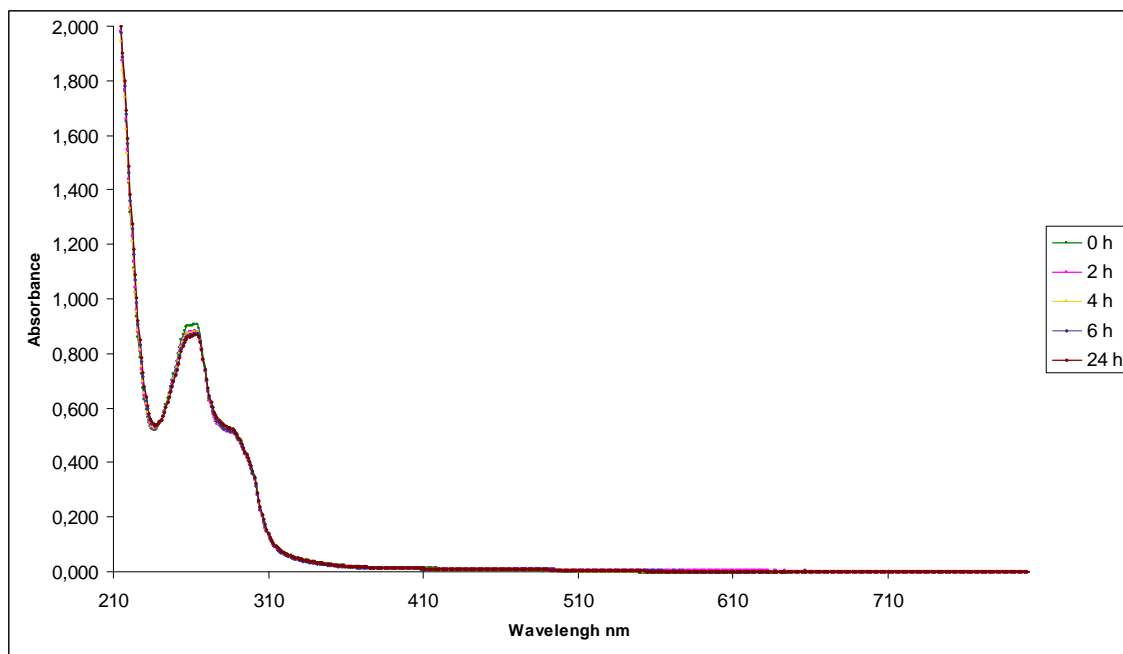
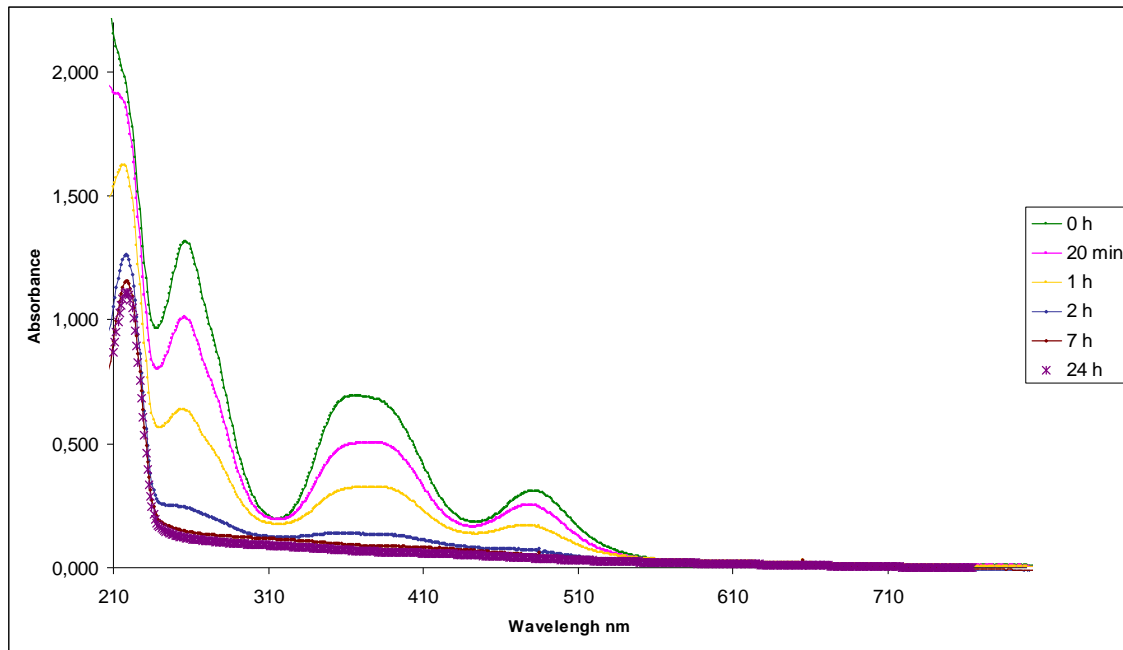


Figure 11. Time dependent UV-ivs spectra of $[\text{Ru}_2\text{Cl}_5\text{O}](3,5\text{-dimepz})_4$ (7) (top) and $\text{trans-}[\text{Ru}(\text{OH})(\text{NO})(\text{Hind})_4]\text{Cl}_2$ (2) (bottom) in H_2O (7) and MeOH (2). The spectra were measured immediately after dissolution (green), after 2 h (2) and 20 min (7) (pink), 4 h (2) and 1 h (7) (yellow), 6 h (2) and 2 h (7) (blue), 7 h (braun) and 24 h (violet).

References

- [1] E. Reisner, V. B. Arion, A. Eichinger, N. Kandler, G. Giester, A. J. L. Pombeiro, B. K. Keppler, *Inorg. Chem.*, **2005**, *44*, 6704-6716.
- [2] A. Eichinger, Dissertation, **2003**, University of Vienna.
- [3] E. Reisner, V. B. Arion, M. F. C. Guedes da Silva, R. Lichtenecker, A. Eichinger, B. K. Keppler, V. Yu. Kukushkin, A. J. L. Pombeiro, *Inorg. Chem.* **2004**, *43*, 7083-7093.
- [4] G. M. Sheldrick, *SHELXS-97, Program for Crystal Structure Solution*: University Göttingen: Göttingen, Germany, **1997**.
- [5] G. M. Sheldrick, *SHELXL-97, Program for Crystal Structure Refinement*: University Göttingen: Göttingen, Germany, **1997**.
- [6] M. N. Burnett, G. K. Johnson, ORTEP III. Report ORNL-6895; OAK Ridge National Laboratory: Oak Ridge, TN, **1996**.
- [7] C. K. Johnson, Report ORNL-5138; OAK Ridge National Laboratory: OAK Ridge, TN, **1976**.
- [8] *International Tables for X-ray Crystallography*; Kluwer Academic Press: Dordrecht, The Netherlands, **1992**; Vol. C, Tables 4.2.6.8 and 6.1.1.4.
- [9] Cotton, G. Wilkinson, *Advanced Inorganic Chemistry*, 5th ed, Wiley, New York, 1988, p 486.
- [10] E. Tfouni, M. Krieger, B. R. McGarvey, D. W. Franco, *Coord. Chem. Rev.* **2003**, *236*, 57–69.
- [11] J. A. McCleverty, *Chem. Rev.* **2004**, *104*, 403–418.
- [12] M. Buron-Le Cointe, B. Cormary, L. Toupet, I. Malfant, *Cryst. Struct. Commun.*, **2011**, *67(12)*, 375-377.
- [13] M. G. B. Drew, S. Nag, D. Datta, *Dalton Trans.*, **2008**, 2298-2302.
- [14] D. A. Freedman, D. E. Janzen, K. R. Mann, *Inorg. Chem.*, **2001**, *40*, 6009-6016.
- [15] D. R. Lang, J. A. Davis, L. G. F. Lopes, A. A. Ferro, L. C. G. Vasconcellos, D. W. Franco, E. Tfouni, A. Wieraszko, M. J. Clarke, *Inorg. Chem.* **2000**, *39*, 2294-2300.
- [16] L. G. F. Lopes, E. E. Castellano, A. G. Ferreira, C. U. Davanzo, M. J. Clarke, D. W. Franco, *Inorg. Chim. Acta*, **2005**, *358*, 2883–2890.

-
- [17] B.Serli, E. Zangrando, E Lengo, G. Mestroni, L. Yellowlees, E. Alessio, *Inorg. Chem.* **2002**, *41*, 4033-4043.
- [18] M. Wanner, T. Scheiring, W. Kaim, L. D. Slep, L. M. Baraldo, J. A. Olabe, S. Zalis, E. J. Baerends, *Inorg. Chem.*, **2001**, *40*, 5704-5707.
- [19] P. Singh, B. Sarkar, M. Sieger, M. Niemeyer, J. Fiedler, S. Zalis, W. Kaim, *Inorg. Chem.*, **2006**, *45*, 4602-4609.
- [20] K. G. Dyall, *Theor. Chem. Acc.* **2004**, *112*, 403–409.
- [21] S. Kapitza, M. A. Jakupec, M. Uhl, B. K. Keppler, B. Marian, *Cancer Lett.* **2005**, *226*, 115 -121.
- [22] S. Kapitza, M. Pongratz, M. A. Jakupec, P. Heffeter, W. Berger, L. Lackinger, B. K. Keppler, B. Marian, *J. Cancer Res. Clin. Oncol.*, **2005**, *131*, 101–110.
- [23] C. G. Hartinger, M. A. Jakupec, S. Zorbas-Seifried, M. Groessl, A. Egger, W. Berger, H. Zorbas, P. J. Dyson, B. K. Keppler. *Chem. Biodiversity* **2008**, *5*, 2140–2155.
- [24] G. Sava, S. Zorzet, C. Turrin, F. Vita, M. R. Soranzo, G. Zabucchi, M. Cocchietto, A. Bergamo, S. DiGiovone, G. Pezzoni, L. Sartor and S. Garbisa, *Clin. Cancer Res.*, **2003**, *9*, 1898-1905.
- [25] M. A. Jakupec, E. Reisner, A. Eichinger, M. Pongratz, V. B. Arion, M. Galanski, Ch. G. Hartinger, B. K. Keppler, *J. Med. Chem.* **2005**, *48*, 2831–2837.
- [26] D. A.Wink, Y. Vodovotz, J. Laval, F. Laval, M. W. Dewhirst, J. B. Mitchell, *Carcinogenesis* **1998**, *19*, 711–721.

Curriculum vitae

Ewelina Orłowska BSc.



Education

10/2012 – present day	Master thesis at the Institute of Inorganic Chemistry Master thesis: <i>Synthesis, characterization and electrochemical studies of ruthenium–nitro and –nitrosyl complexes withazole heterocycles as potential anticancer drugs</i>
03/2011 – present day	Chemistry at the University of Vienna (Master)
03/2007 – 03/2011	Chemistry at the University of Vienna (Bachelor) Bachelor thesis: <i>Isolation and spectroscopic characterization of herbal compounds from Chassalia curviflora</i>
09/2003 – 06/2006	High school Nr. 3 in Cracow
09/2000 – 06/2003	Secondary school No. 38 in Cracow
09/1994 – 06/2000	Primary school No. 89 in Cracow

Work Experience

01.10.2012 – 30.07.2013	Tutor at the University of Vienna in inorganic chemistry laboratory
-------------------------	---

Languages

Polish – native tongue
German – C-level niveau
English – B-level niveau
French – A-level niveau

Publications

J. Schinnerl, E. A. Orłowska, E Lorbeer, A. Berger,

L. Brecker. Alstrofines in Rubiaceae: *Alstrofline A* from *Chassalia curviflora* var. *ophioxyloides* and a novel derivative, *rudgeifoline* from *Rudgea cornifolia*. *Phytochemistry Letters* **2012**, 5(3), 586-590

International Experience

01.02.2013 – 29.03.2013

Work in the context of the master thesis in the group of Prof. Dominique Luneau (Groupe de Cristallographie et d'Ingénierie Moléculaire, Laboratoire des Multimatériaux et Interfaces) at the University Claude Bernard in Lyon

Other

German courses at the University of Vienna

10.07.2006 – 04.08.2006

basics, phase 3

07.08.2006 – 01.09.2006

basics, phase 4

16.10.2006 – 01.02.2007

advanced, phase 1-3

French courses in Alliance Française de Lyon

01.02.2013 – 29.03.2013

basics A1

A and B license

Personal Interests

Painting - Airbrush
Nature Photography
Sports, Motorcycle
Exotic squirrels